Reverse Osmosis Desalination: A State-of-the-Art Review

Muhammad Qasim[a], Mohamed Badrelzaman[a], Noora N. Darwish[b], Naif A. Darwish[1a*], Nidal Hilal[c,d*]

[a]*Department of Chemical Engineering, American University of Sharjah, P.O. Box 26666, Sharjah, United Arab Emirates*

[b]*The Research Institute of Science and Engineering (RISE), University of Sharjah, P.O. Box 27272, Sharjah, United Arab Emirates*

[c]*Centre for Water Advanced Technologies and Environmental Research (CWATER), College of Engineering, Swansea University, Fabian Way, Swansea SA1 8EN, UK.*

[d]*NYUAD Water Research Center, New York University Abu Dhabi, Abu Dhabi, United Arab Emirates*

Abstract

Water scarcity is a grand challenge that has always stimulated research interests in finding effective means for pure water production. In this context, reverse osmosis (RO) is considered the leading and the most optimized membrane-based desalination process that is currently dominating the desalination market. In this review, various aspects of RO desalination are reviewed. Theories and models related to concentration polarization and membrane transport, as well as merits and drawbacks of these models in predicting polarization effects, are discussed. An updated review of studies related to membrane modules (plate and frame, tubular, spiral wound, and hollow fiber) and membrane characterization are provided. The review also discusses membrane cleaning and different pre-treatment technologies in place for RO desalination, such as feed-water pre-treatment and biocides. RO pre-treatment technologies, which include conventional (e.g., coagulation-flocculation, media filtration, disinfection, scale inhibition) and non-conventional (e.g., MF, UF, and NF) are reviewed and their relative attributes are compared. As per the available literature, UF, MF and coagulation-flocculation are considered the most widely used pre-treatment technologies. In addition, this review discusses membrane fouling, which represents a serious challenge in RO processes due to its significant contribution to energy requirements and process economy (e.g., flux decline, permeate quality, membrane lifespan, increased feed pressure, increased pre-treatment and membrane maintenance cost). Different membrane fouling types, such as colloidal, organic, inorganic, and biological fouling, are addressed in this review. Principles of RO process design and the embedded economic and energy considerations are discussed. In general, cost of water desalination has dropped to values that made it a viable option, comparable even to conventional water treatment methods. Finally, an overview of hybrid RO desalination processes and the current challenges faced by RO desalination processes are presented and discussed.

Keywords:
Reverse Osmosis; Membranes; Pre-treatment; Fouling; Desalination; Concentration polarization

[1] Corresponding authors: ndarwish@aus.edu: n.hilal@swansea.ac.uk

Highlights

- An updated review of RO desalination is provided.
- Concentration polarization and transport models are discussed.
- Studies related to RO membranes are reviewed.
- Design, energy, and economic factors are discussed.
- Hybrid RO processes are reviewed.
- Technological challenges are addressed.

Table of Contents

1. Introduction

Clean water is a scarce and stressed resource since only a small portion (around 2.5%) of all the water present on Earth is suitable for direct human use and consumption [1,2]. Currently, there is a high imbalance between clean water demand and supply and around one quarter of the global population is facing economic water shortage [3]. In addition, latest statistical forecasts have revealed that about half of the Earth's population may be subjected to water stressed conditions by the year 2030 [4]. The problem of water scarcity is further exacerbated by factors such as exponentially growing population, continuing industrialization, expanding agricultural activities, water pollution, poor water management, and climate change [5–7]. In order to address the global challenge of water scarcity, extensive efforts are being made to develop and advance alternative water production technologies. In addition, the scientists and leaders are making great efforts in increasing the awareness regarding the importance of water management and water conservation [8].

Water desalination is considered as the main source of producing clean water from a variety of sources [9]. Desalination refers to the process of removing the salts and minerals (contaminants) from either seawater or brackish water in order to attain clean water suitable for human consumption and industrial and domestic usage [6]. Strict regulations, imposed by the different governments, on potable water quality have necessitated improvements in water desalination plants and enhancement of their efficiency [10]. Historically, thermal desalination methods utilizing phase change processes (such as evaporation and condensation) have been used to produce fresh water. Common thermal desalination processes include multi-stage flash evaporation (MSF), multiple-effect distillation (MED), and thermal vapor compression (TVC) [11]. These processes, however, exhibit high capital and operational costs and are considered to be highly energy-intensive due to their inherent reliance on thermal energy mainly gained from fossil fuels [12,13]. For instance, producing 1000 m^3/day of fresh water through thermal desalination may require an annual amount of 10,000 tons of fossil fuels [2]. With the advancements in membrane science, membrane-based processes are now considered to be the most promising and practical desalination options owing to their high energy efficiency [14,15]. In addition, these processes offer advantages such as low space requirement, process and plant compactness, operational simplicity, and ease of process automation [16]. Pressure-driven membrane-based processes utilize semipermeable membranes to purify water during which water molecules diffuse through the membrane while the salts are rejected [17,18]. Many different membrane-based processes have been utilized for seawater and brackish water treatment obtained from a variety of sources. Among these, the most widely used processes include reverse osmosis (RO), nanofiltration (NF), and membrane distillation (MD) [19].

RO is currently the most reliable state-of-the-art technique for seawater and brackish water desalination and has been used as an alternative source for producing clean water in order to minimize the desalination-associated costs [20–22]. The utilization of RO for desalination has significantly increased since the 1950s [23]. Based on the quality of the input processed, RO

processes can be grouped into brackish water RO plants (BWRO) where the salinity is in the range of 500 mg/L to 10,000 mg/L and seawater RO plants (SWRO) where the salinity is around 30,000 mg/L. BWRO is further sub-grouped into low salinity BRWO that process feed water with salinity between 500 and 2,500 mg/L and high salinity BRWO plants that process water with salinity between 2,500 and 10,000 mg/L. Currently, around 50% of the desalinated water available globally is produced by using RO [22]. The efficiency of RO depends on a number of factors including the operational parameters, the employed membrane, and the feed water characteristics. This review paper aims to provide an overview on the state of the art of various aspects of the RO desalination process. The fundamentals, theory, and modeling of RO desalination are extensively reviewed. The membrane cleaning as well as the pre-treatment technologies for RO membranes are discussed. In addition, advancements in membrane development (both integrally-skinned asymmetric and thin-film composite) and membrane modification have been reviewed. The principles of RO process design and the embedded economic and energy considerations are also highlighted. Finally, the main technological challenges faced by RO desalination are summarized.

2. Theoretical background

The physical phenomenon of osmosis has been known to mankind since many years [24,25]. Osmosis, in simplest terms, can be defined as a natural process in which water molecules spontaneously move from a solution of low solute concentration (low osmotic pressure) to a solution of high solute concentration (high osmotic pressure) across a semipermeable membrane (Fig. 1a). The membrane, being semipermeable, rejects the solutes and only allows water molecules to pass through. The process of osmosis continues until a state of osmotic equilibrium is reached where the chemical potentials across the membrane become equal (Fig. 1b). The flow of water molecules can be stopped or reversed by application of an external pressure on the solution of higher concentration (feed solution) [26]. In case the applied pressure difference is greater in magnitude than the osmotic pressure difference across the membrane, water molecules are forced to flow in a direction opposite to that of the natural osmosis phenomenon. In such a case, the process occurring is known as RO and is depicted in Fig. 1c.

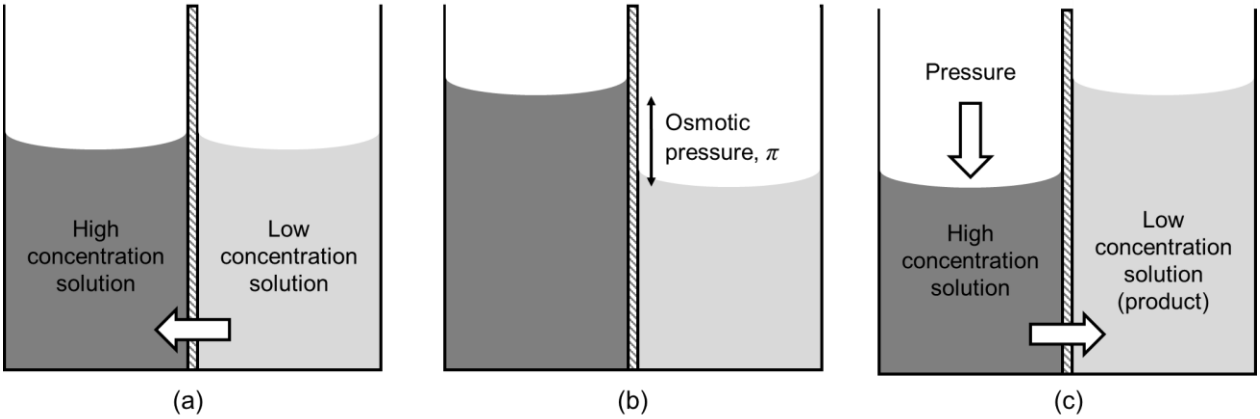

Fig. 1. Schematic of (a) osmosis (b) osmotic equilibrium (c) RO

2.1. Osmotic pressure

Osmotic pressure is closely related to the colligative properties of a solution such as freezing point depression and boiling point elevation [27]. For ideal dilute solutions, the osmotic pressure (π) can be estimated using the van't Hoff equation given below [28]:

$$\pi = CRT \quad (1)$$

where, C is the molar concentration of a non-permeable solute in the solution (mol/L), R is the universal gas constant (0.08206 L atm/mol K), and T is the absolute temperature (K).

In case of non-ideal dilute solutions, the osmotic pressure is given by the power series shown below [29]:

$$\pi = RT\left(\frac{\rho_2}{M_2} + A_2\rho_2^2 + A_3\rho_2^3 + \cdots\right) \quad (2)$$

where, M_2 is molar mass of the solute, A_2, A_3, and so on are the second, third, etc. virial coefficients, and ρ_2 is the solute mass concentration (g/L).

For non-ideal concentrated solutions, the following logarithmic equation is valid for the estimation of osmotic pressure [29]:

$$\pi = -\frac{RT}{V_1^0}\ln(a_1) \quad (3)$$

where, a_1 is the activity of the solvent and V_1^0 is the molar volume of pure solvent (L/mol).

When several electrolytes are present in the solution, the osmotic pressure can be calculated as follows [30]:

$$\pi = \varphi RT\sum v_i C_i \quad (4)$$

where, v_i and C_i represent the number of ions and molar concentration of the electrolyte i and φ is the osmotic coefficient that can be determined by conducting experiments (such as freezing point depression measurements or vapor pressure osmometry) or using Pitzer correlation [31]. In case of RO using seawater feed, the following approximate expression for osmotic pressure can be employed [23,26,32]:

$$\pi = 1.12T\sum m_i \quad (5)$$

where, π is in psia, T is in K, and the term $\sum m_i$ represents the summation of molarities (mol/L) of all the dissolved species (both ionic and non-ionic) in the solution.

As a rule of thumb, osmotic pressure ranges from 0.60 to 1.1 psi for every 100 ppm of total dissolved solids (TDS) in the solution [33]. For instance, the osmotic pressure of seawater with TDS content of 35,000 ppm would be around 350 psi. However, it should be noted that due to the high resistance of the membrane, the pressure applied in RO must be significantly higher than the

osmotic pressure. For example, in case of RO using seawater with TDS content of 35,000 ppm, pressures as high as 1,500 psi may be required [33].

2.2. Water recovery

In a continuous RO process, the feed water stream splits into two streams as shown in Fig. 2. The first stream consists of water molecules that have permeated through the membrane. This stream of low solute concentration is called permeate or product water. The second stream consists of a decreased amount of water molecules and the rejected solutes. This stream is of higher solute concentration compared to the feed and is termed as brine, concentrate, or reject.

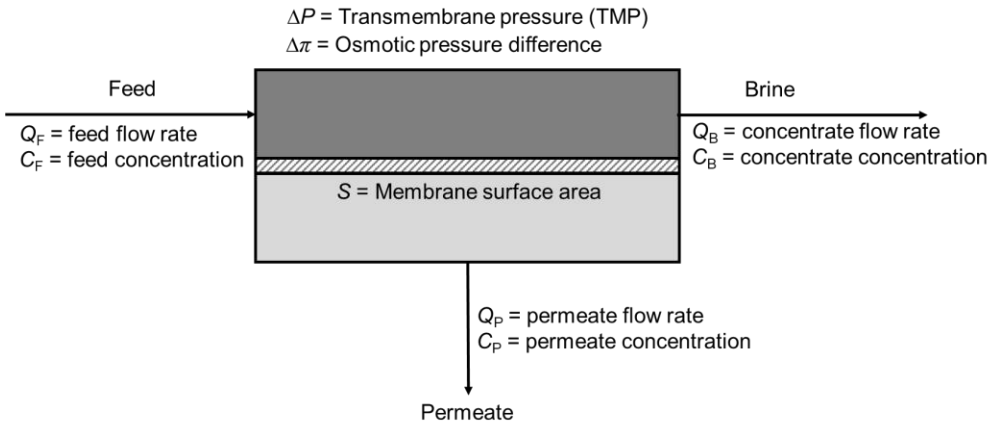

Fig. 2. Schematic of a continuous RO system

Recovery or conversion of an RO process is defined as the volume fraction of feed water that is recovered as permeate or product water. Considering the RO process streams in Fig. 2, the percentage recovery (r) can be calculated as follows:

$$r = \frac{Q_p}{Q_F} \times 100\% \quad (6)$$

where, Q_P and Q_F are the flow rates of the permeate and feed streams, respectively. In most RO systems, recovery ranges from 50-85% [33] and typically depends on the feed characteristics, feed salinity, pre-treatment, design configuration, and brine disposal considerations [34]. Recovery is an important design parameter that requires careful selection in order to balance the tradeoff between the concentrate volume generated and the permeate purity. A higher recovery results in lower amount of concentrate that needs to be disposed. However, this advantage is gained at the expense of lower permeate purity.

2.3. Solute rejection and passage

Solute or salt rejection (SR) is defined as the percentage of a particular incoming solute that is rejected by the RO membrane. Mathematically, the apparent (observed) SR is given as follows:

$$SR = \left(1 - \frac{C_p}{C_F}\right) \times 100\% \quad (7)$$

where, C_P and C_F represent permeate and feed solute concentrations (mg/L), respectively.

Salt passage (*SP*) is opposite of *SR* and represents the percentage of a particular incoming solute that permeates through RO membrane. Mathematically, *SP* and *SR* are related as follows:

$$SP = 100\% - SR \quad (8)$$

Rejection depends on the type of feed constituents, their characteristics, and the type of RO membrane. In general, solutes with high degree of dissociation and hydration, high molecular weight, and low polarity exhibit high rejection [33].

2.4. Permeate and salt flux

Permeate or water flux (J_w) is the volumetric flow rate of permeate per unit surface area of the RO membrane. It is typically proportional to the net pressure driving force across the membrane. Salt flux (J_s), on the other hand, is the amount of salt passing through unit membrane surface area per unit time and is proportional to the salt concentration difference across the membrane. Mathematical expressions for permeate and salt flux are given by various RO transport models outlined in Section 2.6.

2.5. Concentration polarization

During RO desalination, there is convective flow of solutes from the bulk feed towards the membrane. This maximizes the solute concentration on the membrane surface and, consequently, creates a boundary layer within which the solute concentration is higher than the bulk solute concentration. Higher solute concentration within the boundary layer also causes diffusional back-transport of the solutes away from the membrane. However, the dominance of convection over diffusion builds up the solutes in the boundary layer and on the membrane surface. As a result, the concentration on the membrane surface (C_m) is always higher than the solute concentration in the bulk feed water (C_F) [23,26,33]. This phenomenon due to accumulation of rejected solutes near the RO membrane surface is known as concentration polarization (CP).

2.5.1. Effects of concentration polarization

The effects of CP on the performance of RO desalination are highly undesirable. The main adverse effect of CP is to decrease the permeate flux by increasing the hydraulic resistance for the flow of water and decreasing the net pressure driving force across the membrane by increasing the osmotic pressure within the boundary layer [33,35,36]. Permeate flux decline can also be attributed to membrane fouling (Section 3.3) which is almost always an adverse consequence of CP [37]. In addition, due to increased solute concentration on the membrane surface, CP increases the solute flux across the membrane [36]. This decreases the membrane solute rejection due to an increase in the permeate concentration as described by Eq. (7). Also, CP exacerbates the probability of precipitation (scaling) of divalent ions and sparingly soluble salts by enhancing their concentrations on the membrane surface [35,36]. In case of feed water containing colloidal particles, the formation of a cake layer on the membrane surface and the resulting hindrance of the

diffusional back-transport further enhances the CP effects and the associated permeate flux decline. This phenomenon is termed as cake-enhanced concentration polarization (CECP) or cake-enhanced osmotic pressure (CEOP) [38,39]. The severity of CP is typically governed by the solute and membrane properties and the hydrodynamics (flow conditions, pressure, and geometry of the flow channel) of the RO process [40,41]. Although the aforementioned effects are severe, CP is considered to be reversible and can be mitigated by employing appropriate feed velocity, rotating or vibrating modules, reactive micro-mixing, pulsation, or feed spacers [40,42–46].

2.5.2. Concentration polarization models

A thorough understanding and accurate prediction of CP is highly critical to the design, performance prediction, and elucidation of fouling mechanisms in the RO desalination process [41]. Neglecting the effects of CP during RO modeling can lead to underestimation of the energy requirements and overestimation of the recovery and permeate quality [47]. Several studies have focused on the modeling of CP in membrane systems. The classical boundary layer film model represents the simplest CP model and assumes one dimensional flow and a fully developed boundary layer [35]. The model is based on steady-state solute mass balance as shown below [35]:

$$J_w C + D\frac{dC}{dx} = J_w C_p \tag{9}$$

where, the terms $J_w C$, $D\frac{dC}{dx}$, and $J_w C_p$ represent convective salt flux towards the membrane, diffusive salt flux away from the membrane, and salt flux through the membrane, respectively. In Eq. (9), D is the diffusivity of solute in water, x is the distance from the membrane, and C is the concentration at any point within the boundary layer of thickness δ (Fig. 3).

Solving Eq. (9) over the boundary layer thickness (boundary conditions: $C = C_F$ at $x = \delta$ and $C = C_m$ at $x = 0$) gives the following film model that describes the extent of CP [35,36]:

$$\frac{C_m - C_P}{C_F - C_P} = exp\left(\frac{J_w}{k}\right) \tag{10}$$

where, C_m is the solute concentration at the membrane surface and $k = D/\delta$ is the solute mass transfer coefficient. A more rigorous mathematical development of the film model is given Zydney [48]. It should be noted that the use of film model in practical RO applications is only justified under operating conditions of high cross-flow and low permeate flux where the effects of CP are small [49].

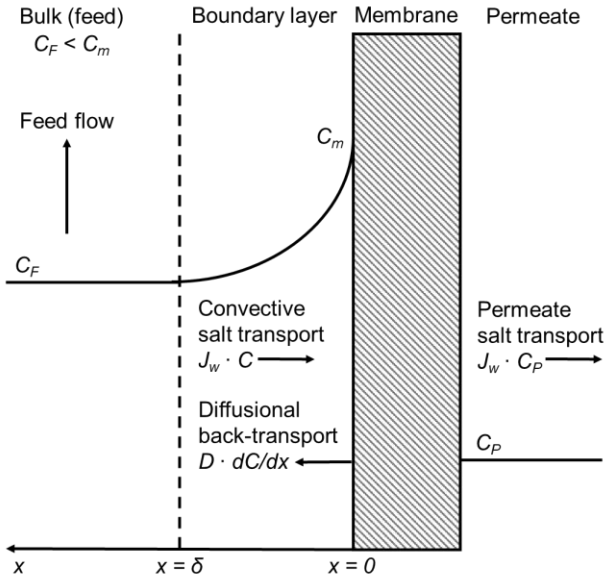

Fig. 3. Schematic of concentration gradient developed by concentration polarization

Prediction of C_m from Eq. (10) requires accurate estimation of the mass transfer coefficient. Experimental techniques such as optical or microelectrode measurements and velocity or flux variation method can be used to estimate the mass transfer coefficient [35,50]. Also, the mass transfer coefficient can be estimated using the Sherwood correlation [36,40]:

$$Sh = \frac{kd_h}{D} = \gamma_1 Re^{\gamma_2} Sc^{\gamma_3} \tag{11}$$

where, *Sh* is the Sherwood number, *Re* is the Reynolds number, *Sc* is the Schmidt number, d_h is the hydraulic diameter of the flow channel, and γ_1, γ_2, and γ_3 are empirical constants.

In case of spiral wound RO membranes and fully developed turbulent flow, the mass transfer coefficient in the channel of the feed spacer can be predicted by the following relation [23,51]:

$$k = 0.023 \frac{D}{d_h} Re^{0.875} Sc^{0.25} \tag{12}$$

For a fully developed laminar flow, the mass transfer coefficient has the following form [52]:

$$k = 1.86 \left(Re\, Sc \frac{d_h}{L} \right)^{\frac{1}{3}} \tag{13}$$

where, *L* is the channel length.

Bhattacharya and Hwang [53] showed that the mass transfer coefficient *k* in the film model is equal to the ratio D/δ only when the average modified Peclet number approaches zero. Therefore, the generalized model given below was presented that expressed the extent of CP in terms of modified Peclet number [53]:

$$I = \frac{C_m}{C_F} = \exp(Pe^M) \quad (14)$$

where, I is the polarization index that represents the extent of CP, and Pe^M is a dimensionless component of the average modified Peclet number and is equal to the ratio of the convective to diffusive velocities.

It should be noted that the film model in Eq. (10) assumes that the velocity and concentration profiles are fully developed, the permeate flux is constant and axially invariant, the axial velocity profile is unaltered, axial solute convection is negligible, and there is uniform CP layer over the membrane [30,49,54]. These assumptions may not be valid in actual RO systems. For instance, in cross-flow systems, the CP effects vary locally and the CP layer builds gradually over the length of the filtration channel [30]. As a result, several attempts (both analytical and numerical) have been made to create a better understanding of the CP phenomenon. De and Bhattacharya [55] considered the case of developing boundary layer and provided Sherwood-number relations for rectangular channel, tubular, and radial cross-flow channels in the presence of suction effects through the membrane. Local Sherwood-number relations were developed which were integrated over the entire channel to obtain the average Sherwood number and the average mass transfer coefficient. The study showed that the suction through the membrane had a profound effect on the mass transfer coefficient. The predicted permeate flux values were within ±10% of the experimental values.

Mariñas and Urama [56] used the film model with Sherwood correlation but considered the local variation of CP along the length of a spiral wound RO membrane element. This was done by dividing the membrane into a number of sub-elements and treating each sub-element as an ideal continuous stirred tank reactor. Both Schmidt number and kinematic viscosity were evaluated at the logarithmic average concentration within the boundary layer. The model results were compared with the experimental permeate flux data obtained by RO of $MgSO_4$ and $NaCl/Na_2SO_4$ feeds using commercial membranes. The model performed well except at low feed water flow rates.

The local variation of CP in the filtration channel was confirmed by Song and Yu [30]. The authors concluded that the assumption of uniform CP layer oversimplified the cross-flow RO process. The following equation for polarization index was provided through analytical solution of the model equations [30]:

$$I = \frac{\Delta p - R_m J_w(y)}{\Delta \pi} \quad (15)$$

where, R_m is the membrane resistance and $J_w(y)$ is the local permeate flux. In Eq. (15), $\Delta\pi$ is the osmotic pressure difference between the bulk feed and permeate sides of the membrane. The model was, however, not validated against experimental data. In a later study [49], it was shown that the model does not perform well in predicting CP during RO experiments.

Song and Elimelech [57] developed a mechanistic model for CP based on mass balance and transport equations in cross-flow membrane channels. The model uses the concept that solute mass

balance cannot be performed in the direction perpendicular to the membrane since the solute is always brought into the CP layer by the permeate flow [58]. The following analytical expression for permeate velocity (V) was proposed based on mass balance for the retained solute [57,58]:

$$V = \frac{V_0}{\left(1+\frac{\alpha x}{L}\right)^{1/3}}\left\{\left[\left(\frac{1}{1+\frac{\alpha x}{L}}+4\right)^{1/2}+2\right]^{1/3}-\left[\left(\frac{1}{1+\frac{\alpha x}{L}}+4\right)^{1/2}-2\right]^{1/3}\right\} \quad (16)$$

where, V_0 is the initial permeate velocity at the entrance of the membrane channel, α is a dimensionless parameter, and L is the membrane channel length. The model, however, is not suitable for long narrow RO channels since it assumes that the permeate amount is negligible compared to the total cross-flow in the channel [59].

Elimelech and Bhattacharjee [60] developed a theoretical model for CP in cross-flow membrane filtration of small hard spherical solute particles. The model was developed by considering the equivalence of the hydrodynamic and thermodynamic principles related to the equilibrium in the CP layer and predicts the surface concentration and the local permeate flux along the filtration channel.

For industrial applications where the feed water is multi-ionic, the applicability of the film model given by Eq. (10) becomes limited since several ions and solutes move at different rates within the boundary layer. In order to overcome this limitation, Geraldes and Afonso [61] developed a simple and accurate model for predicting CP effects in RO of dilute multi-ionic solutions. The model assumes coupling of ionic fluxes, enforces electroneutrality at the feed/membrane interface, and does not need assumption of the film layer thickness.

Besides analytical models, numerical models have also been proposed to simulate CP in RO systems. Madireddi et al. [62] developed an unsteady-state finite difference model for the prediction of CP in commercial spiral wound RO membranes. The model was based on mass balance equations and axial velocity profiles for laminar, completely mixed, and spacer-induced (partial) mixing regimes. In comparison with the experimental data, permeate flux predictions exhibited errors as high as 10%. The error in the predictions was attributed to numerical errors and model limitations attributed to the description of the membrane, module and, spacers. However, the model is useful in long-term prediction of CP effects and the resulting flux decline. Wiley and Fletcher [63] developed a computational fluid dynamic (CFD) model for CP and permeate flow in pressure-driven membrane processes using commercial finite volume code CFX4. Although the model performed well, it was not tested in spacer-filled RO systems. In order to account for spacer-filled channel, Ma et al. [64] developed a finite element model for CP in spiral wound RO membranes. Numerical solution of the model equations was obtained by employing the streamline upwind Petrov/Galerkin (SUPG) method. The results were found to be in agreement with the experimental data of Merten et al. [65]. Similarly, Zhou et al. [66] conducted a numerical study on CP in long spacer-filled RO membranes. However, this study also included the effect of depolarization induced by the spacers. The numerical simulation results were supported by

experimental data. Also, it was concluded that CP effects in long RO membranes are negligible when the so-called hydraulic dispersion coefficient is eight times higher than the salt diffusion coefficient.

Kim and Hoek [49] developed a numerical CP model that considered two-dimensional mass transfer in cross-flow RO processes. The model assumed that the axial velocity was independent of CP and the thickness of the CP layer was negligible compared to the channel height. Compared to the experimental values, the proposed numerical model under and overestimated the CP at low and high operating pressures, respectively, with accuracy improving at higher cross-flow velocities. However, the model performed better at predicting the average permeate flux. Overall, the predictions were better than those from the film model. Subramani et al. [67] proposed a finite element model to predict CP in open and spacer-filled channels. In open channels, the model overestimated the CP effects at high permeation rates especially at the end of the channel. The study showed the zigzag spacers resulted in dramatic changes in CP due to the stagnant zones produced by directional changes of the flowing fluid. Lyster and Cohen [54] studied the CP effects in rectangular and plate-and-frame RO channels using a numerical model that coupled equations of motion and mass transfer. The study considered the impact of concentration dependence of the model parameters (viscosity, density, diffusivity, and osmotic pressure). In case of rectangular channel, ignoring the concentration dependence of model parameters resulted in a small but noticeable overestimation of CP. Also, the film model underestimated the CP effects at the entrance and exit of the rectangular channel. In case of plate-and-frame channel, the model was able to predict CP in the entrance and exit regions.

Song [59] presented a numerical total salt balance (TSB) model for unbounded and bounded CP in a narrow RO membrane channel. In unbounded CP, the thickness of the CP layer was assumed to be small compared to the channel height whereas in bounded CP, the CP layer extended to the whole height of the membrane channel. The TSB along the channel, derived using a plug flow, was used to account for the variable cross-flow velocity. In a later study, Song and Liu [58] introduced shear flow within the TSB model. In this study, the TSB model with shear flow was compared with Song and Elimelech [57] model and the TSB model with plug flow by Song [59]. The model by Song and Elimelech [57] was found to be unsuitable for predicting CP in long narrow RO channels since large channel height was the basic assumption in its development. Also, in case of long narrow channel, the use of plug or shear flows did not produce significant changes in CP predictions. As a result, due to its relative simplicity, the TSB model with plug flow was recommended for CP predictions in practical RO processes.

Recently, Ishigami and Matsuyama [68] proposed a numerical model with permeable wall boundary condition for describing CP in spacer-filled channel of a spiral wound RO membrane. Water and salt permeation across the membrane were modeled using non-equilibrium thermodynamics. The proposed model was reported to be useful for understanding local variations in solute concentration, water flux, and mass transfer coefficient. However, the model results were not validated against experimental data. Li et al. [69] developed a three-dimensional CFD model

that was able to predict the polarization index in an industrial spiral wound RO membrane. More recently, Bernales et al. [70] developed a two-dimensional numerical model based on the solute conservation equation and the steady Navier-Stokes equations under the Prandtl approximation. The model was able to predict CP and local permeate flux in cross-flow channels. The CP profiles obtained from the model were slightly over predicted compared to the experimental results. This was attributed to model assumptions such as total rejection by the membrane and a two-dimensional geometry. Chaudhuri and Jogdand [71] provided a model for CP in a closed roto-dynamic RO system without retentate outlet. The model was based on unsteady-state equations related to conservation of mass, momentum, and species transport in an axisymmetric set up. It was, however, not validated against experimental data.

2.6. Transport models

Membrane transport models are important tools in understanding the transport of solutes and water through the RO membrane. Such models hold immense significance in predicting the membrane performance and designing novel membrane with improved characteristics [72]. The various transport models developed over the years can generally be classified into two distinct types, namely, phenomenological and mechanistic models [73]. Details of these models are provided below.

2.6.1. Phenomenological models

Phenomenological models are based on the principles of irreversible thermodynamics (IT) and are independent of the transport mechanism and the membrane structure. These models assume that the membrane is a black box which is not far from equilibrium and that the system can be divided into smaller subsystems where local equilibrium exists [74,75]. Based on the phenomenological thermodynamic relationships, the membrane performance and flux are described in terms of measureable quantities such as water flux and salt rejection [73,76]. Generally, the phenomenological models are considered to be convenient since they require less input data and can be utilized for cases where the membrane structure is unknown. However, they do not provide insights into the actual transport mechanism involved [77].

The IT theory states that the flux of each component (J_i) in a solution can be related to the forces (F_i) acting on the system. Onsager [78,79] showed that J_i and F_i are interrelated through the so-called phenomenological coefficients (L_{ij}) according to the following linear relation [80]:

$$J_i = L_{ii}F_i + \sum_{\substack{i=1 \\ i \neq j}}^{n} L_{ij}F_j \quad (17)$$

For systems that are not far from equilibrium, the following relation applies for $i \neq j$ [80]:

$$L_{ij} = L_{ji} \quad (18)$$

The Kedem-Katchalsky [81] and Spiegler-Kedem [82] models are two of the well-known phenomenological membrane transport models. According to the Kedem-Katchalsky model, the

hydraulic pressure difference (Δp) and osmotic pressure difference ($\Delta \pi$) govern the water and solute flux across the membrane. Using the concepts of linear thermodynamics of irreversible processes, the model defines the water flux and the solute flux through the membrane as follows [80,83]:

$$J_w = l_p(\Delta p - \sigma \Delta \pi) \tag{19}$$

$$J_s = \omega \Delta \pi + (1 - \sigma) J_w C_{avg} \tag{20}$$

where, Δp and $\Delta \pi$ are the hydraulic and osmotic pressure differences across the membrane, C_{avg} is the logarithmic mean solute concentration across the membrane, and the coefficients l_p, ω, and σ are functions of L_{ij}. The coefficient σ is also known as the reflection coefficient which is equal to unity for complete solute rejection or less than unity for semipermeable solute [73]. The Kedem-Katchalsky model, however, has limited applicability to RO systems due to concentration dependence of the model coefficients and invalidity of the linear relations at high concentration difference across the membrane [80]. In order to avoid these limitations, the Spiegler-Kedem model defines the local water and solute fluxes using the following equations [75]:

$$J_w = -P_w \left(\frac{dp}{dz} - \sigma \frac{d\pi}{dz} \right) \tag{21}$$

$$J_s = -P_s \frac{dC}{dz} + (1 - \sigma) J_w C \tag{22}$$

where, P_w, P_s, and σ are the model coefficients and z is the coordinate perpendicular to the membrane. Assuming constant fluxes and coefficients, Eqs. (21) and (22) can be integrated to obtain the following relations for the water flux and the real solute rejection (SR_r) [73]:

$$J_w = \frac{P_w}{\Delta z} (\Delta p - \sigma \Delta \pi) \tag{23}$$

$$SR_r = 1 - \frac{C_P}{C_m} = \sigma \left[\frac{1 - exp\left(-\frac{J_w (1-\sigma) \Delta z}{P_s} \right)}{1 - \sigma exp\left(-\frac{J_w (1-\sigma) \Delta z}{P_s} \right)} \right] \tag{24}$$

where, Δz is the membrane thickness. Although the Spiegler-Kedem model is accurate in describing the membrane transport, it is not a mechanistic model and does not explain the transport mechanism. Complete derivations of Kedem-Katchalsky and Spiegler-Kedem models are provided by Soltanieh and Gill [84]. An equation similar to Eq. (24) was developed earlier by Starov and Churaev [85] where both the maximum value of rejection coefficient and corresponding optimum filtration velocity were estimated. The study also explained the possibility of negative rejection of some ions and a change in pH of the filtrate. Hall et al. [86] provided a model (based on Extended Nernst-Planck equation) for RO separation of electrolyte solutions. The model incorporated a mechanism for varying-membrane-fixed-charge as a function of ion concentrations and pH inside the membrane. The model was verified in another study [87] by comparing the model results with the values obtained from single salt experiments performed over a wide range of concentration and pH using NaCl and $CaCl_2$. The model results matched well with the

experimental data and it was concluded that the model can be used for prediction of multicomponent separations using data from single salt experiments.

2.6.2. Mechanistic models

Mechanistic models assume a certain type of transport mechanism and relate the membrane performance to the physical and chemical properties of the membrane and the solutes [73]. These models can be classified into non-porous and porous transport models.

The non-porous models assume that the membrane is non-porous or homogeneous. Common non-porous transport models include the solution-diffusion (SD) model, the extended solution-diffusion (ESD) model, and the solution-diffusion-imperfection (SDI) model.

The SD model assumes that the membrane is homogeneous and non-porous and both solute and solvent species dissolve in the non-porous layer of the membrane and, thereafter, diffuse independently across the membrane [36,73]. Separation of solute from the solvent is achieved by the difference in the amount dissolved and the diffusion rate of each species [88]. According to the SD model, the water flux is proportional to the net pressure driving force across the membrane while the solute flux is proportional to the solute concentration difference across the membrane. Mathematically, the water flux is given as follows for constant flux RO systems [73,76,88]:

$$J_w = A(\Delta p - \Delta\pi) \tag{25}$$

where, A is known as the water permeability coefficient. The value of A depends on the type of membrane and also varies with temperature and pH [33]. The water permeability coefficient given by the following equation [34,73,88,89]:

$$A = \frac{D_w K_w \bar{V}_w}{RT\Delta z} \tag{26}$$

where, D_w is the water diffusivity in the membrane, K_w is the water-membrane distribution coefficient, and $\bar{V}_w$ is the partial molar volume of water. The salt flux, on the other hand, is defined as follows [73,88]:

$$J_s = B(C_m - C_P) \tag{27}$$

where, B is the membrane permeability coefficient for the solute defined as follows [34,73,88]:

$$B = \frac{D_S K_S}{\Delta z} \tag{28}$$

where, D_s is the salt diffusivity in the membrane and K_s is the solute-membrane distribution coefficient. Based on the solution-diffusion model, the real salt rejection is defined as follows [73]:

$$SR_r = \frac{J_w}{J_w + B} \tag{29}$$

The SD model is simple and highly suitable for RO processes due to the non-porous behavior of RO membranes and the presence of diffusion as the prevalent transport mechanism [90]. However, it is only appropriate for cases where the solute rejection is close to unity [80].

In Eq. (27), the SD model neglects the effect of pressure on solute transport across the membrane. In case of organic solutes, the following ESD model is utilized which considers the effect of pressure on solute flux [80]:

$$J_s = B(C_m - C_P) + l_{sp}\Delta p \tag{30}$$

where, l_{sp} is a pressure-induced parameter.

Although the SD and ESD models assume that the membrane is non-porous, industrial RO membranes inevitably contain some imperfections (pores) induced during the synthesis process. These imperfections allow for leakage of the solution through the RO membranes [33]. In order to account for the imperfections, the SDI model extends the SD model by considering the solvent and solute flow through the imperfections in addition to the diffusion through the membrane. The water and solute flux are expressed as follows [33,91]:

$$J_w = A(\Delta p - \Delta\pi) + K_3\Delta p \tag{31}$$

$$J_s = B(C_m - C_P) + K_3\Delta p C_m \tag{32}$$

where, K_3 is known as the coupling coefficient and the second term in each equation signifies flow through the imperfections.

In porous transport models, the membrane is assumed to be porous. Common porous transport models include frictional, preferential sorption-capillary flow (PS-CF), finely porous (FP), surface force-pore flow (SF-PF), and modified surface force-pore flow (MD-SF-PF) models.

The frictional model considers that the membrane pores are too small to allow free permeation and friction occurs between solute-pore wall, solvent-pore wall, and solute-solvent [80]. The driving forces for any species are balanced by the exerted frictional forces [84]. The frictional force on any component is assumed to be proportional to the velocity difference between that component and the component that is causing the frictional drag [92]. Mathematically, the frictional forces are expressed as follows [84]:

$$F_{ij} = f_{ij}\left(u_i - u_j\right) \tag{33}$$

where, F_{ij} represents the frictional force between component *i* and *j* (component *w*: solvent, component *s*: solute, and component *m*: membrane), u is the component velocity with membrane as reference ($u_m = 0$), and f_{ij} is the friction coefficient. Using Eq. (33), the total force acting on water and solute can be expressed as follows [84]:

$$F_w = (C_s/C_w)f_{sw}(u_w - u_s) + f_{wm}u_w \tag{34}$$

$$F_s = f_{sw}(u_w - u_s) + f_{sm}u_w \quad (35)$$

where, C_s and C_w are the solute and water molar concentrations per unit membrane volume. Eqs. (34) and (35) can be written as follows in terms of fluxes [84]:

$$J_w = \frac{(f_{sm}+f_{sw})C_w^2}{d}F_w + \frac{f_{sw}C_wC_s}{d}F_s \quad (36)$$

$$J_s = \frac{f_{sw}C_wC_s}{d}F_w + \frac{(f_{wm}C_w+f_{sw}C_s)C_s}{d}F_s \quad (38)$$

where, $d = f_{sm}f_{wm}C_w + f_{sm}f_{sw}C_s + f_{sw}f_{wm}C_w$.

In the frictional model, the frictional coefficients are related to Spiegler-Kedem coefficients in Eqs. (21) and (22) as follows [84]:

$$\sigma = 1 - \left(\frac{C_s/C_s^b}{C_w/C_w^b}\right)\left(\frac{1+(f_{wm}/f_{sw})(\bar{V}_s/\bar{V}_w)}{1+(f_{sm}/f_{sw})}\right) \quad (39)$$

$$P_w = \left(C_w/C_w^{b^2}\right)\frac{(1/f_{wm})(1+f_{sm}/f_{sw})}{1+f_{sm}/f_{sw}(1+f_{ws}/f_{wm})} \quad (40)$$

$$P_s = 2RT(C_s/C_s^b)(1/f_{sm})/(1 + f_{sw}/f_{sm}) \quad (41)$$

where, the superscript b denotes the bulk solution and $\bar{V}_s$ is the partial molar volume of the solute.

The PS-CF model is based on the assumption of a microporous membrane [26,93]. According to this model, preferential sorption of the solvent molecules results in the formation of a solvent layer over the membrane surface and in the membranes pores. Subsequently, the solvent molecules in the solvent layer pass through the membrane capillary pores under the influence of applied pressure. Solute, on the other hand, is rejected by the membrane and does not form any surface layer [26,94]. The water flux is given by the following expression [26]:

$$J_w = A[\Delta p - \{\pi(C_m) - \pi(C_P)\}] \quad (42)$$

where, $\pi(C_m)$ is the osmotic pressure at the membrane surface and $\pi(C_P)$ is the osmotic pressure of the permeate solution. The solute flux in the PS-CF model is given by the same expression as in the SD model (Eq. (27)). Thus, according to the PS-CF model, solute transport is solely governed by diffusion and not partially by pore flow as dictated by the SDI model [26].

The FP model assumes that water transport occurs by viscous flow through the membrane pores and solute transport takes place by both diffusion and convection [26]. The model expresses the solute rejection as follows [84]:

$$SR_r = 1 - \frac{k_s'\exp(u\tau\delta/bD_e)}{k"_s - b\epsilon + b\epsilon\, exp(u\tau\delta/bD_e)} \quad (43)$$

where, k_s' and k_s'' are the partition coefficients with respect to total membrane volume, u is the permeation velocity, τ is the membrane tortuosity, δ is the skin layer thickness, ϵ is the void fraction, and b and D_e are defined as follows [84]:

$$b = 1 + \frac{f_{sm}}{f_{sw}} \quad (44)$$

$$D_e = \frac{RT}{f_{sw} b} \quad (45)$$

A complete derivation of the FP model is provided by Soltanieh and Gill [84].

The SF-PF model [95] extends the FP model in two dimensions (radial and axial coordinates) [26]. This model considers the membrane to be microporous consisting of perfect cylinders in which the solute velocity and concentration are assumed to vary in both the radial and the axial direction. The model equations are highly complex and based on a balance between the applied forces and the frictional forces. Details of this model are provided elsewhere [76]. Mehdizadeh and Dickson [96,97] highlighted that the SF-PF model employs a form of material balance that is incorrect and a potential function that is unsuitable for cylindrical pores. The authors modified the SF-PF model to account for these limitations. According to the MD-SF-PF model, the water and solute fluxes averaged over the pore cross-sectional area are given as follows [72,73,76]:

$$\bar{J}_w = 2\left(\frac{CRT}{\delta_p f_{sw}}\right)\int_0^1 \alpha(\rho)\rho d\rho \quad (46)$$

$$\bar{J}_s = 2\left(\frac{1}{\delta_p f_{sw}}\right)\int_0^{1-\frac{r_s}{r_p}} \frac{\alpha(\rho)}{b(\rho)}\left(\pi_2 + \frac{\pi_2 - \pi_3}{e^{\alpha(\rho)}-1}\right)e^{-\emptyset(\rho)}\rho d\rho \quad (47)$$

where, ρ is the dimensionless radial distance in the pore ($\rho = r/r_p$), r_s is the solute Stokes radius, r_p is the pore radius, δ_p is the pore length, C is the solution molar density, $\emptyset$ is the surface wall potential, π_2 and π_3 are the osmotic pressures in the boundary layer and the permeate, respectively, $\alpha(\rho)$ is the dimensionless velocity profile, $b(\rho)$ is the dimensionless friction parameter that can be given by a modified form of the Faxen equation [72].

3. Reverse osmosis membranes

3.1. Membrane modules

Membranes for RO desalination exist in four different type of modules: (1) plate and frame, (2) tubular, (3) spiral wound, and (4) hollow fiber. For industrial applications, RO membrane modules must possess a high packing density such that a large membrane area can be packed into a relatively small volume in order to ensure compactness of the process, ease of membrane installation, cleaning, and replacement, and low capital cost [33,98,99]. Initially, RO membranes were based on tubular and plate and frame configurations. However, due to inherently low packing density, these two membrane modules were phased out and replaced with hollow fiber and spiral wound modules [100,101]. Table 1 compares the four RO membrane modules in terms of packing density, fouling propensity, ease of cleaning, and manufacturing cost [33,102].

Table 1. Comparison of RO membrane modules [33,102]

Module type	Packing density (ft^2/ft^3)	Fouling propensity	Ease of cleaning	Manufacturing cost
Plate and frame	45-150	Moderate	Good	High
Tubular	6-120	Low	Excellent	Very high
Spiral wound	150-380	High	Poor	Moderate
Hollow fiber	150-1500	Very high	Poor	Low

3.1.1. Plate and frame modules

Plate and frame modules are among the earliest RO membrane modules. In such modules, a flat sheet RO membrane is attached to the two sides of a rigid plate that is composed of solid plastic, porous fiberglass, or reinforced porous paper [98,103]. A number of plates are used that are stacked within a pressurized support framework [33,103]. The plates contain grooved channels that provide a path for the permeate flow. As the feed solution enters the module from one end, water molecules permeate the membrane and are collected as permeate solution in a central permeate collection manifold [44,98]. The brine or concentrate solution leaves the module from the other end. A typical plate and frame module is shown in Fig. 4 [104].

Plate and frame modules exhibit low packing density and are expensive owing to their tedious design and construction. In addition, these modules are prone to fouling due to the presence of dead zones within the modules. The modules are, however, easy to clean which makes them suitable for feed streams containing high content of suspended solids [33].

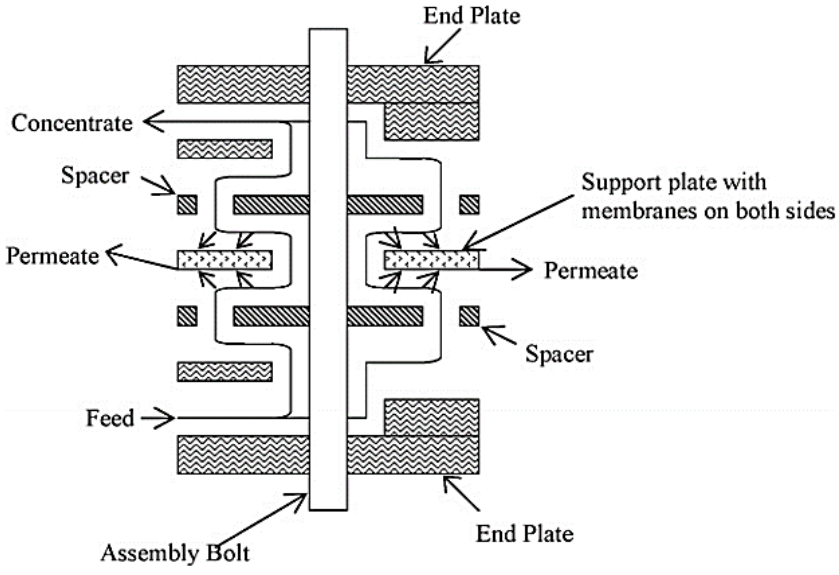

Fig. 4. Plate and frame membrane module (adopted from [104])

3.1.2. Tubular modules

Tubular modules are relatively simple in construction. A typical tubular module, shown in Fig. 5, consists a porous tube with an inserted or surface-coated RO membrane. The tubes are made of ceramic, carbon, paper, plastic, or fiberglass [44,101,103]. As pressurized feed water enters the tube from one end, water molecules permeate radially through the membrane to produce the product water. Concentrate solution, on the other hand, leaves from the other end of the tube. Multiple tubes can be arranged in series or parallel to increase the system capacity [101].

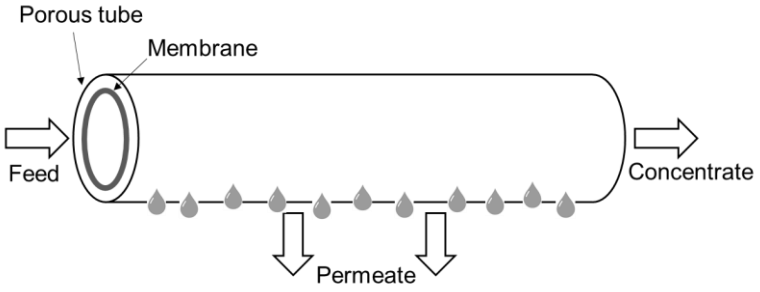

Fig. 5. Tubular RO membrane module (modified after [101])

Tubular membrane modules are uneconomical but easy to clean [33,98]. Although applicable to RO desalination [105–107], tubular modules are more common in microfiltration (MF) and ultrafiltration (UF) applications due to their low packing density [33].

3.1.3. Hollow fiber modules

A hollow fiber module is composed of numerous small-diameter (hair-like) fibers contained within a pressure vessel. On one side, the module consists of an epoxy tube sheet where the fibers ends are potted in epoxy while keeping them open for permeate flow. On the other side, the fiber ends are sealed in epoxy to form an epoxy nub which prevents bypassing of the feed to the concentrate outlet. The module also contains a porous feed distributor (core tube) that runs along the entire length of the module [98]. Fig. 6 [108] shows the structure of a hollow fiber module. As pressurized feed water enters the module through the core tube, water molecules permeate radially into the fibers and exit through the open fiber ends in the epoxy tube sheet while the concentrate leaves the module at the same end as the feed inlet.

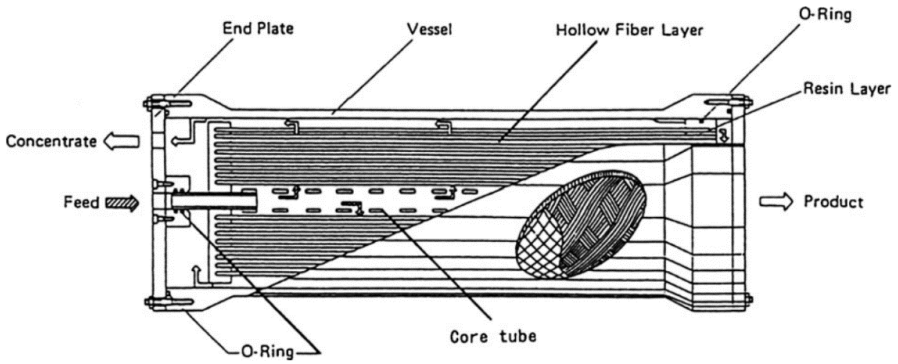

Fig. 6. Hollow fiber RO membrane module (adopted from [108])

Hollow fiber modules are economical and exhibit high packing density and recovery [109–111]. However, they are difficult to clean and highly susceptible to fouling due to small fiber spacing [33,98,101]. Commercial hollow fiber RO membranes, known as HOLLOSEP®, are available from Toyobo Co., Ltd. (Osaka, Japan). These membranes are suitable for industrial scale desalination of both brackish and seawater and exhibit salt rejections up to 99.6% [112].

3.1.4. Spiral wound modules

Spiral wound modules are currently the most common type of module used for RO desalination. In a spiral wound module, shown in Fig. 7, two membrane sheets are placed together with a permeate spacer (made of nylon or dacron) in between to form a leaf [33,98,100]. The membrane sheets are glued from three sides with the fourth side left open and connected to a central perforated permeate collector tube. The leaves are then placed together with a feed/concentrate mesh spacer to induce turbulence and minimize the CP effects. The combination of leaves and feed/concentrate spacers is wrapped around the permeate collector tube to create a spiral configuration and finally placed inside a pressure vessel (also known as housing) [33].

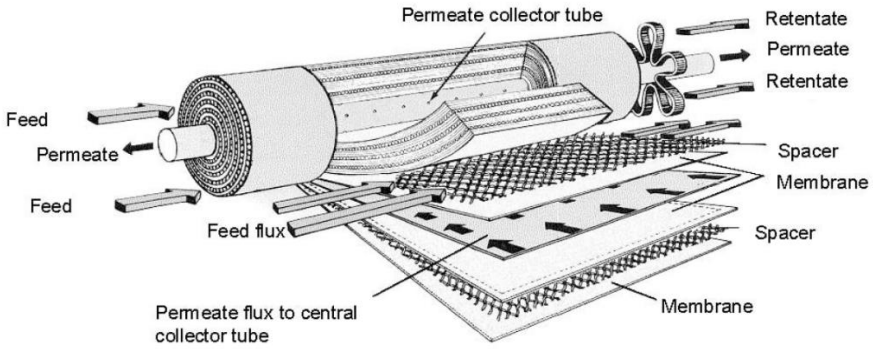

Fig. 6. Spiral wound RO membrane module (adopted from [36])

Feed water is introduced from one end of the module and travels axially along the length of the module. Water molecules are forced through the membrane and are collected as permeate through the perforated permeate collector tube. The concentrate leaves the module at the end opposite to the feed.

Spiral would modules are cost effective, possess high packing density, and allow for high mass transfer rates due to the presence of feed spacers. However, they are difficult to clean and are susceptible to fouling if pre-treatment is inadequate. In addition, spiral would modules result in high feed side pressure drop [36]. Commercial spiral wound RO membranes are available from manufacturers such as the Dow Chemical Company (Michigan, USA), Toray Membrane (California, USA), Koch Membrane Systems Inc. (Massachusetts, USA), and Suez Water Technologies (Pennsylvania, USA). Most industrial spiral would modules are available in standard 8 inch diameter [36].

3.2. Membrane characterization

Characterization of RO membranes is important in understanding the membrane structure, morphology, chemical composition, and physiochemical properties. In addition, characterization plays a critical role in membrane selection, membrane fabrication, and novel membrane material design [113–115]. In case of RO membranes, the methods used for membrane characterization are summarized below:

3.2.1. Pore characterization

The classical way of characterizing a membrane is to determine its pore size and pore size distribution (PSD) [116]. RO membranes are considered to be tight due to inherently small average pore radii (0.2-1 nm) [117]. As a result, conventional techniques such as thermoporometry, gas adsorption-desorption, and bubble point cannot be employed for determining the pore size [117,118]. Typically, for RO membrane, the pore size and PSD are determined indirectly by means of solute transport method utilizing separation data of reference solutes [117,119–123]. Also, membrane's flux dependency on pressure can be used to determine characteristic parameters that can be related to PSD [121]. In addition, atomic force microscopy (AFM) can be employed to obtain information about the pores on the membrane surface [121,124,125]. The free volume or open cavities in the membrane can be characterized by small-angle X-ray scattering (SAXS) and small-angle neutron scattering (SANS) techniques [114,126]. Also, the free volume cavities in the membrane can be studied using positron annihilation spectroscopy (PAS) which is the most viable technique to characterize the internal structure of RO membranes [114,118,127–131].

3.2.2. Physico-chemical characterization

Various techniques can be used to study the physical characteristics of the membrane surface. Scanning electric microscopy (SEM) is widely used to visualize and study the membrane morphology by examining and magnifying the top layers and cross-sections using high quality and high resolution images [132–135]. Transmission electron microscopy (TEM) can also be used to characterize the morphology, crystalline structure, and elemental information of the membrane and obtain 3D images of the membrane structure [135,136]. AFM represents another important microscopic technique that can be utilized to obtain quantitative nanoscale measurements of the lateral and vertical morphology and high resolution 3D images of the membrane surface topography [135]. AFM can also quantify the interaction force between the membrane surface and the probe used which allow for studying the nano-mechanical surface properties, adhesion forces, and long range interaction forces [135,137]. In addition, AFM can be used to estimate the surface roughness of RO membranes [132]. This is of immense significance since surface roughness has been reported to influence the permeate flux and fouling propensity [138,139]. Besides SEM, TEM, and AFM, electron spin resonance technique (ESR) can be used to study the structure of RO membranes [140].

For surface chemistry analysis, Fourier transform infrared (FTIR) spectroscopy is typically employed in order to identify the functional groups and determine the molecular bonds between chemical compounds of the membrane [125]. In addition, Raman spectroscopy (RS) can be used to study the orientation of polymer chain and the degree of crystallinity of the polymer in the membrane [141]. Both FTIR and RS are nondestructive tests and can be used to probe the lateral and vertical chemical composition of membranes [137]. The chemical composition of the membrane surface can also be studied using electron dispersive X-ray spectroscopy (EDX/EDS), X-ray photoelectron spectroscopy (XPS), Rutherford backscattering spectrometry (RBS), auger electron spectroscopy (AES), and secondary ion mass spectrometry (SIMS) [132,137,142]. Generally, a combination of different techniques must be used in order to confirm the surface chemistry of an unknown membrane. Details on the working principle of all the aforementioned characterization techniques can be found elsewhere [125,135,137].

3.2.3. Other characterizations

The thermal stability and thermal properties of RO membranes can be characterized using thermo-gravimetric analysis (TGA) [143,144]. Also, characterizing the membrane hydrophilicity or hydrophobicity is an important consideration. The hydrophilicity of a membrane is related to the surface wetting phenomenon that governs the interaction between fluids and the membrane surface and plays a critical role in dictating the permeate flux, salt rejection, and membrane fouling. The degree of surface wetting depends on the properties of the membrane surface, the interfacial interaction energy, and the fluid pH and temperature [135]. Membrane hydrophilicity is commonly indicated by means of contact angle measurement using a contact angle analyzer (drop shape analyzer) [132]. This measurement technique is based on either sessile drop method or captive bubble method, with the former being the simplest and the most commonly applied method [137]. Besides indicating the hydrophilicity, contact angle can provide information about the surface free energy of the membrane [137].

The surface charge or electrical properties of RO membranes have a profound effect on their separation performance, fouling propensity, and CP effects [135]. Therefore, characterization of the membrane surface charge is of great interest in RO desalination. Surface charge is acquired when the RO membrane comes in contact with an aqueous electrolyte solution which causes dissociation of the functional groups and adsorption of ions/molecules [137]. Typically, the surface charge of a membrane is characterized by zeta potential that can be obtained using standard electrokinetic methods such as streaming potential, electrophoresis, electro-osmosis, and sedimentation potential [135]. These methods are well explained in a recent review by Johnson et al. [135].

3.3. Membrane fouling

Membrane fouling is an inevitable phenomenon and represents an extreme operational and economic challenge in RO desalination. It involves complex physical and chemical interactions between unwanted impurities (foulants) present in the feed and the membrane surface. Generally,

membrane fouling can be external or internal. In external (surface) fouling, the foulants accumulate on the membrane surface. In contrast, internal fouling involves fouling mechanisms occurring within the membrane pores. Owing to the compact and nonporous nature of RO membranes, external fouling is more frequent during the RO desalination process [145]. Membrane fouling can cause significant decline in the water permeation rates by decreasing the active membrane area and increasing the resistance across the membrane. In addition, fouling can lead to CEOP effects where the CP effects are exacerbated due to an unstirred layer over the membrane surface [146]. Overall, membrane fouling is a serious challenge due to its significant contribution to the decline in flux, productivity, permeate quality, and membrane lifespan, increase in feed pressure and energy requirement, and increase in the pre-treatment and membrane maintenance, cleaning, and replacement costs [16,145,147]. Depending on the foulants encountered during RO desalination, membrane fouling can be classified as colloidal fouling, organic fouling, inorganic fouling, or biofouling.

In RO, fouling including the formation of bacterial biofilms, colloidal deposition and organic adhesion and precipitation of sparingly soluble minerals is directly associated with the reduction of plan efficiency and the increase of cost of water produced [148]. Although, RO processes are characterized with its high reliability, ability to treat wide range of salinities, high water recovery rate as well as salt rejection rate [149], it is very limited in treating effluents with low suspended solids concentrations which may reduce the efficiency of the process and increase energy consumption due to membrane fouling [5,150]. Thus, research and development efforts are directed towards preventing and/or mitigating the RO membrane fouling as well as developing new prediction tools. This is currently being done through analyzing the experimental and theoretical results of different studies which would lead to a better understanding of the membrane fouling such as studying the membrane surface, foulants interactions as well as developing membranes with specific anti-fouling properties [151,152]. Studies have shown that there is no established approach for understanding the membrane fouling, many approaches are currently followed and used in this regard including investigating the fouling resistance through the use of foulants models, measuring fouling layer morphology and growth, and measuring the rheological properties of fouling layers [152,153]. Generally, current research lines are mainly focused in minimizing the effects of membrane scaling and fouling and obtaining higher permeate flux and reducing its associated energy consumption [115]. The different types membrane fouling are summarized in the sections below.

3.3.1. Colloidal fouling

Colloids (particulates) are fine suspended particles with size ranging from few nanometers to micrometers. Typically, colloids can be classified into: (1) settleable solids (>100 μm), (2) supra-colloidal solids (1 μm to 100 μm), (3) colloidal solids (10 Å to 1 μm), and (4) dissolved solids (<10 Å) [147]. Alternatively, colloids may be classified as inorganic or organic colloids. Typical inorganic colloids in feed water include aluminum silicate minerals, silt, colloidal silica, sulfur, precipitated iron, and corrosion products [145,147]. Organic colloids, on the other hand, include

proteins, carbohydrates, bio-colloids, fats, oils, surfactants, and greases [146,147,154]. During colloidal fouling, the colloids present in the feed are driven from the bulk to the membrane surface as a result of permeate flow resulting in formation of a cake layer. The cake layer hinders the back-diffusion of salts and, consequently, increases the salt concentration near the membrane surface. This CEOP phenomenon combined with the cake layer formation causes significant decline in the permeate flux [146]. Colloidal fouling is influenced by the colloid characteristics such as size, shape, and charge as well as the feed solution chemistry (pH, ionic strength, and ionic interactions) [151]. In general, small colloids are more problematic since large colloids can be easily removed by backwashing [147]. Colloidal fouling also depends on the membrane surface properties. Membranes with smooth, more hydrophilic, and low charge surface are less susceptible to colloidal fouling at the initial fouling stage [151]. In addition, colloidal fouling is effected by the hydrodynamic conditions such as flux and cross flow velocity. High flux and low cross flow velocity tend to increase the severity of colloidal fouling [151].

In case of colloidal foulants, the feed fouling propensity can be rapidly estimated using water-quality sensors based on the silt density index (SDI), turbidity measurement, and particle count [146]. Besides these, various other fouling indices have been developed over the years to assess the colloidal fouling propensity. SDI is the most common index for colloidal fouling propensity that is performed according to the standard method ASTM D4189 – 95. To determine SDI, the feed water is filtered through a 0.45 μm membrane in dead-end mode at a constant pressure of 2.07 bar and the following equation is used [146]:

$$SDI = \frac{1-t_i/t_f}{T} \times 100 \quad (48)$$

where, t_i is the time initially required to collect a sample of volume V, t_f is the time required to collect the same volume V at the end of the test, and T is the time interval. Typically, SDI is based on constant T of 15 min and is reported as SDI_{15}. For long term operations, SDI_{15} below 3 is recommended [146]. Unfortunately, SDI is not based on a filtration model and does not quantify the colloids. Also, its applicability is limited to colloids with size >0.45 μm. The modified fouling index (MFI) has been introduced (ASTM D8002 – 15) in order to quantify the particle concentration and the flux decline. It is based on the mechanism of cake filtration and is defined as follows [146]:

$$MFI = \frac{\mu I}{2\Delta p S^2} \quad (49)$$

where, I is the cake resistivity and S is the active filtration area. Again, the applicability of MFI is limited to colloids with size >0.45 μm. In order to account for smaller colloids, the MFI-UF test was introduced which involved a tighter UF membrane [155]. This index provided better and more realistic estimations of the flux decline by accounting the smaller colloids. The MFI-UF test is conducted under dead-end mode and at constant pressure. In contrast, most RO systems are operated in cross flow mode and at constant flux. This difference results in dissimilar cake composition and structure between the cross flow and dead-end modes [146]. In order to account

for the actual hydrodynamics in RO systems, the cross-flow sampler-modified fouling index (CFS-MFI) was developed [156]. In this test, a cross flow cell is used which consists of a filter with large pores. The cross flow hydrodynamics only allow a portion of particles to pass through cross flow cell. These particles subsequently enter a dead-end MFI device in which their fouling potential is determined. Choi et al. [157] developed a combined fouling index (CDI) that utilized three MF/UF membranes for MFI tests with the purpose of increasing the sensitivity to fouling potential of particles, hydrophobic organics, and sub-micron colloids. The index was based on a linear combination of the fouling index for each membrane filter. Overall, utilization of a set of different membrane filters provided better prediction of RO/NF fouling. The approach, however, is tedious since different types of membranes and constant pressure conditions are required [158]. Similarly, Hong and co-workers [159–161] developed a multiple membrane array system (MMAS) in which MF, UF, and NF membranes were connected in series to separate the target foulants and determine their corresponding fouling potential. Particulate, colloids, and organic matters were separated by MF, UF, and NF membranes in a consecutive manner and the MFI was measured during each separation. The fouling potentials predicted by MMAS were more accurate than those predicted by SDI or single MFI. However, MMAS is tedious since different types of membranes and constant pressure conditions are required [158].

Recently, a novel on-line flow simulator known as the feed fouling monitor (FFM) was developed for estimating colloidal fouling propensity [162,163]. The technique is based on cross flow where foulants are detected in a stream continuously passing over a small collection UF membrane [146]. FFM can be used to provide online measurement of specific cake resistance of foulants and trends in foulant cake height can be measured by ultrasonic time domain reflectometry (UTDR) [162].

3.3.2. Inorganic fouling

Inorganic fouling (scaling) is caused by inorganic compounds such as calcium sulfate, calcium carbonate, calcium phosphate, barium sulfate, and silica present in the feed water [147]. It is a complex phenomenon consisting of both crystallization and transport mechanisms. Crystallization occurs when the ion activity exceeds the saturation limit resulting in a supersaturated feed solution. Inorganic fouling due to crystallization can occur by two pathways: bulk (homogeneous) crystallization and surface (heterogeneous) crystallization. Surface crystallization refers to lateral growth of crystals on the membrane surface. Bulk crystallization, on the other hand, involves deposition of crystals on the membrane surface after the crystal particles are formed in the bulk phase through homogeneous crystallization. The supersaturated solution causes agglomeration of scale-forming ions due to random collisions between the ions in motion. The ion cluster coalesces to form a crystal and once it grows above a critical size, precipitation occurs [164,165]. Fig. 7 depicts the bulk and surface crystallization phenomena.

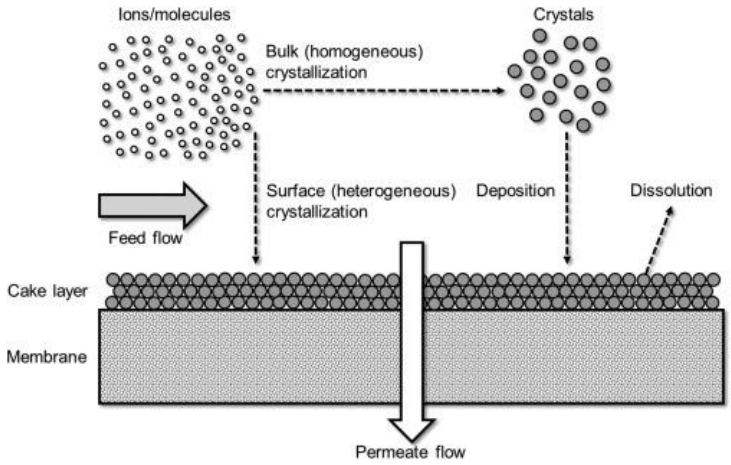

Fig. 7. Schematic illustration of surface and bulk crystallization (adopted from [16])

Inorganic fouling is influenced by a number of physical and chemical parameters such as membrane surface roughness and hydrophilicity, shear or drag across the membrane surface, transmembrane pressure, surface and bulk temperatures, feed solution chemistry, and particle size and concentration [166].

The feed scaling potential can be determined using the Langelier saturation index (LSI) (ASTM D3739-06). This index provides a measure of the ability to dissolve or deposit calcium carbonate from an aqueous solution and is defined as follows [146]:

$$LSI = pH - pH_s \tag{50}$$

where, pH is the actual feed solution pH and pH_S is the pH at saturation defined as follows [146]:

$$pH_s = pCa^{+2} + pAlk + K \tag{51}$$

where, pCa^{2+} and pAlk are the negative of the logarithm of the calcium ion concentration and of the alkalinity, and *K* is a TDS and temperature-dependent factor given as follows [146]:

$$K = 0.03742 \ln(TDS) - 0.0209T + 2.5 \tag{52}$$

A positive LSI indicates that scaling will occur. It should be noted that the LSI index is valid over TDS range of 10-10,000 ppm [146]. For TDS above 10,000 ppm, the Stiff and Davis saturation index (S&DSI) must be used (ASTM4582-05). This index is similar to the LSI index with *K* factor in Eq. (52) defined as follows [146]:

$$K = (0.0016T + 0.5528)I^3 + (0.002T^2 - 0.0142T - 2.2695)I^2 + (-0.0004T^2 + 0.0266T + 2.907)I + (-0.0206T + 2.598) \tag{53}$$

where, *I* is the ionic strength. In addition, the supersaturation index (SI) defined as follows can be used [146,165]:

$$SI = \frac{IAP}{K_{sp}} \tag{54}$$

where, *IAP* is the ion activity product and K_{sp} is the solubility product. SI can be used to estimate the scaling potential of $CaCO_3$, $CaSO_4$, $BaSO_4$, and SiO_2. SI index greater than unity indicates that the solubility limit for the mineral salt has been exceeded which may result in scaling. It should be noted that K_{sp} for a given salt changes in a mixed salt solution. In order to account for the ionic interactions of individual and mixed salts, the scaling potential index (SPI), defined as follows, can be used to predict the scaling potential of mixed salt solutions [146]:

$$SPI = log\left[\frac{IAP}{K_{sp}}\right]^{\frac{1}{v}} \quad (55)$$

where, v is the number of ions and K_{sp} is temperature-dependent solubility product given as follows:

$$-RTln(K_{sp}) = \frac{T}{298.15}\Delta_{reac}G^{298} + \left(1 - \frac{T}{298.15}\right)\Delta_{reac}H^{298} \quad (56)$$

where, $\Delta_{reac}G^{298}$ and $\Delta_{reac}H^{298}$ represent free energy of reaction and enthalpy of reaction, respectively.

3.3.3. Organic fouling

Organic fouling is a consequence of organic matter (OM) present in the feed. Typically, OM can be classified as: (i) allochthonous natural organic matter (NOM) consisting of humic substances (humic acids, fulvic acids, and humin) derived from plant and animal residues, (ii) autochthonous or algal organic matter (AOM) consisting of extracellular and intracellular macromolecules and cellular debris, and (iii) wastewater effluent organic matter (EfOM) (polysaccharides, proteins, enzymes, nucleic acids, antibiotics, and steroids) consisting of background (drinking water) NOM plus soluble microbial products (SMPs) derived from biological wastewater treatment [147,167,168]. Organic fouling is challenging in RO desalination since conventional pre-treatment cannot assure complete removal of NOM in the feed. As a result, OM is ubiquitously present in the RO feed water [146]. Organic fouling is known to be influence by feed water chemistry, membrane properties, foulant-membrane interactions, foulant-foulant interactions, hydrodynamic operating conditions, and NOM characteristics such as molecular size and hydrophilicity [169].

The organic fouling potential of RO feed water can be determined using standard online techniques such as total and dissolved organic carbon (TOC and DOC) and ultraviolet absorbance at 254 nm (UV254) and other sophisticated techniques such as liquid chromatography-organic carbon detection (LC-OCD) and fluorescence excitation-emission matrix (F-EEM) [146].

3.3.4. Biofouling

Biofouling is recognized as a contributing factor to more than 45% of all membrane fouling [170]. It is caused by the deposition, proliferation, and metabolism of microorganisms (bacteria, algae, protozoa, and fungi) and creation of a biofilm on the membrane surface. Biofouling is initiated by attachment of microorganisms to the membrane surface. This is a dynamic process in which the

microorganisms approach the membrane surface and, subsequently, adhere to it. A number of factors control the microorganism attachment to the membrane surface. Common factors include microbial properties, membrane surface characteristics, microbial-surface interactions, feed characteristics, and operating conditions such as cross flow velocity and permeate flux [145]. After attachment, the microorganisms reproduce and grow by feeding on the feed water nutrients. During this stage, metabolic activities release extracellular polymeric substances (EPS) which provide an anchoring effect to the biofilm structure. After sufficient growth, the microorganisms are detached from the membrane surface from where they are dispersed to new sites to reinitialize the biofilm formation [171]. Fig. 8 depicts the different stages involved in biofouling.

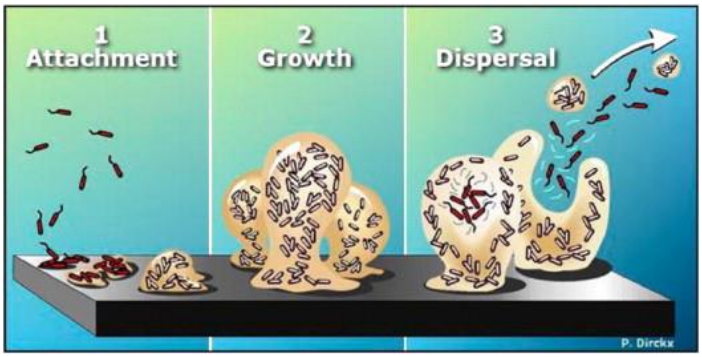

Fig. 8. Schematic illustration of biofilm formation on membrane surface (adopted from [171])

The biofouling potential of a feed can be determined using the heterotrophic plate counts (HPC) method. In this method, a sample of feed water is placed over plates with an R2A (Reasoner's 2A agar) culture medium. After incubation, the number of colonies are reported as CFU/mL. In addition, the epifluorescence microscopy counting method can be utilized where the membrane sample is stained with a fluorescence dye. A fluorescent microscope is then used to find the bacterial density. Other helpful analyses for biofouling include OPTIQUAD sensor system, adenosine triphosphate (ATP) analysis, and analysis of assimilable organic carbon (AOC) and transparent exopolymer particles (TEP) [146].

3.3.5. Fouling monitoring and prediction

Monitoring of RO membrane fouling is an important consideration in order to conduct timely membrane cleaning and avoid any process disruption. Typically, operating parameters such as decline in permeate flux, increase in transmembrane pressure, pressure drop, and product quality are good indicators of the extent and severity of membrane fouling [146]. In addition, membrane autopsy can be used where the RO module is sacrificed in order to identify the foulants [145,146]. However, these techniques cannot provide an early insight into membrane fouling and its causes. To overcome this issue, ultrasonic time-domain reflectometry (UTDR) has been developed for non-invasive, in-situ, and real-time monitoring of membrane fouling. UTDR relies on the transmission and reflection of ultrasonic waves to detect the thickness and growth of the fouling layer in real time [172]. The technique has been applied to RO systems to characterize colloidal fouling [173] and biofouling [174]. The ex-situ scale observation detector (EXSOD) can be used

for real-time monitoring of scale crystals before the onset of flux decline [175]. This technique is limited to inorganic fouling and uses a high resolution digital camera and an optical microscope to detect subtle changes of crystal boundaries. As a result, very early stages of scale formation can be detected before the onset of any measurable decrease in the permeate flux. Besides UTDR and EXSOD, electrical impedance spectroscopy (EIS) has been proposed as a non-invasive technique for monitoring of membrane fouling [172,176–178]. This technique is based on fouling-induced changes in the electrical properties of the membrane and requires electrodes within the RO cell combined with a high resolution impedance spectroscope. Using the EIS data, Nyquist plots are used to characterize the dynamic fouling process [145]. This technique is applicable to all types of fouling [146]. Optical coherence tomography (OCT) is another recent technique to monitor membrane fouling. It consists of a light beam that is split into the membrane cell and a reference arm. The backscattered beam from the membrane cell is then combined with the reference beam to create an interference spectrum which is finally Fourier-transformed. At the end, a 3D view of the fouled surface can be obtained. Also, this technique is applicable to all types of fouling [146]. Although the aforementioned techniques are effective in monitoring membrane fouling, large scale applicability of these techniques still needs to be assessed.

A number of studies have presented predictive models to estimate the fouling-induced decline in water flux due to changes in the water permeability coefficient (*A*). For example, Wilf and Klinko [179] used extensive experimental data (over a period of three years from different SWRO desalination plants) to develop the following model for the change in the coefficient *A* [179]:

$$A = t^m \tag{57}$$

where, *m* is a parameter with values between -0.035 and -0.041 related to permeate flow decline of 20 and 25% respectively and *t* is the operating time (days).

Similarly, Abbas and Al-Bastaki [180] presented the following equation for the change in the coefficient *A* using operational data spanning over 500 days and related to brackish water desalination using FilmTec spiral wound membrane:

$$A = 0.68e^{\left(\frac{79}{t+201.1}\right)} \tag{58}$$

Zhu et al. [181] presented the following exponential decay model for the change in the coefficient *A* [158]:

$$A = A_0 e^{\frac{-t}{328}} \tag{59}$$

where, A_0 is the initial value of the permeability coefficient. The model was obtained by using operational data over a period of one year for DuPont B-10 hollow-fiber RO modules.

Recently, Ruiz-García and Nuez [182] developed a new model for the decline of coefficient *A*. The decline was studied in two stages. The first stage represented a more pronounced decline due to initial compaction and irreversible fouling. The second stage, on the other hand, described a

more stable period with less slope. Using ten years of operational data related to brackish water desalination using BW30-400 Filmtec™ membrane, the following model was presented by superposition of two exponential functions:

$$A = \delta_1 e^{\frac{-t}{\tau_1} k_{fp}} + \delta_2 e^{\frac{-t}{\tau_2} k_{fp}} \quad (60)$$

where, δ_1, δ_2, τ_1, and τ_2 are the model parameters and k_{fp} is the feed fouling potential.

3.4. Advances in membrane materials

The performance of RO desalination, in terms of flux and rejection, is highly dependent on the structure and chemical composition of the employed membrane [33]. As a result, development of RO membranes and advancements in RO membrane materials and properties have always been critically important to the technological progress and the economical and operational efficiency of the RO desalination process [183]. An ideal RO membrane must exhibit desirable characteristics such as high mechanical robustness, thermal stability, permeate flux, solute rejection, useful membrane life, and resistance to chemical and biological degradation, and low fouling propensity and cost [184,185]. Research investigations until the late 1980s focused on exploring novel RO membrane materials and membrane formation methods. Since then, the research activities have oriented towards improving the conventional RO membrane materials [186]. Synthetic RO membranes composed of cellulose acetate (CA) and aromatic polyamide (PA) polymers are conventional and currently dominate the commercial desalination applications [186–189]. Conventional polymeric RO membranes are asymmetric (anisotropic) and possess a gradient in in structure where a thin dense layer (skin layer) is supported on a porous sublayer [190]. The top skin layer dictates the flux and rejection properties of the membrane while the porous sublayer acts as a mechanical support [191,192]. Based on the structure, asymmetric RO membranes are typically classified into two distinct groups: (1) integrally-skinned asymmetric membranes, and (2) thin film composite (TFC) membranes [193]. Besides these two groups, novel RO desalination membranes have also been developed over the years. Research activities related to the development of RO membranes and their modifications for performance enhancement are reviewed below.

3.4.1. Integrally-skinned asymmetric membranes

In integrally-skinned asymmetric membranes, both the top skin layer and the porous sublayer are composed of the same material. These membranes are synthesized using the phase inversion (polymer precipitation) method where a polymer is transformed from a liquid to a solid state in a controlled manner [191,192]. Among the various phase inversion methods, the nonsolvent-induced phase separation (NIPS) (also known as immersion precipitation, dry-wet phase inversion, or the Loeb-Sourirajan method) represents the most versatile and commonly used phase inversion method for membrane synthesis [44,194]. In NIPS, a polymer solution is prepared by mixing the polymer, solvent, and nonsolvent and, subsequently, casted on a surface using a doctor blade. In order to achieve polymer precipitation, the cast film is immersed into a coagulation (gelation) bath

(containing the nonsolvent) after partial evaporation of the solvent. The skin layer is formed on top of the cast film as a result of solvent loss during the solvent evaporation step. The porous sublayer, on the other hand, is formed during the solvent-nonsolvent exchange step where the nonsolvent diffuses in and the solvent diffuses out of the polymer solution film [191,195,196]. Besides NIPS, other methods can be employed to induce phase inversion. For instance, temperature-induced phase separation (TIPS) method can be used to induce phase inversion by reducing the temperature of polymer solution. In addition, evaporation-induced phase separation (EIPS) method (also known as solution casting method) can be employed where a polymer solution is prepared in a solvent and precipitation is induced by allowing the solvent to evaporate. Also, vapor-induced phase separation (VIPS) method can be used where the absorption of a nonsolvent causes precipitation once the polymer solution is exposed to the nonsolvent-rich atmosphere [192,197].

Table 2. Examples of commercial CA-based membranes

Manufacturer	Brand name	Configuration	Material	Dimensions (diameter x length) (inch × inch)	Permeate flow (m^3/d)	Salt rejection (%)	Reference
Toyobo Co., Ltd	HOLLOSEP® HA8130 (brackish water)	Hollow fiber	CTA	11.6 × 52*	60[(a)]	94	[112]
Toyobo Co., Ltd	HOLLOSEP® HJ9155 (seawater)	Hollow fiber	CTA	11.6 × 80.7*	34[(b)]	99.6	[112]
Applied Membranes Inc.	M-C4040A	Spiral wound	CTA	4.0 × 40.0*	3.8[(c)]	96.0	[198]
Suez Water Technologies	CD series (brackish water)	Spiral wound	CDA/CTA blend	7.9 × 40*	23.8[(d)]	98.5	[199]
Suez Water Technologies	CE series (brackish water)	Spiral wound	CDA/CTA blend	7.9 × 40*	25.4[(d)]	97.5%	[200]

*Other dimensions available on the market (a) Test conditions: 29.4 bar, 1,500 ppm NaCl, 25 ^{o}C, 75% recovery (b) Test conditions: 53.9 bar, 35,000 ppm NaCl, 25 ^{o}C, 30% recovery (c) Test conditions: 16.0 bar, 500 ppm tap water, 25^{o}C, 15% recovery, pH 7-8 (d) Testing conditions: 29.3 bar, 2,000 ppm NaCl, 25 ^{o}C, pH 6.5, 15% recovery.

The discovery of integrally-skinned asymmetric membranes is credited to Loeb and Sourirajan who synthesized the first defect-free, high-flux asymmetric membrane composed of cellulose

acetate (CA) [201–204]. The membrane consisted of a dense 200 nm skin layer on a thick micro-porous support [186] and provided one of the earliest critical breakthroughs leading to commercialization of the RO desalination process [205,206]. Subsequent research efforts focused on membranes composed of cellulose diacetate (CDA), cellulose triacetate (CTA), and their blends in order to enhance the membrane characteristics [33,186]. Compared to CDA membranes, CTA membranes are suitable for wider ranges of temperature and pH and offer higher resistance to chemical and biological attack. A blend of CDA and CTA, on the other hand, offers higher flux and rejection along with higher resistance to compaction compared to CTA membranes [186]. In general, CA membranes exhibit good fouling tolerance owing to their relatively smooth surface morphology and neutral surface charge [33,207]. They are also low in cost and possess some resistance to chlorine [207,208]. However, the membranes have a tight operating pH range of 4-6 beyond which the membrane lifetime decreases owing to the hydrolysis of the acetate group [33]. In addition, CA membranes are susceptible to microbial attack and exhibit low silica rejection (~80%) and low temperature tolerance (up to 30 ^{o}C) [33]. Despite being one of the earliest membrane materials, CA membranes are still available for commercial desalination applications. Table 2 provides a list of CA membranes currently on the market.

Besides CA, integrally-skinned asymmetric membranes can be composed of non-cellulosic materials. One such non-cellulosic membrane material is aromatic polyamide (PA). Aromatic PA membranes were, in fact, commercialized by Du Pont under the trade name Permasep® B-9 and B-10 for brackish and seawater desalination, respectively [33,209,210]. These membranes were popular until the early 1990s due to inherently higher rejection, durability, and stability compared to the CA membranes available during that time [33,186]. In addition, PA membranes are known to be insusceptible to hydrolysis and biological attack and suitable for wide operating range for both pH and temperature [84]. The membranes are, however, sensitive to disinfectants such as chlorine and ozone [186]. Polybenzimidazole (PBI) [211–214] and Polybenzimidazoline (PBIL) [215,216] membranes have also been tested in RO desalination. Both PBI and PBIL membranes exhibit low salt rejection. In case of PBIL membranes, Goldsmith et al. [215] reported good resistance to extreme pH values of 2-12. However, the performance of the membranes was significantly affected by chlorine at pH of 7 and below. In order to improve chlorine resistance, integrally-skinned asymmetric membranes based on polypiperazinamides (PPA) were developed [217–220]. Despite their high chlorine resistance, PPA membranes were not commercialized due to unfavorable salt rejections [186]. Polyimide (PI) has also been used to synthesize asymmetric RO membranes [221,222]. These membranes exhibited poor salt rejection and, therefore, were not commercialized. Similarly, polyoxadiazole (POD) membranes were commercially unattractive due to low permeability and salt rejection [186,223]. Table 3 and Fig. 9 summarize the RO performance of the aforementioned integrally-skinned asymmetric membranes.

Table 3. Summary of integrally-skinned asymmetric membranes for RO desalination

Membrane material	Test conditions	Permeate flux (m^3 m^{-2} day^{-1})	Salt rejection (%)	Reference
Cellulose acetate (CA)	100 bar, 40,000 ppm NaCl	0.35	99.0	[186,202]
Polyamide (PA)	27.6 bar, 5,000 ppm NaCl	0.05	99.0	[209]
Polybenzimidazole (PBI)	5.89 bar, 1,050 ppm NaCl	0.13	95.0	[214]
Polybenzimidazoline (PBIL)	18.3 bar, 5,000 ppm NaCl	0.61-0.65	90.0-95.0	[215]
Polyimide (PI)	28.6 bar, 5,000 ppm NaCl	0.49	97.0	[222]
Polyoxadiazole (POD)	44.1 bar, 5,000 ppm NaCl	1.50×10^{-7}	92.0	[223]
Polypiperazinamide (PPA)	80.0 bar, 3,600 ppm NaCl	0.67	97.2	[186,218]
Polyvinylchloride/cellulose acetate (PVC/CA)	40.0 bar, 38,528 ppm Red seawater	0.96	99.9	[224]
Cellulose acetate/polyvinylpyrrolidone (CA/PVP)	0.35 bar, pure water	0.60-1.56	-	[225]

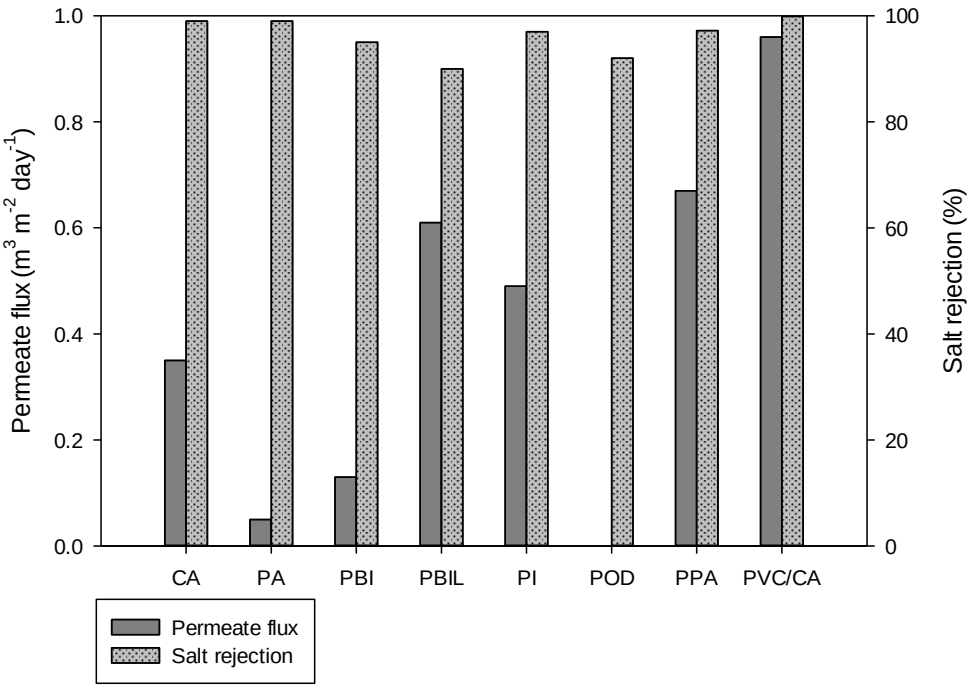

Fig. 9. Performance of integrally-skinned asymmetric membranes for RO desalination

Research activities related to integrally-skinned asymmetric membranes have become infrequent since the introduction of thin film composite (TFC) RO membranes. Very few studies appear in recent literature. For example, blended polyvinylchloride/cellulose acetate (PVC/CA) membranes for seawater desalination were proposed by El-Gendi et al. [224]. Among the various polymeric solution compositions used, blended PVC/CA membrane synthesized using 16% PVC, 3% CA, and 1% polyethylene glycol (PEG) exhibited the highest tensile strength. The membrane was able to work at pressures up to 50 bar without cracking. Similarly, Saljoughi and Mohammadi [225] synthesized cellulose acetate/polyvinylpyrrolidone (CA/PVP) blend asymmetric membranes. Addition of 3 wt% PVP to the cast film solution and using a coagulation bath temperature of 25 ^{o}C significantly increased the pure water flux. However, the synthesized membranes were not tested with saline feed. Also, the salt rejection values were not reported.

3.4.1.1. Surface modification of CA membranes

CA-based membranes have been modified in several studies in order to tailor and improve membrane properties such as permeate flux, salt rejection, and fouling resistance. One such post-synthesis membrane modification technique is the surface modification. Worthley et al. [226] used the surface modification technique to enhance the biofouling resistance of commercial CA membranes. The membrane surface hydroxyl groups were reacted with 2-bromoisobutyryl bromide and then grafted with 2-hydroxyethyl methacrylate (pHEMA). In order to test the biofouling resistance, the modified membrane samples were immersed in a natural seawater aquarium (TDS: 20,000 ppm) for three weeks. Biofouling prevention of the pHEMA-modified membrane samples improved by 24-28% compared to the unmodified membrane samples. However, this improvement was realized at the expense of decreased water flux and salt rejection. It was recommended to use a low graft density in order to avoid significant loss of function in terms of water flux and salt rejection. Ferjani et al. [227,228] modified CA membranes by coating the surface with a thin film of polymethylhydrosiloxane (PMHS). The resulting membranes consisted of a hydrophobic top layer and were employed in desalination of brackish waters from the Sahel region of Tunisia (TDS: 4100 ppm). Results from RO performance tests indicated that surface modification with PMHS increases the salt rejection of CA membranes, however, at the expense of 15-50% lower permeate flux. Similarly, Guezguez et al. [229] used a mixture of PMHS and polydimethylsiloxnae (PDMS) to coat the surface of CA membranes. Unlike the membranes modified by PMHS alone, a mixture of PMHS and PDMS improved the pure water permeability of the CA membranes.

Morsy et al. [230] used graft polymerization to modify the surface of CA membranes. The grafting reaction was induced by placing 15 wt% of 2-acrylamido-2-methylpropanesulfonic acid (AMPSA) monomer onto the membrane top surface. The modified membrane was found to be more hydrophilic and exhibited higher salt rejection compared to the unmodified membrane. Despite these improvements, the modification technique was unsuccessful in enhancing the permeate flux without significantly effecting the salt rejection. Also, the study showed that AMPSA concentrations above 15 wt% can cause significant decline in the salt rejection. Fei et al. [231]

quaternized the surface of CTA membranes using 3-chloro-2-hydroxypropyl-trimethyl ammonium chloride (CHPTA). The CTA membranes were partially hydrolyzed, deacetylated, and subsequently immersed in CHPTAC to allow for the etherification reactions. The resulting membranes consisted of CHPTAC covalently immobilized onto the membrane surface. The modification enhanced the membrane hydrophilicity, positive surface charge, and water permeation without compromising the salt rejection, mechanical properties, crystalline and thermal stability. In addition, the modified membranes exhibited increased resistance to biofouling and good bacterial activity against *E. coli* and *S. aureus*.

3.4.2. Thin film composite (TFC) membranes

Thin film composite (TFC) membranes are essentially composites of two polymers that are cast on a fabric support. These membranes are prepared using the well-known interfacial polymerization (IP) technique developed by Cadotte et al. [232,233]. In this technique, polymerization occurs at the interface of two immiscible liquids. First, a nonselective microporous support substrate is prepared (without annealing) using the Loeb-Sourirajan method. The substrate is then exposed to monomers (e.g., polyamine) that are known to exhibit high water permeability and low salt permeability. The membrane is then immersed in a water-immiscible solvent containing a reactant (e.g. diacid chloride in hexane). Polycondensation occurs at the water-solvent interface resulting in a highly-crosslinked thin film (active or barrier layer) that dictates permeate flux and salt rejection of the membrane [33,186,195]. In commercial membranes, the substrate is also cast on woven or non-woven fabric (e.g., polyester web) for mechanical support [234]. TFC membranes are distinctively attractive since they allow for optimization of the individual layers. In particular, the barrier layer can be tailored and optimized to achieve the optimum combination of permeate flux and salt rejection. The substrate, on the other hand, can be optimized to increase its strength, compression resistance, and permeate flow resistance [234].

3.4.2.1. Barrier layers

TFC membranes composed of aromatic PA are by far the most common membranes for RO desalination applications and their spiral wound configuration account for over 90% of the market sales [235].

Table 4. Examples of commercial PA TFC RO membranes in spiral wound configuration

Manufacturer	Brand name	Dimensions (diameter × length) (inch × inch)	Permeate flow (m^3/d)	Salt rejection (%)	Reference
Axeon	HF1	4.0 × 40*	9.46[(a)]	99.0	[236]
Dow	FILMTEC™ BW30-365 (brackish water)	7.9 × 40*	36.0[(b)]	99.0	[237]

Dow	FILMTEC™ SW30HR-380 (seawater)	7.9 × 40*	24.6[c]	99.7	[238]
Toray Industries, Inc.	TM700 (brackish water)	8.0 × 40*	42.6[d]	99.7	[239]
Toray Industries, Inc.	TM800 (seawater water)	8.0 × 40*	24.6[e]	99.8	[240]
Suez Water Technologies	Osmo HR (brackish water)	7.9 × 40*	36.3[f]	99.0	[241]
Hydranautics	CPA series (brackish water)	7.9 × 40*	37.9[g]	99.7	[242]
Hydranautics	SWC series (brackish water)	7.9 × 40*	24.6[h]	99.7	[243]
Koch Membrane Systems	FLUID SYSTEMS® TFC® HR (brackish water)	8.0 × 40	41.6[i]	99.6	[244]
Koch Membrane Systems	FLUID SYSTEMS® TFC® SW	8.0 × 40	27.2[j]	99.8	[245]

*Other dimensions available on the market (a) Test conditions: 10.34 bar, 550 ppm NaCl, 25 ^{o}C, 15% recovery (b) Test conditions: 15.5 bar, 2,000 ppm NaCl, 25 ^{o}C, pH 8, 15% recovery (c) Test conditions: 55 bar, 32,000 ppm NaCl, 25 ^{o}C, pH 8, 8% recovery (d) Test conditions: 15.5 bar, 2,000 ppm NaCl, 25 ^{o}C, pH 7, 15% recovery (e) Test conditions: 55.2 bar, 32,000 ppm NaCl, 25 ^{o}C, pH 7, 8% recovery (f) Test conditions: 15.5 bar, 2,000 ppm NaCl, 25 ^{o}C, pH 7.5, 15% recovery (g) Test conditions: 15.5 bar, 1,500 ppm NaCl, 25 ^{o}C, pH 6.5-7, 15% recovery (h) Test conditions: 55 bar, 32,000 ppm NaCl, 25 ^{o}C, pH 6.5-7, 10% recovery (i) Test conditions: 15.5 bar, 2,000 ppm NaCl, 25 ^{o}C, pH 7.5, 15% recovery (j) Test conditions: 55.2 bar, 32,800 ppm NaCl, 25 ^{o}C, pH 7.5, 7% recovery

Table 4 lists some of the well-known PA TFC membranes available on the market. Compared to CA membranes, PA TFC membranes exhibit higher salt and silica rejections and can operate under wider ranges of temperature (up to 45 ^{o}C) and pH (2-12). In addition, PA TFC membranes require a lower operating pressure due to their intrinsically thin active layer and highly porous substrate layer. However, surface morphology of PA TFC membranes is rough which increases their fouling propensity. Also, PA TFC membranes are highly sensitive to free chlorine and oxidizers [33]. For

instance, Dow FILMTEC™ SW30HR-380 membrane element for seawater desalination has free chlorine tolerance of less than 0.1 ppm [238].

PA TFC membrane was first prepared by Cadotte [246] using IP between polythylenimine (PEI) and toluene 2,4-diisocyanate (TDI). Although the resulting membrane (designated as NS-100) exhibited high salt rejection, the resistance to chlorine was critically low [186]. Soon after, Riley and coworkers [247,248] synthesized and commercialized PA TFC membranes by using polyepiamine (PEA). The membranes were synthesized with isophthaloyl chloride (IPC) or TDI and were designated as PA-300 or RC-100, respectively [234]. PA-300 exhibited high permeate flux and, therefore, its spiral wound configuration was employed in the desalination plant at Jeddah, Kingdom of Saudi Arabia [186,234]. Also, RC-100 was employed in Umm Lujj II desalination plant in Saudi Arabia due to its high biofouling resistance [234].

While attempting to improve TFC membranes, Cadotte [249] discovered that PA composite membranes with high flux and high salt rejection can be synthesized by avoiding heat curing and utilizing monomeric aromatic amines with aromatic acyl halides of functionality greater than 2 (i.e., three or more carbonyl halide groups). Also, addition of acid acceptor or surfactant was not required [234]. The best PA TFC membrane was obtained by using 1,3-diaminobenzene (*m*-phenylenediamine, MPDA) and trimesoyl chloride (TMC). The resulting membrane was commercialized as FILMTEC™ FT-30 [186] and exhibited high water flux and high salt rejection when tested against real seawater (Table 5) [250]. This membrane was a turning point in the commercialization of aromatic PA TFC membranes. In fact, PA TFC membranes produced by interfacial polymerization of MDP and TMC (depicted in Fig. 10) represent the most commercially successful products [251]. Besides FT-30, aromatic PA membranes were commercialized as CPA2 and NTR-759 by Hydranautics [234]. Also, Toray Industries [252] developed the UTC-70 membrane that consisted of aromatic PA barrier layer from a blend of MPDA and 1,3,5-trisaminobenzene (TAB) interfacially reacted with a blend of TMC and terephthaloyl chloride (TCL) [234]. Besides PA, TFC membranes may also contain polypiperazinamide (PPA), polyvinylamine (PVAM), polypyrrolidine (PPY), or polyurea barrier layers [186,234]. However, compared to aromatic PA TFC membranes, commercial use of these barrier layers for desalination applications is infrequent.

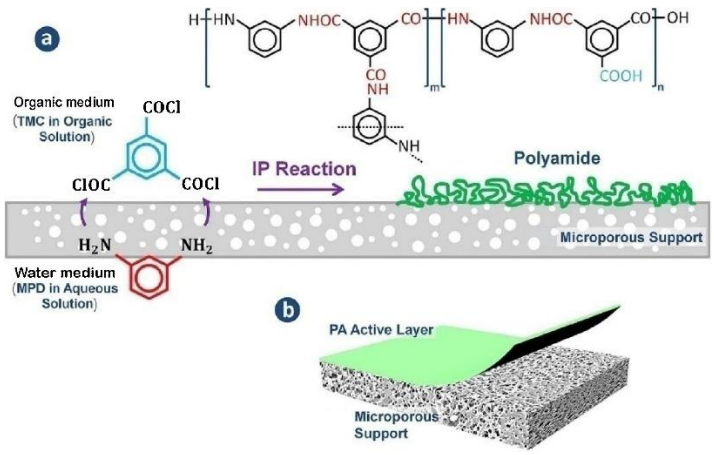

Fig. 10. Schematic illustration of IP reaction between TMC and MPDA (b) Structure of resultant PA TFC membrane (adopted from [253])

Table 5. Summary of studies on barrier layer for TFC RO membranes

Barrier layer	Test conditions	Permeate flux (m^3 m^{-2} day^{-1})	Salt rejection (%)	Reference
PA from polythylenimine (PEI) and toluene 2,4-diisocyanate (TDI) (NS-100)	104.4 bar, 35,000 ppm NaCl	0.25	99.8	[246]
PA from polyepiamine (PEA) and isophthaloyl chloride (IPC) (PA-300)	104.4 bar, 35,000 ppm NaCl	0.81-1.0	99.4	[234]
Polypiperazinamide (PPA) from piperazine and IPC	104.4 bar, 35,000 ppm NaCl	1.1	98.0	[234]
Aromatic PA from 1,3-diaminobenzene (MPDA) and trimesoyl chloride (TMC) (FT-30)	55.16 bar, real seawater	0.94	99.5	[250]
Aromatic PA from a blend of MPDA and 1,3,5-trisaminobenzene (TAB) and a blend of TMC and terephthaloyl chloride (TCL) (UTC-70)	14.71 bar, 1,500 ppm NaCl	1.0	99.6	[252]
PA from MPDA and 3,3’,5,5’-biphenyl tetraacyl chloride (I, mm-BTEC)	20 bar, 2,000 ppm NaCl	0.72	98.6	[254]
PA from MPDA and 3,4′,5-biphenyl triacyl chloride (BTRC)	20 bar, 2,000 ppm NaCl	0.80	98.9	[254]
PA from MPDA and 2,2′,4,4′-biphenyl tetraacyl chloride (II, om-BTEC)	20 bar, 2,000 ppm NaCl	1.2	97.8	[255]
PA from MPDA and 2,2′,5,5′-biphenyl tetraacyl chloride (III, op-BTEC)	20 bar, 2,000 ppm NaCl	1.3	97.2	[255]

PA from blend of MPDA, sulfonated cardo poly(arylene ether sulfone) (SPES-NH_2) and TMC	20 bar, 2,000 ppm NaCl	1.2	97.3	[256]
PA from blend of MPDA, 3,5-diamino-N-(4-aminophenyl) benzamide (DABA) and TMC	20 bar, 2,000 ppm NaCl	1.3	98.1	[257]
PA from MPDA, 2,2′-benzidinedisulfonic acid (BDSA), and TMC	16 bar, pure water	1.1	97.7	[258]
PA from MPDA and 2,4,4′,6-biphenyl tetraacyl chloride (BTAC)	15.5 bar, 2,000 ppm NaCl	1.0	99.1	[259]
PA from MPDA and 2,3′,4,5′,6-biphenyl pentaacyl chloride (BPAC)	15.5 bar, 2,000 ppm NaCl	0.75	99.0	[259]
PA from MPDA and 2,2′,4,4′,6,6′-biphenyl hexaacyl chloride (BHAC)	15.5 bar, 2,000 ppm NaCl	0.53	99.1	[259]
PA from 2,6-diaminotoluene (DAT) and TMC	35 bar, 35,000 ppm NaCl	0.22	98.3	[260]
TFC from 4,4′-(1,2-ethanediyldiimino)bis(benzenesulfonic acid) (EDBSA) and TMC	12 bar, 2,000 ppm NaCl	0.20	96.8	[261,262]
TFC from 3,3′-(ethane-1,2-diylbis(azanediyl))bis(2,6-dimethylbenzenesulfonic acid) (EDADMBSA) and TMC	15.5 bar, 1,000 ppm NaCl	0.63	96.0	[261,262]
PA from MPDA and TMC (toluene solvent)	15.5 bar, 2,000 ppm NaCl	0.59	99.9	[263]
PA from MPDA and TMC (xylene solvent)	15.5 bar, 2,000 ppm NaCl	0.58	99.8	[263]
PA from m-phenylenediamine-4-methyl (MMPD) and cyclohexane-1,3,5-tricarbonyl chloride (HTC)	15 bar, 1,500 ppm NaCl	1.3	97.5	[264]
PA from MPDA and 5-isocyanato-isophthaloyl chloride (ICIC)	16 bar, 2,000 ppm NaCl	1.4	98.6	[139]
PA from MPDA and 5-chloroformyloxy-isophthaloyl chloride (CFIC)	16 bar, 2,000 ppm NaCl	0.96	98.7	[139]
Sulfonated poly(arylene ether sulfone) containing sulfonic acid and amino groups (SDADPS) with MPDA and TMC	55 bar, 32,000 ppm NaCl	0.77	95.0	[265]
PA from N,N ’-dimethyl-m-phenylenediamine (N,N’-DMMPD) and a mixture of TMC and IPC	15 bar, 1,500 ppm NaCl after heat treatment at 100 °C for 30 s	1.3	97.0	[266]

PI from MPDA and 1,2,4,5-benzene tetracarbonyl chloride (BTC) with thermal imidization	15 bar, 2,000 ppm NaCl	0.57	96.7	[267]
PI from MPDA, BTC, and TMC with thermal imidization	15 bar, 2,000 ppm NaCl	0.77	98.8	[267]
PA from MPDA and 2,4,6-pyridinetricarboxylic acid chloride (PTC)	13.8 bar, 1,500 ppm NaCl	0.88	73.0	[268]
PA from MPDA, PTC, and TMC	13.8 bar, 1,500 ppm NaCl	1.3	93.0	[268]
TFC from hyperbranched polyesteramide (HPEA) and TMC	6 bar, 2,000 ppm NaCl	5.2	14.0	[269]
TFC from hyperbranched polyesteramide (HPEA), 4-dimethylaminopyridine (DMAP), and TMC	6 bar, 2,000 ppm NaCl	0.9	93.0	[269]

Recent studies have focused on the aqueous and hydrocarbon solution chemistry and properties involved in the IP technique used for the synthesis of barrier layer in TFC membranes. Different monomers have been used in order to study their effect on the TFC membrane structure and separation performance. Li et al. [254] prepared PA TFC membranes from MPDA and 3,3′,5,5′-biphenyl tetraacyl chloride (I, mm-BTEC) or 3,4′,5-biphenyl triacyl chloride (BTRC) and found that the new membranes had inferior flux but higher salt rejection compared to the membrane prepared from MPDA/TMC. Also, the membrane from MPDA/BTRC exhibited higher flux and rejection compared to that from MPDA/BTEC. In a later study [255], PA TFC membranes were prepared from MPDA with 2,2′,4,4′-biphenyl tetraacyl chloride (II, om-BTEC) and 2,2′,5,5′-biphenyl tetraacyl chloride (III, op-BTEC). Compared with the previous study [254], it was concluded that the flux performance was in the order op-BTEC > om-BTEC > mm-BTEC while the salt rejection was in the order op-BTEC < om-BTEC < mm-BTEC. In general, the flux enhancement was attributed to rougher and larger surface area of op-BTEC membrane that led to greater contact with water molecules during RO desalination. Chen et al. [256] used a blend of sulfonated cardo poly(arylene ether sulfone) (SPES-NH_2) and MPDA with TMC for the synthesis of PA TFC membranes. The optimum preparation conditions were reported to be 1% acyl chloride monomer concentration, MPDA to SPES-NH_2 ratio of 2:1, and 4 min contact time with the organic solution. At optimum conditions, the flux for membrane from TMC/MPDA/SPES-NH_2 was higher than that from MPDA/TMC due to the hydrophilic nature of SPES-NH_2. However, the salt rejection was slightly lower. Wang et al. [257] also increased the hydrophilicity of PA TFC membrane by using MPDA and 3,5-diamino-N-(4-aminophenyl) benzamide (DABA) with TMC during the IP synthesis procedure. Water flux increased with increasing DABA concentration in the aqueous solution. The salt rejection, on the other hand, was maintained around 98%. Baroña et al. [258] prepared PA TFC membranes using MPDA, 2,2′-benzidinedisulfonic acid (BDSA),

and TMC. Results showed that the water flux increased with increasing BDSA content in the barrier layer due to increased hydrophilicity. In particular, the membrane prepared using 10% BDSA in MPDA solution exhibited 100% higher water flux than that of the control membrane sample prepared without BDSA. The membranes containing 2.5, 5, and 7.5% BDSA content also exhibited higher salt rejections than that of the control sample. Above 10% BDSA content, the salt rejection slightly decreased. Wang et al. [259] compared PA TFC membranes synthesized from MPDA and three different polyacyl chloride monomers: 2,4,4′,6-biphenyl tetraacyl chloride (BTAC), 2,3′,4,5′,6-biphenyl pentaacyl chloride (BPAC) and 2,2′,4,4′,6,6′-biphenyl hexaacyl chloride (BHAC). The permeate flux was observed to be in the order TMC > BTAC > BPAC > BHAC. The salt rejection was, however, the same for all the membranes and close to that of conventional MPDA-TMC membrane. It was concluded that the barrier layer based on polyacyl acid chloride monomer with higher functionality was more negatively charged, thinner, and smoother. This was attributed to the higher crosslinking degree of the PA film with heavier resistance of amine diffusion into organic phase during the IP process.

Studies employing different type of novel monomers have also appeared in very recent times. For instance, Said et al. [260] proposed fabrication of a novel PA TFC membrane by IP of 2,6-diaminotoluene (DAT) and TMC. The salt rejection of the fabricated membrane was high and performed reasonably well with both brackish and seawater feeds. The membrane allowed for seawater desalination under reduced pressure (35 bar) and had a potential to lower the energy consumption in the RO desalination process. Ghosh and Bindal [270] prepared aliphatic-aromatic PA TFC membranes using PEI and IPC and compared the performance with conventional PA TFC membrane from MPDA and TMC. The study also focused on the effect of different post-synthesis heat treatment media (hot air, hot water, and steam) on the hydrophilicity and separation performance of the membranes. Membranes from PEI and IPC exhibited lower water flux compared to the conventional membranes from MPDA and TMC. However, salt rejections were comparable. Results also showed that the surface hydrophilicity and water flux of the steam and hot water-cured membranes was higher than that of hot air-cured membranes. Zhang and co-workers [261,262] used 4,4′-(1,2-ethanediyldiimino)bis(benzenesulfonic acid) (EDBSA) and 3,3′-(ethane-1,2-diylbis(azanediyl))bis(2,6-dimethylbenzenesulfonic acid) (EDADMBSA) separately with TMC to fabricate novel TFC membranes. For seawater desalination, TFC membranes from EDBSA and TMC revealed a higher rejection of salts than the commercially available SW30 membrane (from Dow Chemical Company) and conventional membrane from MPDA and TMC. The high salt rejection was attributed to the hydrophilic-hydrophobic-hydrophilic alternating monomeric structure that resulted in charge-aggregate induced (CAI) cavities on the membrane surface. The water flux was, however, slightly lower than that for SW30 membrane. Membranes synthesized from EDADMBSA and TMC were tested with brackish water. The membrane synthesized from 0.1 wt% EDADMBSA displayed an excellent rejection ability to both monovalent and divalent ions. The rejections were rather comparable or even better than that of commercially available BW30FR membrane (from Dow Chemical Company). However, the flux was slightly lower than that of BW30FR membrane. The study concluded that the use of

EDADMBSA monomer produced more free volumes within the polymer network and resulted in high flux. Also, the salt rejection was high since the methyl groups next to the amine group could occupy the free spaces within the porous structure. Also recently, Park et al. [263] suggested to use toluene and xylene as an organic solvent phase (instead of hexane) in the IP technique in order to achieve high water flux and salt rejection. In comparison to hexane, toluene and xylene solvents can increase the amine diffusion during IP and expand the miscible interface zone due to the enhanced miscibility of toluene/xylene with water. The resulting membranes can have roof-like structures, thin and highly cross-linked PA barrier layer, and consequently, superior performance in RO desalination.

Some studies have also focused on using novel monomers in order to improve the chlorine resistance of the barrier layer. For example, PA membranes developed by Yu et al. [264] showed good chlorine resistance to more than 3000 ppmh Cl. These membranes were synthesized from m-phenylenediamine-4-methyl (MMPD) and cyclohexane-1,3,5-tricarbonyl chloride (HTC). The use of aromatic diamine with a mono CH_3 substituent at the ortho position was believed to be the main factor contributing to the enhancement of chlorine resistance. In addition to good chlorine resistance, the water flux and salt rejection values were fairly high. Liu et al. [139] studied the effect of polyacyl chloride structure on the surface properties and chlorine stability of PA TFC membranes. Membranes were synthesized using TMC, 5-isocyanato-isophthaloyl chloride (ICIC), or 5-chloroformyloxy-isophthaloyl chloride (CFIC) with MPDA. The hydrophilicity of the three PA TFC membranes was found in the order ICIC > TMC > CFIC while the surface roughness was observed to be in the order ICIC < TMC < CFIC. Also, chlorine resistance was measured by subjecting the prepared membrane to 2,500 ppmh Cl. Membrane formed from CFIC was found to exhibit the highest chlorine resistance followed by membrane from TMC and ICIC. The low chlorine resistance in the case of ICIC membrane was attributed to the existence of urea bond and –NHCOOH group that increased the susceptibility of N-chlorination reaction in the barrier layer. Kim et al. [265] prepared novel TFC membranes using sulfonated poly(arylene ether sulfone) containing sulfonic acid and amino groups (SDADPS), MPDA, and TMC. The fabricated membrane exhibited higher chlorine resistance when compared to a typical PA TFC membrane. Shintani et al. [266] synthesized chlorine-resistant PA TFC membranes from N,N′-dimethyl-m-phenylenediamine (N,N′-DMMPD) and a mixture of TMC and IPC. The membranes exhibited good chlorine resistance and the salt rejections did not change significantly upon immersion for 94 h in aqueous NaOCl solution (200 ppm) containing calcium chloride (500 ppm) at pH = 7.0 and 40 ^{o}C. Hong et al. [267] prepared chlorine-resistant PI TFC membranes using MPDA and 1,2,4,5-benzene tetracarbonyl chloride (BTC) with subsequent thermal imidization. Results indicated that the water flux decreased with increasing imidization. Salt rejection, on the other hand, increased to a maximum and then decreased with increasing imidization. Also, the flux and salt rejection increased upon the addition of TMC to BTC in the organic phase. Overall, compared to a conventional PA TFC membrane, BTC-based membranes exhibited higher chlorine resistance due to the elimination of chlorine-sensitive sites caused by the replacement of amide linkage with imide linkage. In an attempt to synthesize chlorine-resistant PA TFC membranes, Jewrajka et al.

[268] used 2,4,6-pyridinetricarboxylic acid chloride (PTC) with or without TMC in the interfacial polymerization reaction with MPDA. Compared to the control membrane sample obtained from MPDA and TMC alone, the membrane samples synthesized in the presence of PTC showed superior antimicrobial activity towards both Gram-negative and Gram-positive bacteria. However, the use of PTC requires mixed solvent system in the organic phase due to its limited solubility in hexane. Qin et al. [269] developed novel TFC membranes from interfacial reaction between hyperbranched polyesteramide (HPEA) and TMC with or without 4-dimethylaminopyridine (DMAP) in the aqueous phase. Without DMPA, the membrane performance in terms of water flux and salt rejection was extremely poor. However, addition of DMPA into the aqueous phase significantly increased the degree of the crosslink reaction between highly steric-hindered HPEA and TMC. As result, the membrane synthesized from HPEA, DMAP, and TMC exhibited high water flux and moderate salt rejection. Although the chlorine resistance ability of this membrane was high, it suffered from hydrolysis in an acidic solution. The aforementioned studies on the barrier layer in TFC membranes are summarized in Table 5. Not only PA represents the most common type of barrier layer in commercial TFC membranes, it is also the most widely studied barrier layer as indicated by the number of studies in Table 5.

3.4.2.2. Substrates

The importance of the substrate in influencing the formation and the performances of the barrier layer in TFC membranes has been acknowledged. An ideal substrate in any TFC membrane must be hydrophilic in order to allow for high water flux. However, very high substrate hydrophilicity can also reduce the adhesion between the barrier layer and the substrate [271]. Also, substrates with wide variations in the pore size may result in non-uniform barrier layer thickness due to larger amount of IP solution permeating into the larger pores compared to the smaller pores [272]. Selection of suitable substrate is, therefore, of great significance in order to ensure high flux, consistent and defect-free barrier layer, and strong barrier layer adhesion. Compared to the extensive studies on the barrier layers, less attention has been paid to the substrates in TFC membranes and their role in influencing the membrane performance.

Polysulfone (PSf) UF membranes are the most widely used substrates in laboratory and commercial TFC membranes due to their favorable properties such as wide pH operating range and high hydrophilicity [185]. These substrates are also known to be mechanically robust, thermally and chemically stable, and cost-effective [272]. Besides PSf, other substrate materials have been proposed as substrates in TFC membranes. Wei et al. [273] proposed the use of poly(phthalazinone ether sulfone ketone)s (PPESK) as substrate for PA TFC membranes. Using 2,000 ppm NaCl feed solution and 12 bar test pressure, the salt rejection and water flux of fully aromatic PA/PPESK TFC membrane were 98% and 0.24 m^3 m^{-2} day^{-1}, respectively. The PA/PPESK also exhibited higher thermal stability than that of PA/PSf membrane. Polyvinylidene fluoride (PVDF) UF membrane has also been used as a support substrate layer in PA TFC membranes [274]. Fluorinated polymers, such as PVDF, are known for their chemical, thermal, and mechanical stabilities as well as toughness and resistance to corrosion [272,274]. However,

the hydrophobic nature of PVDF membranes necessitates the use of plasma modification in order to improve the substrate surface hydrophilicity before TFC membrane synthesis. Using plasma-modified PVDF UF membranes, the TFC membranes synthesized by Kim et al. [274] not only produced higher pure water permeability but also exhibited higher salt rejections compared to those of TFC membranes containing the conventional PSf substrate. Kim and Kim [275] also used plasma treatment with hydrophilic monomers such as acrylic acid (AA), acrylonitrile (AN), allylamine (AM), ethylenediamine (ED), and n-propylamine (PAM) to hydrophilize polypropylene (PP) MF and PSf UF substrates. Hydrophilic plasma treatment of PSf substrate showed a slight enhancement in flux and rejection of resulting TFC membrane. However, the performance of membrane with PP substrate increased significantly (8 times rejection increase from 11%). In addition, plasma treatment also increased the chlorine resistance of the membranes with PP and PSf supports. Recently, Mauf et al. [276] used nanoimprinting on commercial PES UF membrane to fabricate patterned TFC membranes with water flux and salt rejection comparable to that of commercial TFC RO membranes. The study showed that surface pattern can reduce CP effects and scaling during salt solution filtration. Park et al. [277] used HKUST-1 [$Cu_3(BCT_2)$] (treated with sulfuric acid) to prepare novel metal organic framework (MOF)-PSf substrate for the fabrication of PA TFC membrane. The novel membrane showed improved flux along with enhanced fouling resistance compared to the TFC RO membrane with conventional PSf substrate. Also, the salt rejection was not compromised.

Some studies have focused on additive-incorporated substrates. For example, Ba and Economy [278] used poly(pyromellitic dianhydride-*co*-4,4′-oxydianiline) (PMDA/ODA) with $ZnCl_2$ as additive to fabricate PI substrates. Immersion precipitation of casting solutions composed of polyamic acid (PAA) and $ZnCl_2$ additive were used for the synthesis. SEM analysis showed that the $ZnCl_2$ additive played an important role in suppressing the macrovoid formation, increasing the surface smoothness, and enhancing the substrate strength of the PI substrates. Also, it was reported that, in the absence of $ZnCl_2$, PI was not a good substrate since the resulting TFC membrane had a very low salt rejection (61.4%). In comparison, incorporation of $ZnCl_2$ in the substrate improved the TFC membrane performance. For example, TFC membrane from PI substrate with 6% $ZnCl_2$ exhibited a water flux of 0.60 $m^3\ m^{-2}\ day^{-1}$ and a rejection of 95.3% when tested with 2,000 ppm NaCl solution at 55.2 bar. Choi and coworkers [279,280] prepared TFC membranes using polyethersulfone (PES) substrate blended with functionalized carbon nanotubes (fCNT). Results showed that fCNT incorporation increased the hydrophilicity, average pore width, total pore area, and porosity of the resulting TFC membranes. As a result, the water flux was enhanced (by 10-20% for seawater desalination and 90% for brackish water desalination) without sacrificing the salt rejection. In addition, the surface charge of the membranes became more negative which decreased the fouling propensity towards negatively charged foulants. Recently, Dizajikan et al. [281] prepared UF membranes from poly(vinyl chloride) (PVC) as main polymer, poly(vinyl pyrrolidone) (PVP) as additive, and 1- methyl- 2- pyrrolidone (NMP) as solvent. When used to prepare TFC RO membranes, the NaCl rejections were lower than commercial membranes.

The pore size/porosity of the substrate plays an important role in determining the performance characteristics of TFC RO membranes [272]. For example, Ramon et al. [282] used 2D and 3D models to show the importance of substrate pore size and porosity in diffusive transport through TFC membranes. Singh et al. [283] used two PSf substrates (average pore size distribution of 0.07 and 0.15 μm) to prepare PA TFC membranes. The study emphasized on the importance of substrate pore size by showing that the substrate with lower pore size distribution exhibited superior salt rejection. This was attributed to increased thickness of the barrier layer caused by reduced penetration of PA into the substrate. In case of substrate with higher pore size distribution, a lower salt rejection was observed since the barrier layer was thin and, consequently, prone to defects. Yan et al. [284] used a secondary pore-forming method for improving the surface porosity of PSf substrates in TFC RO membranes. In this method, SiO_2 nanospheres were added to the casting solution during the substrate synthesis step and, subsequently, removed by alkali treatment after solidification [284]. The secondary pore-forming method resulted in an increased substrate porosity and, consequently, increased flux of the resulting TFC membranes. In addition, the salt rejection of the resulting membranes was not compromised. Compared to the TFC membrane formed on pure support, at the optimal condition, the flux improved by 55.4% (0.84 to 1.3 m^3 m^{-2} day^{-1}) with a slight increase in rejection (98.74% to 99.10%). Recently, Wang et al. [285] explained the effect of substrate layer pore size on the formation of PA layer bottom surface. The study showed that the morphology of PA layer is affected by the PSf substrate. In case of PSf with small surface pores, the PA layer bottom was found to be porous and the top layer showed the typical ridge-and-valley structure. On the other hand, featureless and flat bottom surface morphology of the PA layer was observed with PSf containing large surface pores.

The aforementioned mentioned studies show that the substrate has a profound effect on the performance of TFC RO membranes. Substrate properties such as pore size, pore size distribution, porosity, and hydrophilicity are important considerations due to their influence on the IP process and the performance on the resulting TFC membranes. Despite their importance, substrates have been given less attention in the literature compared to the barrier layers.

3.4.2.3. Additives

Several research efforts have been made in order to optimize the performance of TFC RO membranes by embedding novel additives in the aqueous or organic phase during the IP process. Such additives can alter the monomer diffusion rate and dissolution and, consequently, effect the performance of the resulting TFC membranes [253]. Common additives include organic materials, surfactants, co-solvents, and nanoparticles [251,253].

Addition of surfactants to the amine solution during IP has been reported to improve the TFC membrane performance. For example, Khorshidi et al. [286] added sodium dodecyl sulfate (SDS) surfactant into the amine solution and reported that addition of SDS produced less permeable membranes with higher salt rejection. Studies on addition of surfactants during IP are limited and

further studies are required in order to develop a better understanding of the effects of surfactants on the IP process and the resulting TFC membranes.

Besides surfactants, various co-solvents have been used as additives in order to decrease the immiscibility between the aqueous and organic phases in the IP process [253]. Liu et al. [287] used MPDA and TMC with ethyl formate as a co-solvent in the organic phase to fabricate PA TFC membranes. Due to more hydrophilic surface of the synthesized membranes, the water flux improved in comparison with the conventional PA TFC membrane fabricated from MPDA and TMC. Also, the salt rejection was found to exceed 90% when the content of ethyl formate was less than 4 wt%. Similarly, Kong et al. [288] used acetone as a co-solvent in the organic phase. The observed water flux was found to increase significantly with increasing acetone in the organic phase. However, the salt rejection decreased at the same time. Kim et al. [289] suggested the use of dimethyl sulfoxide (DMSO) as co-solvent in the aqueous phase. With 3 wt% DMSO, flux was 5 times higher (2.8 m^3 m^{-2} day^{-1} with 2,000 ppm NaCl at 15.5 bar) compared to that of the non-additive membrane (0.62 m^3 m^{-2} day^{-1}). Salt rejection, on the other hand, decreased by 7% (89.6% compared to 96.4% for the non-additive membrane). Qiu et al. [290] used 2-propanol as co-solvent in the aqueous phase to enhance the water flux while maintaining the salt rejection. The flux enhancement was attributed to the fast reaction between hydroxyl group of 2-propnaol and the acid chloride monomer, polarity change of the aqueous system, swelling of the PA layer. Recently, Khorshidi et al. [291] used ethanol, ethylene glycol, and xylitol as co-solvents in the MPDA aqueous solution to prepare TFC membranes. The results showed that addition of ethanol and ethylene glycol significantly improved water flux of the synthesized membranes. However, in case of xylitol, an optimum (maximum) flux value was found at xylitol concentration of 1 wt%. In addition, all membranes exhibited higher salt rejection compared to the non-additive membrane.

Organic materials can also serve as additives during the synthesis of TFC RO membranes. For example, Abu Tarboush et al. [292] used hydrophilic surface modifying macromolecules (LSMM) as additives during TC membrane synthesis using MPDA and TMC. The LSMMs were named as cLSMM or iLSMM depending on whether they were synthesized before (cLSMM) or during (iLSMM) the in situ polymerization. Results indicated better performance of iLSMM incorporated membrane than that of cLSMM incorporated membrane. Using 35,000 ppm NaCl and 55 bar pressure, the iLSMM incorporated membrane exhibited higher rejection (96.1%) but lower flux (0.58 m^3 m^{-2} day^{-1}) compared to LSMM-free membrane (with rejection of 90.4% and flux of 0.78 m^3 m^{-2} day^{-1}). Rana et al. [293] also incorporated iLSMM with into the TFC membranes, however, in the presence of silver salts. This combination of additives improved the antimicrobial fouling intensity of the resulting membranes. Duan et al. [294] studied the influence of hexamethyl phosphoramide (HMPA) additive on TFC RO membrane performance. Results showed that addition of HMPA facilitated the diffusion rate of MPDA from the aqueous phase to the organic phase resulting in a thicker reaction zone during IP. In addition, HMPA also assisted in increasing the reaction rate between MPDA and TMC. As a result, with 3 wt% HMPA addition, the flux was 1.24 m^3 m^{-2} day^{-1} higher than that of non-additive membrane (0.72 m^3 m^{-2} day^{-1}) using 2,000 ppm

NaCl at 15.5 bar. The increase in flux was attributed to the enhanced hydrophilicity and increased cross-linking extent of the PA barrier layer. However, the salt rejection was slightly lower (98.3% compared to 98.5% for non-additive membrane). Gol and Jewrajka [295] used poly(ethylene glycol)diacrylate (AA-PEG-AA), poly(ethylene glycol)methyl ether acrylate (MeO-PEG-AA), and amine terminated poly(ethylene glycol) (H_2N-PEG-NH_2) as additives in the amine solution for in situ PEGylation of TFC RO membranes. Addition of H_2N-PEG-NH_2 to the MPDA solution for IP with TMC produced hydrophilized TFC with poor salt rejection (79-83%). The best performance was demonstrated with a 0.25-0.5% (w/v) of AA-PEG-AA or MeO-PEG-AA when reacted with excess MPDA for in situ generation of amine terminated PEG for IP with TMC. The PEGylated membranes exhibited superior antifouling properties compared to TFC membrane prepared by reacting MPDA and TMC under similar experimental conditions. In addition, the flux and salt rejection was not greatly compromised. Bera et al. [296] also produced PEGylated TFC membranes using MeO-PEG-AA, however, with the incorporation of triazine ring. The resulting membranes exhibited simultaneous enhancement of anti-organic fouling and anti-biofouling properties. However, the performance was lower than that of conventional TFC membrane from MPDA and TMC. Zhao et al. [297] used o-aminobenzoic acid-triethylamine salt (o-ABA-TEA), m-aminobenzoic acid-triethylamine salt (m-ABA-TEA), 2-(2-hydroxyethyl) pyridine, and 4-(2-hydroxyethyl) morpholine as hydrophilic additives in the MPDA solution during TFC membrane synthesis with TMC. At optimum concentrations, all additives produced higher water flux without significant change in the salt rejection of the resulting membranes. In case of o-ABA-TEA salt, the water flux increased dramatically from 0.88 $m^3\ m^{-2}\ day^{-1}$ to 1.5 $m^3\ m^{-2}\ day^{-1}$ (with 2,000 ppm NaCl at 15.5 bar) as the o-ABA-TEA salt concentration increased from 0 to 2.85 wt% while the salt rejection increased slightly. The increased performance was due to increased hydrophilicity and charge repulsion caused by o-ABA-TEA salt additive. However, o-ABA-TEA salt concentrations above 2.85 wt% resulted in decreased performance due to interference with the IP process that resulted in deterioration of the subsequently formed PA barrier layer. In case of m-ABA-TEA salt, similar trends were observed and the optimum additive concentration was found to be 2.375 wt%. The optimum concentration of both 2-(2-hydroxyethyl) pyridine and 4-(2-hydroxyethyl) morpholine was 2.4 wt%. Recently, Zhang et al. [298] used 1,3-propanesultone (PS) as an additive in the organic phase to fabricate PA TFC membranes. Compared to conventional the PA TFC membrane without PS, the optimal membrane (synthesized using 0.04% (w/v) PS) produced higher water flux (1.16 $m^3\ m^{-2}\ day^{-1}$) without compromising the salt rejection (99.4%). Wu et al. [299] utilized dimethyl sulfoxide (DMSO) and glycerol as additives in the preparation of PA TC membranes. The MPDA/TMC/DMSO/glycerol membrane was found to be more hydrophilic with a rougher surface compared to the conventional MPDA/TMC membrane. In the presence of additives, the flux improved slightly (~12% when test with 1,000 ppm NaCl at 10.3 bar) without any decrease in the salt rejection.

Table 6. Summary of studies on surfactants, co-solvents, and organic materials as additives in TFC RO membrane synthesis

Additive type	Additive name	Test conditions	Comments on performance	Reference
Surfactant	Sodium dodecyl sulfate (SDS)	15.2 bar, 2,000 ppm NaCl	Salt rejection increased at the expense of decreased flux	[286]
Co-solvent	Ethyl formate	16 bar, 2,000 ppm NaCl	TFC membrane had hydrophilic surface leading to water flux twice as high as that of the conventional TFC without ethyl formate. The change in salt rejection was low	[287]
	Acetone	15 bar, 2,000 ppm NaCl	With 2% acetone, flux was three times higher compared to the membrane synthesize without acetone (salt rejection remained the same). Further increase in acetone concentration increased the flux but reduced the salt rejection	[288]
	Dimethyl sulfoxide (DMSO)	15.5 bar, 2,000 ppm NaCl	Flux was increased by up to 5 times with small decrease in salt rejection compared to the non-additive membrane	[289]
	2-propanol	16 bar, 32,800 ppm NaCl	Flux was enhanced without compromising the salt rejection	[290]
	Ethanol, ethylene glycol, and xylitol	15.2 bar, 2,000 ppm NaCl	Flux increased with increasing concentration of ethanol and ethylene glycol. In case of xylitol, an optimum flux value existed at 1 wt% concentration. Salt rejection was higher than that of non-additive membrane	[291]
Organic additive	Hydrophilic surface modifying macromolecules (LSMM)	56.2 bar, 35,000 ppm NaCl	5.7% increase in rejection was observed (at expense of 26% decline in flux)	[292]
	In-situ hydrophilic surface modifying macromolecules (iLSMM) with silver salts	56.2 bar, 35,000 ppm NaCl	Antimicrobial fouling properties improved	[293]
	Hexamethyl phosphoramide (HMPA)	15.5 bar, 2,000 ppm NaCl	The flux increased by 73% and the salt rejection decreased by less than 0.21% compared with the non-additive membrane	[294]

	Poly(ethylene glycol)diacrylate (AA-PEG-AA), poly(ethylene glycol)methyl ether acrylate (MeO-PEG-AA), and amine terminated poly(ethylene glycol) (H_2N-PEG-NH_2)	13.8 bar, 2,000 ppm NaCl	PEGylation improved fouling resistance without compromising flux and salt rejection	[295]
	MeO-PEG-AA with triazine	13.8 bar, 2,000 ppm NaCl	Anti-organic fouling and anti-biofouling were simultaneously enhanced with decreased RO performance	[296]
	o-aminobenzoic acid-triethylamine salt (o-ABA-TEA), m-aminobenzoic acid-triethylamine salt (m-ABA-TEA), 2-(2-hydroxyethyl) pyridine, and 4-(2-hydroxyethyl) morpholine	15.5 bar, 2,000 ppm NaCl	With 2.85 wt% o-ABA-TEA and 2.375 wt% m-ABA-TEA, flux increased by ~70% with minor increase in salt rejection. With 2.4 wt% 2-(2-hydroxyethyl) pyridine and 4-(2-hydroxyethyl) morpholine, flux increased by ~85% and ~88%, respectively, with minor change in salt rejection	[297]
	1,3-propanesultone (PS)	15.5 bar, 2,000 ppm NaCl	Under optimum conditions, flux improved by 41% compared to that of the conventional PA TFC membrane. Salt rejection was not compromised	[298]
	Dimethyl sulfoxide (DMSO) and glycerol	3.4-17.2 bar, 1,500 ppm NaCl	Flux improved slightly without any decrease in salt rejection	[299]

The use of nanotechnology in membrane science has opened doors to a complete new class of RO membranes known as mixed matrix membranes (MMM) or thin film nanocomposite (TFN) membranes [253]. Fig. 11 illustrates the concept of TFN membranes where nanoparticles are embedded within the membrane barrier layer. Recently, considerable attention has been given to the use of nanofillers (nanoparticle additives) in the synthesis of RO membranes in order to enhance the membrane performance and thermal, chemical, and mechanical stability. Jeong et al. [300] introduced the concept of TFN membranes by dispersing NaA-type zeolite nanoparticles in the organic phase to synthesis membranes with zeolite-PA barrier layer. The synthesized TFN

membranes had smoother and more hydrophilic, negatively charged surfaces. As a result, at the maximum zeolite loading (0.4% (w/v)), the water flux was double than that of the conventional PA membrane with equivalent solute rejection.

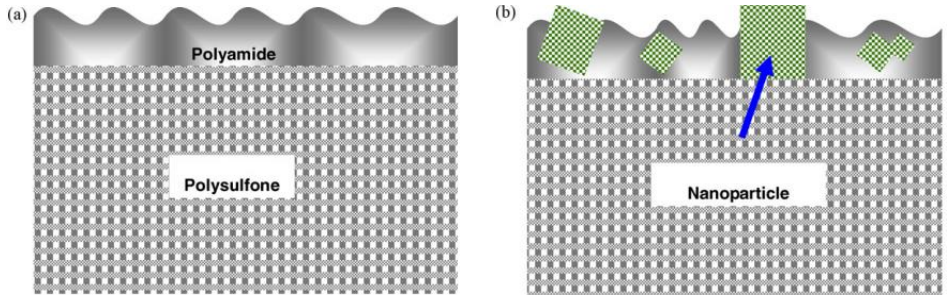

Fig. 11. Conceptual illustration of (a) TFC and (b) TFN membrane structures (adopted from [300])

Later, other zeolite nanoparticles were also used to fabricate TFN RO membranes. For example, Fathizadeh et al. [301] used added NaX nano-zeolite into PA layer. The resulting membranes had higher thermal stability and more water permeability than the pure PA TFC membranes due to improved surface roughness, contact angle, and solid-liquid interfacial free energy, decreased film thickness and, increased pore size. Dong et al. [302] used NaY zeolite nanoparticles to synthesize PA TFN membranes with good salt rejection and higher water flux compared to the conventional PA TFC membrane. Safarpour et al. [303] embedded plasma treated natural zeolite into the PA layer. The resulting membranes exhibited lower surface roughness and increased hydrophilicity. The flux, salt rejection, and antifouling ability were found to be higher than the conventional PA TFC membrane. Similarly, Cay-Durgun et al. [304] used Linde type A (LTA) zeolite nanoparticles to synthesize TFN membranes with higher flux and salt rejection compared to the TFC counterpart. In general, zeolite nanoparticles can improve the flux of RO membranes without significant compromise in the salt rejection by providing favorable flow channels for water molecules.

Table 7. Summary of studies on TFN RO membrane synthesis

Nanoparticle class	Nanoparticle name	Test conditions	Comments on performance	Reference
Zeolite	NaA-type zeolite	12.4 bar, 2,000 ppm NaCl	A maximum zeolite loading (0.4% (w/v)), the water flux was double than that of the conventional PA membrane with equivalent solute rejection	[300]
	NaX nano-zeolite	12 bar, 2,000 ppm NaCl	TFN membrane synthesized with 0.2% (w/v) nano-NaX zeolite, 0.1% (w/v) TMC and 2% (w/v) MPD produced 1.8 times higher flux than that of conventional PA	[301]

			TFC membrane without any change in salt rejection	
	NaY zeolite	15.5 bar, 2,000 ppm NaCl	Compared to conventional PA TFC membrane, the TFN had higher flux (1.78 m^3 m^{-2} day^{-1} compared to 0.95 m^3 m^{-2} day^{-1}). Salt rejection was 98.8%	[302]
	Plasma treated natural zeolite	15 bar, 16,000 ppm NaCl	The membrane modified with 0.01 wt% zeolite treated under 1.0 Torr oxygen as the plasma gas showed the highest water flux improvement (39%) and fouling recovery ratio (88%) compared to the unmodified membrane	[303]
	Linde type A (LTA) zeolite	13.9 bar, 734 μS cm^{-1}	All TFN membranes demonstrated higher salt water flux than the TFC membranes while maintaining similar average salt rejection	[304]
Silica	Monodispersed spherical mesoporous nanosilica	16 bar, 2,000 ppm NaCl	Flux improved by 2.8 times and salt rejection stayed above 96%	[305]
	Hydrophilic silica nanoparticles	44 bar, 11,000 ppm NaCl	Maximum flux enhancement was 1.6 times that of non-modified membrane. Salt rejection did not changed significantly	[306]
	MCM-41 silica nanoparticles	20.7 bar, 2,000 ppm NaCl	Maximum flux enhancement was 1.6 times that of non-modified membrane. Salt rejection did not changed significantly	[307]
	Hollow mesoporous silica nanoparticles	15 bar, 2,000 ppm NaCl	Flux was 40% higher that of non-modified membrane. Salt rejection did not changed significantly	[308]
	Polyethylenimine modified silica nanoparticles	15 bar, 2,000 ppm NaCl	A slight increase in flux and salt rejection was observed	[309]
Carbon-based	Graphene oxide (GO)	15.5 bar, 2,000 ppm NaCl	Flux and biofouling resistance were enhanced by 80% and 98%, respectively, without loss of salt rejection. Salt rejection was retained upon high chlorine exposure	[310]

	GO	15 bar, 2,000 ppm NaCl	At 100 ppm GO, water flux was 0.71 m^3 m^{-2} day^{-1} and salt rejection was ≥97%. Stability in acidic and basic solutions was also enhanced	[311]
	Reduced graphene oxide (rGO)/titanium dioxide (TiO_2)	15 bar, 2,000 ppm NaCl	With 0.02 wt% rGO/TiO_2, flux was 1.5 times higher than that of control non-additive membrane. Salt rejection was also increased from 97.4% to 99.45%. Antifouling and chlorine resistance was enhanced. Salt rejection decreased by only 3% for 0.02 wt% rGO/TiO_2 membrane. This was 10 times lower than the control membrane	[312]
	GO nanosheets	20.7 bar, 2,000 ppm NaCl	With 0.015 wt% GO, flux was 1.52 times higher than that of non-additive membrane. Slight decrease in salt rejection was observed	[313]
	Multi-walled carbon nanotubes (MWCNT)	15.5-55 bar, 2,000-35,000 ppm NaCl	With 0.001 wt% CNT, flux enhancement was ~30% with a slight drop in salt rejection. The fouling potential was decreased	[314]
	Acid treated MWCNT-titania nanotube (TNT) hybrid	15 bar, 2,000 ppm NaCl	With 0.05 wt% additive, flux improved by 57.45% compared to that of neat PA membrane. Salt rejection stayed the same	[315]
	Carboxy-functionalized MWCNTs	16 bar, 2,000 ppm NaCl	With 0.1 wt% additive, flux was 1.9 times higher to that of non-additive membrane. Salt rejection stayed the same while antifouling and antioxidant properties improved	[316]
	Zwitterion functionalized carbon nanotubes (CNTs)	24.1 bar, 2,000 ppm NaCl	With 20 wt% additive, flux was 2.3 times higher compared to PA TFC membrane. Salt rejection remained unchanged while biofouling resistance improved significantly	[317]
	Amine-functionalized	15 bar, 2,000 ppm NaCl	With 0.002 wt% additive, flux was 1.38 times higher than non-additive membrane. Salt rejection	[318]

	MWCNT ($MWCNT-NH_2$)		increased slightly (from 95 to 96%)	
	Oxidized MWCNT	15 bar, 2,000 ppm NaCl	With 0.005 wt% additive, flux was 1.15 times higher than that of unfilled membrane. Salt rejection remain unchanged. Antifouling performance was better than the unfilled membrane	[319]
	Carbide derived carbon (CDC)	14.15 bar, 2,000 ppm NaCl	With CDC loading of 0.003 w/v%, flux was 1.15 times higher than that of un-modified membrane. Salt rejection increased from 91 to 96%	[320]
	Nano carbon dots (CDs)	15.5 bar, 2,000 ppm NaCl	With 0.02 wt% additive, flux was 1.2 times higher when compared to control TFC membrane. Salt rejection increased from 98.5 to 98.8%	[321]
	Nitrogen-doped graphene oxide quantum dots (N-GOQD)	15 bar, 2,000 ppm NaCl	With 0.02 wt/v% N-GOQD, water permeability increased by approximately 3 times, while maintaining similar salt rejection as the pristine PA membrane	[322]
Other	Aluminum doped ZnO nanoparticles	15.5 bar	With 0.5 wt% nanoparticle concentration, flux was 1.23 times higher than non-modified membrane. Salt rejection was 98%	[323]
	Amino functionalized titanate nanotubes (NH_2-TNTs)	15 bar, 2,000 ppm NaCl	With 0.05% additive, flux was 93% higher than that of control TFC membrane. Salt rejection was not compromised. Organic fouling was highly reversible	[324]
	MCM-48 nanoparticles	16 bar, 2,000 ppm NaCl	Water flux increased from 0.58 $m^3\ m^{-2}\ day^{-1}$ to 0.96 $m^3\ m^{-2}\ day^{-1}$ with the increase in MCM-48 content in the organic phase, without significantly affecting the salt rejection (95%)	[325]
	Zwitterionic colloid nanoparticles (ZCPs)	15 bar, 2,000 ppm NaCl	With 0.1 wt% additive, flux was 1.3 times higher than that of control TFC membrane. Salt rejection was not compromised.	[326]

			Antifouling properties were improved	
	Silver nanoparticles (Ag-NPs)	E. coli, P. aeruginosa, and S. aureus	Slight reduction (up to 17%) in water permeability was observed. However, antibacterial activity was improved leading to reduction of more than 75% in the number of live bacteria attached to the membrane	[327]
	Polyhedral oligomeric silsesquioxane (POSS)	15.5 bar, 2,000 ppm NaCl	TFN membranes prepared with 0.4 (w/v)% P-8Phenyl in the organic phase showed a 65% increase in water flux compared to the pristine PA membrane while maintaining high salt rejection	[328]
	Zeolitic imidazolate framework-8 (ZIF-8)	15.5 bar, 2,000 ppm NaCl	With 0.4 (w/v)% loading, water permeability increased by 162% compared to pristine membrane while maintaining high salt rejection	[329]
	Montmorillonite (MMT)	16 bar, 2,000 ppm NaCl	At 0.1 wt% loading, flux was 1.4 times higher than that of TFC membrane. Salt rejection remained almost the same	[330]
	Layered double hydroxide (LDH)	16 bar, 2,000 ppm NaCl	At 0.1 wt% loading, flux was 1.13 times higher than that of TFC membrane. Salt rejection increased	[330]
	Metal organic framework (MOF) material-MIL-101 (Cr)	16 bar, 2,000 ppm NaCl	At 0.05 (w/v)% concentration, 44% higher flux was obtained compared to the undoped PA membranes. Salt rejection remained higher than 99%.	[331]
	TiO_2 nanoparticles	20.7 bar, 2,000 ppm NaCl	Water flux increased from 0.96 to 1.56 $m^3\ m^{-2}\ day^{-1}$ by increasing the nanoparticle concentration from 0 to 0.1 wt. %, while NaCl rejection remained above 96%	[332]

Besides zeolite, silica nanoparticles have been used for TFN membrane synthesis. Bao et al. [305] prepared TFN membranes with monodispersed spherical mesoporous nanosilica in the PA layer. The hydrophilicity of the resulting membranes was improved and water flux was increased from

0.56 m^3 m^{-2} day^{-1} (without nanosilica) to 1.27 m^3 m^{-2} day^{-1} (with 0.1% (w/v) mesoporous nanosilica loading) with negligible effect on salt rejection (>96%). Similar results were reported in other studies related to silica nanoparticle-based TFN membranes [306–309]. Based on attractive properties that can be imparted by nanoparticles, several other nanoparticles have been employed to prepare TFN membranes with enhanced performance and, sometimes, enhanced fouling and chlorine resistance. These include graphene oxide (GO), multi-walled carbon nanotubes (MWCNTs), carbon dots (CDs), among others. The performance of the various novel TFN membranes is summarized in Table 7.

3.4.2.4. Surface modification

Modification of the barrier layer in TFC membranes is another effective and feasible method in order to improve the permeate flux, salt rejection, fouling resistance, and chloride stability [185]. Surface modification may be performed physically or chemically. In physical modification, the barrier layer remains chemically intact and physical interactions (van der Waals attraction, electrostatic interaction, or hydrogen bonding) are used to hold the coating material to the membrane surface [253]. Such modification can be in the form of physical adsorption or surface coating. Chemical modification, on the other hand, involves membrane activation using chemical reactions where materials are connected to the surface of RO membranes by covalent bonds. Typical chemical modifications include hydrophilization treatment, radical grafting, chemical coupling, plasma polymerization, and initiated chemical vapor deposition (iCVD) [183].

Physical surface modification has been extensively used to improve the fouling and chlorine resistance of TFC RO membranes and, in some cases, to improve the membrane performance in terms of water flux and salt rejection. Table 8 provides a summary of studies on physical surface modification of TFC RO membranes. Most of these modifications are based on surface coating where a protective layer on the barrier layer helps mitigate the effects of foulants or chlorine. Surface coating is considered as a simple technique and has, therefore, attracted considerable attention among researchers. The selection of coating material, however, is important to avoid an excessive increase in the permeation resistance and a subsequent decrease in the permeate flux. It is crucial to ensure that the coating layer is thin and possesses high water permeability to ensure high permeate flux [183]. Also, it is important to note that, in physical surface modification, only physical interactions such as van der Waals attraction, electrostatic interaction, or hydrogen bonding are used to hold the coating material to the membrane surface. This may make the acquired fouling or chlorine resistance prone to deterioration in long term operations due to loss of the coating layer [183].

Table 8. Summary of studies on physical surface modification of RO membranes

Modification purpose	Modifier	Test conditions	Comments on performance	Reference

Fouling resistance improvement	Methyl methacrylate-hydroxy poly(oxyethylene) methacrylate (MMA-HPOEM)	62.1 bar, 32,000 ppm NaCl, 30 ppm bovine serum albumin (BSA)	Fouling resistance to BSA, *Escherichia coli*, and seawater increased	[333]
	Barium chloride ($BaCl_2$)	5 bar, 500 ppm NaCl, 200 ppm BSA	Mineralized membranes had more hydrophilic and negatively charged surface. Antifouling resistance improved in addition to flux enhancement (by 1.2 times) and increase in salt rejection (from 96.8% for unmodified membrane to 98.2% for modified membrane)	[334]
	Polydopamine (PDA)	7.5 bar, 500 ppm NaCl, (10^7–10^8) cfu/mL bacteria	Water permeability decreased slightly while salt rejection increased. Biofouling resistance and bacterial adhesion resistance increased	[335]
	Sulfonated polyvinyl alcohol (SPVA)	15.5 bar, 2,000 ppm NaCl, 2,000 ppm foulant (BSA or cetyltrimethylammonium bromide (CTAB))	Modification resulted in increased surface smoothness, hydrophilicity, and electronegativity.	[336]

			With 0.5% (w/v) SVPA, the membrane lost only about 10% of the initial flux after fouling by BSA for 12 h, and the flux recovery reached above 95% after cleaning. Salt rejection increased while water flux decreased	
	N-isopropylacrylamide-co-acrylic acid copolymers (P(NIPAm-co-AAc))	5 bar, 500 ppm NaCl, 100 ppm BSA	Modification increased the membrane surface hydrophilicity and surface charge at neutral pH but offer additional resistance to water permeation. Salt permeability decreased and fouling resistance improved	[337]
	Poly(N-isopropylacrylamide-co-acrylamide) (P(NIPAM-co-Am))	10 bar, 2,000 ppm NaCl, 30, 60, and ppm BSA	Surface hydrophilicity, water flux, and fouling resistance improved. Phase transition above the low critical solution temperature (LCST) helped in removing the	[338]

			foulants from membrane surface	
	3-(3,4-dihydroxyphenyl)-lalanine (L-DOPA)	18 and 50 bar, 100 ppm BSA, 100 ppm alginic acid sodium salt (AAS), 50 ppm dodecyl trimethyl-ammonium bromide (DTAB)	Surface hydrophilicity increased while zeta potential remained the same. Maximum flux improvement was 1.27 times that of original membrane. Salt rejection remained almost the same (~97%). Fouling resistance increased and with water-only cleaning, 98% water flux recovery ratio was achieved for the 24-h modified membrane	[339]
	Positively charged anti-biotic tobramycin (TOB) and negatively charged poly acrylic acid	15.5 bar, 2,000 ppm NaCl, 100 ppm BSA/ sodium alginate (SA)	Under optimized condition, the modified membrane showed 18% increase in water flux and slightly enhanced (0.4%) salt rejection. Also, the modified membrane demonstrated 37% and 26% higher flux than the virgin	[340]

			membrane after three-cycling fouling of BVA and SA solution, respectively.	
	Poly[2-methacryloyloxyethyl phosphorylcholine (MPC)-co-2-aminoethylmethacrylate (AEMA)] (p(MPC-co-AEMA))	7.5 bar, 500 ppm NaCl, 10^8 cfu/mL *Sphingomonas paucimobilis* NBRC 13935	Compared to raw membrane with salt rejection 94.7%, the modified membrane had higher rejection of 96.9%. However, flux slightly decreased. The bacterial adhesion resistance improved significantly	[341]
	Polyelectrolyte	7.5 bar, 5,000 ppm NaCl, BSA, humic acid and DTAB solution (each 50 ppm)	Antifouling property of improved while retaining high salt rejection	[342]
	Sericin	5 bar, 500 ppm NaCl, 100 ppm BSA	Modification resulted in increased surface hydrophilicity, enhanced surface negative charge, smoothed surface morphology, and decreased pure water permeability and salt permeability coefficient. Fouling resistance improved	[343]

	Carboxylated chitosan (CCTS) and copper chloride ($CuCl_2$)	15 bar, 2,000 ppm NaCl, *E. coli* MG1655, 2,000 ppm BSA	Modification resulted in more than 99% antibacterial efficiency. Modified membrane exhibited higher hydrophilicity and lower water flux, higher salt rejection and better protein fouling resistance	[344]
	Poly(ethylene glycol) (PEG) acrylate multilayers	55 bar, 30,830 ppm and 2,000 ppm NaCl, 1,110 ppm $CaCl_2$, 100 ppm SA	Water flux declined (9-17% of the uncoated value) while salt rejection improved. Fouling resistance increased	[345]
	PVA with cationic polyhexamethylene guanidine hydrochloride (PHMG)	27.6 bar, 584 ppm NaCl, 10^8 cfu/mL *Pseudomonas aeruginosa*	Modification resulted in higher hydrophilicity, lower roughness, and higher anti-adhesion performance. Water permeability declined by 45-58% while salt rejection remained almost the same	[346]
	Trimethylaluminium ($AlMe_3$)	27.6 bar, 584 ppm NaCl, 10^8 cfu/mL *Pseudomonas aeruginosa*	Modification resulted in higher anti-adhesion performance. However, water permeability and	[347]

			salt rejection declined	
	PEBAX® 1657	11.3 bar, 1,500 ppm NaCl, mixture of 10,000 ppm motor oil and 1,000 ppm silicone glycol	Surface roughness decreased and fouling resistance increased without decline in salt rejection	[348]
	PEG based coating	15.5 bar, 2,000 ppm NaCl, 135 ppm n-decane and 15 ppm surfactant	Water flux decreased while salt rejection remained 99% or higher. Negatively charged membranes showed good fouling resistance against negatively charged foulants	[349]
	Amine-functional polyamidoamine (PAMAM) dendrimers and PAMAM–PEG	6.9 bar, 1,000 ppm NaCl	Coated membrane hydrophilicity could be quadrupled depending on the coating type applied, without deterioration of the salt rejection and acceptable (about 20%) reduction of the permeate flux. High antifouling properties expected	[350]
	PEI	8 bar, 90 ppm NaCl, 50 ppm DTAB	Pure water permeability decreased by	[351]

			37%. salt rejection, fouling resistance, and surface hydrophilicity improved	
Chlorine resistance improvement	Poly(N-isopropylacrylamide-co-acrylamide) (P(NIPAM-co-Am))	15 bar, 2,000 ppm NaCl	Modified membranes with P(NIPAM-co-Am) concentration less than 200 ppm showed increased flux and salt rejection. The flux and salt rejection remained the same after long term exposure to acidic solution and chlorine	[352]
	GO	15 bar, 1,000 ppm NaCl, 6,000 ppm NaOCl	During the first 2 h of chlorine exposure, the salt rejection decreased from 95.3% to 91.6% for the modified membrane while, for the unmodified membrane, salt rejection dropped to 80%. After 16 h of chlorine exposure, the salt rejection for the modified membrane was 75% compared to 63% for the	[353]

			unmodified membrane	
	Terpolymer of 2-acrylamido-2-methyl propanesulfonic acid, acrylamide and 1-vinylimidazole (P(AMPS-co-Am-co-VI))	4 bar, 2,000 ppm $MgSO_4$, 2,000 ppm NaOCl	Modification created a more neutral, hydrophilic, and smooth membrane surface. The chlorine tolerance was improved significantly, especially in acid environment	[354]
	poly(methylacryloxyethyldimethyl benzyl ammonium chloride-r-acrylamide-r-2-hydroxyethyl methacrylate) (P(MDBAC-r-Am-r-HEMA))	15 bar, 2,000 ppm NaCl, 500 ppm NaOCl, 100 ppm BSA	The coated membrane could tolerate chlorine exposure over 16,000 ppmh (7–10 times higher than the pristine membrane). Wettability and fouling resistance also improved	[355]
	Sorbitol polyglycidyl ether (SPGE)	15 bar, 2,000 ppm NaCl, 540, 1,620, and 3,780 ppmh Cl_2	Modification resulted in more neutral, hydrophilic, and smooth membrane surface. With increasing SPGE concentration in the coating solution, water flux declined but salt rejection increased. Also, chlorine stability increased	[356]

Performance improvement	Chlorine treatment and chitosan	8 bar, 1,500 ppm NaCl	With NaClO concentration 200 ppm, chlorination time 2–5 min, and chitosan concentration 1000 ppm, the modified membrane exhibited a water flux of 1.4 m^3 m^{-2} day^{-1} and a salt rejection of 95.4%	[357]

Chemical surface modification, on the other hand, offers a long-term chemical stability when compared to physical modification. Several chemical surface modification techniques appear in the literature. In hydrophilization treatment, the barrier layer is hydrophilized chemically using an appropriate agent such as protic acid (hydrofluoric, hydrochloric, sulfuric, phosphoric, or nitric acid), ethanol, or 2-propanol [358]. Besides hydrophilization, chemical surface modification can be via radical grafting where free radicals, produced from suitable initiators, are reacted with the PA chain (hydrogen in amide bond) in TFC membranes. Surface modification via chemical coupling involves the free carboxylic acid and primary amine groups (on chain ends) on the PA barrier surface. Also, plasma polymerization can be used for chemical surface modification where plasma is used to deposit a polymer of the membrane surface. Lastly, iCVD can be used which is an all-dry free radical polymerization technique performed at low temperatures and low operating pressures [183]. Table 9 summarizes the studies on chemical surface modification using the aforementioned techniques.

Table 9. Summary of studies on chemical surface modification of RO membranes

Modification purpose	Modifier	Modification technique	Test conditions	Comments on performance	Reference
Performance improvement	Protic acids (hydrofluoric, hydrochloric, sulfuric, phosphoric, or nitric acid), ethanol, and 2-propanol	Hydrophilization treatment	17.2 and 24.1 bar, 5,000 ppm NaCl	Ethanol, 2-propanol, hydrofluoric acid and hydrochloric acid improved the flux with no loss in rejection. The other acids caused the flux to increase	[358]

				with some loss in ion rejection properties	
	-	Helium and water gas plasma	15 bar, 2,000 ppm NaCl	Flux was enhanced by up to 66% (from 0.72 to 1.2 m^3 m^{-2} day^{-1}) with 98% rejection	[359]
		Plasma polymerization (maleic anhydride and vinylimidazole)	15 bar, 2,000 ppm NaCl	Enhanced flux (5-10%) and retained salt rejection was observed at low plasma polymerization durations for vinylimidazole monomer. Maleic anhydride monomer resulted in decreased flux (18-33%) but almost the same rejection at low plasma polymerization durations	[360]
Fouling resistance improvement	1-Ethy-3-(3-dimethyl amidopropyl) carbodiimide (EDC)	Chemical coupling	10.5 bar, 1,500 ppm NaCl, 100 ppm milk solution, 100 ppm DTAB	Surface modification caused an acceptable decrease in pure water flux (1.2 to 0.77-0.86 m^3 m^{-2} day^{-1}) but no significant change in salt rejection (>96%). Compared to unmodified membrane, the modified membranes were more hydrophilic and resistant to fouling in protein and cationic surfactant solutions	[361]
	L-cysteine	Chemical coupling	50 bar, 12,500 ppm NaCl, 100 ppm BSA, 50 ppm DTAB	Fouling propensity decreased (due to increased hydrophilicity and lower surface roughness) along with decrease in flux and	[362]

				increase in salt rejection	
	PEI	Chemical coupling	15.5 bar, 2,000 ppm NaCl, 1,000 ppm lysozyme, 60 ppm DTA, 60 ppm CTAC	Modification resulted in high anti-fouling properties against positively charged pollutants. Water flux slightly decreased but salt rejection remained almost the same	[363]
	Lysozyme	Chemical coupling	7.5 bar, 2,000 ppm NaCl, 10^2 cfu/mL B. *subtilis* ISW1214	Water flux decreased to 50% but salt rejection was not compromised. Antibacterial activity improved	[364]
	Poly(amidoamine) (PAMAM)	Chemical coupling	50 bar, 35,000 ppm NaCl, protein solution	The permeability increased by 20–25% with no negative effect on salt rejection. Protein adsorption decreased	[365]
	Glutaraldehyde and PVA	Chemical coupling	5 bar, 500 ppm NaCl, 100, 200, and 10 ppm BSA, SDS and DTAB, respectively	Modification caused improved surface hydrophilicity, a declined surface negative charge and a slightly increased surface roughness. Flux and salt rejection were enhanced. Antifouling properties were also enhanced	[366]
	3-allyl-5,5-dimethylhydantoin (ADMH)	Radical grafting	15 bar, 2,000 ppm NaCl, 1,000 ppmg chlorine, 10^6 cfu/mL *E. coli*	Water flux decreased but salt rejection improved. Chlorine and befouling resistances were enhanced	[367]
	2-bromoisobutyryl bromide (BIBB)	Radical grafting	7.5 bar, 5,000 ppm NaCl, *Sphingomonas paucimobilis* NBRC 13935	The surface morphology became smoother with increasing polymerization time. The modified	[368]

				membranes prevented bacteria adhesion	
	Methacrylic acid (MAA) with ZnO nanoparticle incorporation	Radical grafting	15 bar, 2,000 ppm NaCl, *Escherichia coli*	Modification enhanced the selectivity, permeability, water flux, mechanical properties, and the bio-antifouling properties	[369]
	AA monomer with MWCNT nanoparticle incorporation	Radical grafting	15 bar, 2,000 ppm NaCl, 500 ppm BSA	Modified membranes with 0.75 M of monomer, 3 min contact time and 80 min curing time in an oven at 50 ◦C presented the highest flux and lowest rejection decline. The membrane containing 0.25 wt% COOH-MWCNTs showed the highest fouling resistance	[370]
	N-isopropylacrylamide (NIPAm) and AA	Radical grafting	10 bar, 500 ppm NaCl, 200 ppm BSA, 1,000, 3,000, and 5,000 ppmh Cl_2	Membrane surface became more hydrophilic and negatively charged. Both water flux (maximum 0.85 m^3 m^{-2} day^{-1}) and salt rejection improved (maximum 98.2%). Fouling, acid, and chlorine resistance improved. The phase transition of the grafted NIPAm-polymer chains when washed with lukewarm water (45.0 °C) facilitated the removal of foulants located on the membrane surface	[371]
	N,N′-dimethylaminoethyl methacrylater (DMAEMA) and	Radical grafting	15 bar, 2,000 ppm NaCl, 1,000 ppm lysozyme/BSA,	Flux increased by 22.55% while salt rejection remained the same. Membrane	[372]

	3-bromopropionic acid (3-BPA)		10^6 cfu/mL *E. coli*	acquired higher protein fouling resistance and easy-cleaning and anti-microbial properties	
	Poly(4-vinylpyridine-co-ethylene glycol diacrylate) (p(4-VP-co-EGDA)) followed by quaternization reaction with 3-BPA	iCVD	20.7 bar, 2,000 ppm NaCl, 4.1 × 10^8 cell/mL *E. coli* and *Pseudomonas*	98% reduction in micro-organism attachment was achieved onto the surface of modified membranes compared to bare membranes. Salt rejection improved to 98% but flux decreased slightly	[373]
	HEMA and perfluoro decylacrylate (PFDA)	iCVD	11,700 ppm NaCl, 4 × 10^7 cells/mL *Escherichia coli* K12 MG1655	Increasing the thickness of the coatings increased the surface roughness and decreased the permeation rates (10% decrease with 40% PFA). Increasing PFA content led to higher surface roughness and formed more hydrophobic surfaces. Bacterial adhesion resistance increased	[374]
	Surface-tethered zwitterionic structure	iCVD	20.7 bar, 2,000 ppm NaCl, 4 × 10^7 cells/mL *Escherichia coli*	Water flux showed 15% to 43% reduction in permeation with no change in salt rejection. Biofouling resistance improved	[375]
Chlorine resistance improvement	Imidazolidinyl urea (IU)	Radical grafting	15.5 bar, 2,000 ppm NaCl, 1,000 ppm NaOCl, 6 × 10^7 cfu/mL *E. coli*	The water fluxes decreased by 24.9% after the modification with no change in salt rejection. Hydrophilicity increased along with increase in the anti-biofouling and chlorine resistance	[376]
	Formaldehyde and glutaraldehyde	Chemical coupling	16 bar, 2,000 ppm NaCl, 1 M	With optimal reduction condition at 60 °C, 2h	[377]

			HCl, 60 ppm BSA, 500 ppm NaOCl	and cross linked time at 3hrs, the water flux and the salt rejection was maintained at 98.6% and 0.9 m^3 m^{-2} day^{-1}, respectively, close to that of the pristine membranes (98.7%, 1.03 m^3 m^{-2} day^{-1}). Membranes also exhibited stable acid resistance, better antifouling property to BSA, and improved chlorine resistance both in the acidic and alkaline conditions	

Despite being successful in enhancing the membrane properties, most of the surface modification techniques are limited to laboratory studies due to complex procedures and high costs involved. Research investigations into the stability of surface modifiers require more attention, especially in the presence of cleaning chemicals [187]. Also, studies related to surface modification for chlorine resistance improvement are relatively limited which calls for further investigations. Furthermore, research efforts are required in order to address the tradeoff between decreased permeate flux and enhanced antifouling properties.

3.5. Membrane cleaning

Adequate membrane cleaning is a critical step in maintaining the long term performance of the membrane and attaining an effective and smooth operations of the seawater desalination processes as fouling is inevitable [9]. Many dissolved organic matter such as polysaccharides, amino sugars, proteins, humic and fulvic acids, nucleic acids, and organic acids lead to RO membrane fouling [378]. Fouled membranes would lead to a significant decrease in water productivity, RO flux, and recovery [379]. Studies have shown that there are very limited tools to predict and evaluate the causes and consequences of membrane fouling [380]. Fouling can be controlled through many measures/strategies including feed-water pre-treatment and addition of biocides such as chlorine and monochloramine [381]. Nowadays, one of the main research lines is directed heavily into attaining a better comprehension of the RO membrane fouling and cleaning mechanisms in order to develop and enhance the membrane fouling preventative measures [382]. Routine membrane cleaning is highly required in order to retrieve the membrane performance although complete biofilm removal is never attained. Various membrane cleaning methods are currently in use

including physical, chemical, biological, and enzymatic depending on the configuration of the module, the chemical resistance of the membrane as well as the type of foulants faced [383].

In chemical cleaning, which is the most important membrane cleaning method, the chemical agents added react with the charged foulants. This reduces the cohesion forces between foulants and between foulants and membrane surface through either removing the foulants from the membrane surface, or changing the morphology and the surface chemistry of the foulants [145,384]. Different chemical agents are currently used to remove the foulants accumulated on the RO membrane surfaces including alkaline chemicals, salt solutions, acids, and surfactants [378]. Acids (e.g. citric acid, hydrochloric acid, nitric acid, and sulfuric acid) and alkaline (e.g. sodium hydroxide) chemicals are usually used for RO membrane cleaning, where organics and biofilms are removed using the alkaline chemicals whereas scaling is removed using the acid agents. Moreover, ethylene diamine tetra acetic acid or EDTA is considered the most widely used chelating agent [383], whereas SDS is the most common surfactant used for membrane cleaning. Studies have revealed that unlike the alkaline agents, organic foulants (especially in the presence of calcium) could be removed effectively using surfactants, EDTA, and sodium chloride at high pH [385]. In addition, different parameters need to be considered while using chemical agents for membrane cleaning such as pH, operating conditions (temperature and pressure) as well as the washing time [386]. Moreover, the extensive use of cleaning agents leads not only to significant additional operational costs but also to environmental and health issues [381,387,388].

Different studies have reported interesting results through the chemical cleaning of membranes. For instance, one study has reported the effectiveness of utilizing the two stage cleaning method to clean membrane (fouled with organic and inorganic matters) using a base (NaOH) and a surfactant followed by acid [384]. Another study have revealed that a better membrane cleaning efficiency can be attained by combining different chemical agents given that these agents would have a complementary cleaning mechanisms [378]. Moreover, another study has proved the effectiveness of using EDTA, SDS, and NaOH cleaning agents for the RO membranes fouled with licorice aqueous solutions [383]. In another study [389], the chemical cleaning protocol for membrane fouled with both organic and inorganic matter was investigated. The cleaning method showed that the optimum efficiency and complete restoration of the membrane permeability utilized two cleaning stages including acid cleaning followed by alkaline cleaning with NaOH and surfactant solution. Another study [381] has investigated the effectiveness of utilizing free nitrous acid (FNA) as a cleaning agent for seven different fouled membranes. Results have revealed that FNA can be used for both biomass and calcium carbonate scaling removal [381]. In a study by Yu et al. [390], the effects of common alkaline and acid cleaning on membrane cleaning was investigated. Results have revealed that the use of the common agents have not only removed around 94% and 90% of the total bacteria available on the membranes, but also altered the microbial communities structure. It is worthwhile mentioning that different chemical agents have different efficiencies towards the removal of different foulants. Examples include the limited removal efficiency of both acid and alkaline for calcium salt scales.

On the other hand, current research interests are directed towards improving self-cleaning membranes [391]. Examples include the self-cleaning membrane created through coating the RO membranes with TiO_2 [392].

4. Pre-treatment technologies

Pre-treatment is considered one of the very critical strategies in all RO desalination systems as it has a direct effect on the membrane fouling and could improve the feed water properties in order to ensure a reliable and smooth operation. This would increase the membrane lifetime, as less foulants/contaminants will be deposited on the surface of the membrane. A successful selection of pre-treatment systems is directly related to understanding the feed water composition and type of contaminants encountered. Many researchers are heavily concerned with improving the overall operation of the RO systems through improving the pre-treatment systems in order to minimize membrane fouling and scaling and improve the removal of suspended solids and dissolved organic matters. RO pre-treatment technologies may be either conventional including coagulation-flocculation, media filtration, disinfection, scale inhibition or non-conventional such as MF, UF, and NF [145,391,393–395]. As per the available literature, UF, MF and coagulation-flocculation are considered the most widely used pre-treatment technologies. The following sections will highlights the most widely used pre-treatment technologies.

4.1. Conventional pre-treatment technologies

The most critical step in selecting the most appropriate pre-treatment technology prior to the RO membrane is the full comprehension of the feed water quality. The basic physical RO pre-treatment step include both pre-screening and sedimentation, however, advanced physical and chemical pre-treatments are still required to achieve the best possible feed water quality.

4.1.1. Coagulation–flocculation

Coagulation is related to the removal of organic matters, aqueous particulates, and colloidal foulants that have low molecular weight and cannot be removed the gravitational force [66]. Thus, a better sedimentation and removal of the organic matter can be achieved by adding coagulant chemicals such as aluminum sulfate, ferric sulfate, powdered activated carbon, cationic polyacrylamide, polyaluminum chloride, ferric chloride, etc. [396,397]. Two main coagulation processes are available which are chemical coagulation and electrocoagulation (EC) [398]. Flocculation follows coagulation which is usually referred to as a slow mixing step of the microflocs that leads to the formation visible particles that can be removed by sedimentation (through gravitational force), flotation, or filtration [145].

In a study by Peiris et al. [399], three natural water constituents (humic substances (HS), protein-like and colloidal/particulate matter) were characterized and assessed by adding polyaluminum chloride as coagulant in UF membrane systems. Results have indicated that both HS and protein-like matter contributed to the irreversible fouling unlike the colloidal/particulate matter. Another study [400] has investigated the efficiency of removing both total suspended solids TSS and

turbidity by EC using iron electrodes. Results have revealed that EC can attain up to 99% removal of total suspended solids TSS and 98% removal of turbidity [400]. On the other hand, many studies have investigated the efficiency of coagulation for the removal of arsenic from seawater. Examples include the reported reduction of manganese contained in wastewater using $AlCl_3$ as a coagulant, where the results showed that the initial manganese was reduced by 99.8% [401].

4.1.2. Disinfection

Disinfection is another critical pre-treatment technology due to its important role in destroying microorganisms that are responsible for biofouling. Several disinfection techniques are currently used for pre-treatment mainly chlorination, ozonation, ultraviolet, potassium permanganate, and ultrasound [5,16,402]. Chorine is one of the most widely used disinfectant as it reacts with the water to produce hypochlorous and hydrochloric acids that destroy the microorganisms [145]. However, some of the by-products associated with using chlorine as a disinfection step (such as trihalomethanes and haloacetic acids) has pushed towards finding alternative oxidizing agents such as the ozone [403]. Table 10 summarizes findings of few studies utilizing different disinfection pre-treatment technologies for mitigating membrane fouling.

Table 10. Summary of studies on different disinfection pre-treatment technologies

Pre-treatment Technology used	System Description/Characteristics	Study findings	Reference
Chlorination	• Coagulation and chlorination were tested as pre-treatments of greywater by two-step membrane filtration (ultrafiltration followed by RO desalination). • Feed greywater characteristic were as follow: turbidity of 34 NTU, 24.9 mg/L TOC, 4.6 mg/L TN & 0.7 mg/L TP. • Ferric chloride was utilized as a coagulant	Results revealed that the UF flux decline by 43% utilizing a coagulant dose of 50 mg/L mainly due to 38% decrease of the organic load.	[404]
	• RO pre-treatment of the Fujairah reverse osmosis plant consists of a dose of 25 mg/L H2 SO4, 5 mg/L FeCl3 and 1.5 mg/L polymer	Results showed that intermittent chlorination is a better solution to avoid bio fouling usually resulted from continuous chlorination	[405]
Ozonation	• The effect of Foam fractionators in the absence/presence of ozone, was evaluated for the removal of solids including	Results reported the presence of ozone improved both removal rates of heterotrophic	[406]

	suspended solids, volatile suspended solids and dissolved organic carbon • The effect of ozonation on the removal efficiency of heterotrophic bacteria was evaluated through ozanation	bacteria as well as the suspended solids, volatile suspended solids	
Ultrasound	• The effect of power ultrasound at different frequencies and sonication time on Bacillus subtilis was evaluated	Results have revealed that a significant increase in Bacillus species kill percent is attained as the duration of exposure and intensity of ultrasound is increased (20 and 38 kHz)	[16,407]
	• Industrial water was treated with different combinations of shear, micro-bubbles and high-frequency, low-power ultrasound to test the effect on bacteria and algae growth	Results have shown that both sessile and planktonic biological growth is controlled due to the environment formed by ultrasonic waves which stabilizes and reduces the biofilms formed	[16,408]

4.1.3. Scale inhibitors

The best pre-treatment technology for addressing the membrane scale growth mechanisms is the use of scale inhibitors. Generally, both the chemical and physical properties of the inorganic foulants are changed using scale inhibitors such as polyacrylates, organophosphonates, and sodium hexametaphosphate [409]. In [409], the efficiency of polyaspartic acid and its derivative was evaluated against a commercial antiscalant. Results have revealed that the polyaspartic acid and its derivatives showed better water recovery rates. Other studies have proved the effectiveness of using of different antiscalants including commercial antiscalants, Permatreat 191, Flocon 100, and ammonium biflouride for improving the RO membrane performance [391,410,411].

4.2. Membrane pre-treatment technologies

Membrane pre-treatment technologies have gained an increasing attention due to the various limitations associated with the conventional pre-treatment technologies. The main concept here is to use membranes with higher pore size such as MF (100–5000 nm), UF (10–100 nm) or NF (1–2 nm) prior to the RO membrane so that water with better quality is attained. This will extend the design life of the RO membrane as less foulants would be encountered [5,391,412]. Many studies have shown that utilizing UF and MF may lead to a 100% foulant removal efficiency under certain conditions [413]. Membrane pre-treatment is favored over the conventional pre-treatment due to

its ability to produce better quality water which would lead to an improved RO operation and lower RO pressure drops (due to lower fouling) and thus result in energy savings, increased lifetime of the membranes, enhanced flux and decreased costs associated with chemical agents and sludge disposal. Many recent studies have investigated the performance of MF, UF, and NF pre-treatments. MF can remove suspended solids and bacteria that are higher or equal to 0.1 μm. Many investigations were made using MF pre-treatment to RO, for example, in [414], the efficiency of utilizing a three step pre-treatment system consisting of a flocculation, two-step filtration, and MF was investigated. Results have revealed that the combination of filtration with flocculation is an effective pre-treatment method to MF for desalination. Another study has investigated the efficiency of using both chlorination and MF as pre-treatments of a desalination plant for in the removal of Bacillus sp. Sea-3 and Pseudomonas sp. Sea-5. Results have indicated good removal efficiency, however a negative effects of the chlorination by-products have led to regrowth of the bacteria [415]. In [416], a pre-treatment system consisting of MF and slow sand filtration (SSF) was utilized and compared prior to the RO membrane. Results have shown that the RO membrane was more stable and effective with MF pre-treatment compared to the slow sand filtration (SSF) due to the fact that more foulants were found deposited on the membrane surface during SSF pre-treatment.

UF is used widely with RO systems and has a broader applications compared to the MF. This is due to the various foulants that can be rejected by the UF membranes such as viruses, bacteria, pathogens and suspended organics as well as its ability to produce water with lower fouling potentials when coupled with the RO [417]. Akhondi et al. [418] has recently reported his findings regarding the gravity-driven membrane (GDM) UF that was used as a pre-treatment for RO. The operating parameters were set for the experiments at temperatures of 21 and 29 ^{o}C and hydrostatic pressures of 40 and 100 mbar. Results indicated a significantly lower RO fouling. Another study [419] investigated the use on granular activated carbon (GAC) adsorbent as a step to remove dissolved organic carbon (DOC) prior to using UF. Results showed that this combination for the pre-treatment is very effective in reducing the RO fouling potential as it reduces both slit density and turbidity by 70% and colloids by 90%. Moreover, a study was conducted to evaluate and compare the performance of dissolved air flotation (DAF) - dual-media filter (DMF) and dissolved air flotation (DAF) – UF pre-treatment techniques for the removal of dissolved organic matter. High microbial elimination was maintained by the two treatments with turbidity level maintained at less than 0.1 and SDI maintained at less than 2. Also, it is worthwhile mentioning the UF was removed all algal content compared to only 60% removal through the DMF [420].

Several studies have shown the extensive utilization of NF as a pre-treatment stage in desalination industry in order to overcome the limitations of MF & UF. A recent study by Song et al. [421] explored the use of UF-NF membrane system as a pre-treatment for seawater desalination system. Results have indicated a gradual decrease in the divalent ions rejection rates and permeation flux due to fouling. However, the system has showed effluent with 93.6% TOC removal with time. Another study has highlighted the preparation of novel NF membrane characterized with enhanced

anti-fouling properties. The membrane was prepared through interfacial polymerization of an antibacterial monomer known as polyhexamethylene guanidine hydrochloride (PHGH) and TMC on a polysulfone UF membrane support. Results showed that the membrane salt rejection is in the order $MgCl_2$<$MgSO_4$<Na_2SO_4<NaCl [422].

5. Process design and operation principles

Feed water to the RO plants is generally classified into two broad categories: seawater and brackish water. This widely used classification does not acknowledge the wide variation of the chemical constituents present in the feed. Grouping the water into classes based on the concentration of the chloride ion, and further into subclasses based on the SO_4/HCO_3 molar ratio is suggested by El-Manharawy and Hafez [423]. The "water molar classification" takes into consideration the difference between surface and ground water and correlates the suggested classes to the potential of inorganic scaling after studying 33 running RO plants. Based on these classes, fouling can be predicted, and suitable chemicals for pre-treatment can be identified.

An extensive description of the configurations used to arrange the membranes in either a SWRO or a BWRO plant is available [23]. The terms "stage" and "pass" are indeed identical when looking at the whole process arrangement [23]. The norm, however, is to call the permeate that is further treated with RO (usually in SWRO) a second pass, while the concentrate that is further treated with RO (usually in BWRO) is called a second stage. The RO membrane elements - grouped in one vessel, can be arranged in configurations of passes/stages as the design output dictates.

BWRO and SWRO can be configured in single/multiple stages, single/multiple passes, or a configuration of both. For SWRO, single-pass SWRO systems are used, and addition of a second pass increases the rejection of the solutes and the reliability of the system [424]. Two pass SWRO system can be used when the feed has high salinity, and a permeate suitable for drinking water cannot be produced with good recovery, this is usually the case when there is a limit for a certain constituent like boron, or a disinfection byproduct like bromate [425]. The permeate from the first vessel is sent to a BWRO system that will produce a permeate of low TDS, the reject from the BWRO can be recycled to the first pass to increase the total efficiency of the system. Two pass systems can be either conventional, where all the permeate from the SWRO is further treated in a BWRO or can be split-partial two pass, where the a portion of the permeate in the front SWRO elements (25 to 50%) is collected and blended with the permeate from the second pass, this respectively reduces the cost of pumping in the second pass. However, the total cost reduction should take into account the recovery, and the concentration of the recycled second-pass reject [426].

In multiple passes configuration, the first pass operates at lower pressure than what would be needed in a single pass, the low flux results in low fouling potential; however, the brine lost in the first stage lowers the recovery of the whole process [23].

Regarding the overall layout and arrangement of the RO trains, ref. [23] describes the "three-center" arrangement where the components of the system are grouped in three centers: the high pressure RO feed pumping center, the membrane center, and the energy recovery center. The three center arrangement has the advantage of being flexible to deal with fluctuations in the water demand because only few large pumps are used, the pump curves are flatter for the large pumps, and hence the flow rate can easily be manipulated without much effect on the pressure. Bigger pumps also have the advantage of high efficiency. The distribution piping for the membrane center is costly, but according to reliability analysis, the arrangement has the advantage of being more flexible and reliable, the system availability (the percentage of time in one year during which the plant has operated at or above its design capacity) is 98% compared to the average of 95% in the commonly used train arrangement in which the trains have their own transfer pump, cartridge filter, high pressure pump, and energy recovery system [427]. It has been predicted that the three center arrangement will be used more frequently in the future as the RO systems will become primary source of water and there will be a need for more flexible arrangements to meet the diurnal fluctuation in demand [23].

In designing an RO system there are some technical trade-offs that need to be considered:

- The tradeoff between the permeability and the selectivity of the RO membrane. Brackish water membranes usually have high flux and low salt rejection while on the contrary, seawater membranes have low flux high salt rejection [34]
- Increasing the temperature of the feed increases the flux but decreases the salt rejection. High temperatures also increase the osmotic pressure and accelerate biofouling [34,427]
- Increasing the recovery will decrease the size of the membrane needed to process a certain flow, but increases the pressure needed to process it (capital cost vs. operational cost) [428]

The selection of the RO process configuration is based on engineer's experience and commercial preference. In the pursuit of arriving at the optimum configuration using an objective systematic approach, the problem is formulated as multi-integer non-linear programming problem, and multi-objective optimization is used to obtain the best RO process arrangement by systematically searching for the best arrangement, usually with the objectives of minimizing capital and operating costs (which are usually combined with other costs to obtain the total water price "TWP"), and constraints on water recovery rate, and energy requirements. Vince et al. [429] considered the operating pressure and the total membrane area as an objective. Optimization with other objectives like energy recovery [430], boron rejection [431], split partial second pass operation [432], or increasing the permeate flow under the constraint of a predefined concentration [433] are also studied. Genetic algorithms have been used in other studies [433,434].

The effect of the feed quality and the product specifications was investigated by Lu et al. [435]. The study presented optimum process configurations for different feed water concentrations covering the range of the seawater and the brackish water, and also for different product

concentrations, with the objective of minimizing the total annualized cost while respecting the thermodynamic, technical, and flexibility constraints.

Beside the TWP, Antipova et al. [436] used an environmental indicator to account for the environmental impact of the process. Results by Vince et al. [429] show that 90% of the environmental impact is caused by the electricity consumption which is usually generated off site from non-renewable sources. The difficulty in quantifying the impacts from liquid discharge into water bodies affects the results from such studies. The total recovery rate together with electricity consumption were used as two environmental performance indicators (which are essentially conflicting objectives). So, the design considers a trade-off between the economic objectives and the environmental objectives.

In an effort to aid designers, Kotb et al. [437] developed charts for the determination of the suitable configuration based on the feed flow rate and the pressure. The work is based on the relationship between the permeate flow rate and the permeate cost. Different possible configurations were represented as sagging curves, with the lowest point being the minimum cost for the produced permeate at a certain permeate flow. The same configuration can produce two different flows at the same cost, therefore, the higher flow should be chosen. There are also points where the minimum cost can be achieved by two different configurations, the configuration with the less number of stages is then recommended. Using the aforementioned curves to help in choosing the best configuration and in estimating the production cost without the need for long computations, contour charts were developed. The best configuration can be chosen based on the feed pressure and the feed flow rate. For 10 configurations ranging from single stage, two stage, and three stage arrangements, the charts give the minimum overall cost, the targeted permeate flow, and the targeted membrane area for different configurations. The results should then be compared to arrive at the best choice.

Within the pressure vessel, there are two configurations for the membranes: standard, and internally staged design (ISD). In a standard configuration, all the elements in the vessel are alike, this causes high flux from the first elements and low flux in the last elements downstream due to the drop in pressure and the concentration of the feed as it travels along the vessel. In an ISD, the first element is high rejection/low permeate, the second is standard permeability and salt rejection, and all the other elements are high permeability/low salt rejection elements. This results in feed energy being preserved and allowing higher flux in the downstream elements [427,438].

Much of the energy supplied by the high-pressure pump exists the system in the concentrate stream. Recovery devices are used to recover part of this energy. The energy in the concentrate stream is proportional to the difference in pressure between the feed, and inversely proportional to the recovery, thus energy devices are less frequently used in BWRO [439]. The energy is recovered from the brine side of the process through either [440]:

- Centrifugal energy recovery devices, which are basically small watermills onto which the concentrate is jetted. These include:

    - Reversible pumps (Francis turbine)
    - Pelton turbines
    - Turbochargers (Hydraylic turbo boosters HTB)
- Isobaric systems, recovering 93 to 96% of the concentrate, include:
    - Pressure exchanger (PX) developed by ERI, which is a ceramic rotor mounted in a stationary ceramic sleeve. A brief contact between the concentrate (at high pressure) and the feed (at low pressure) exchanges the pressure with minimal mixing. ERI PX has a modular design, giving it high flexibility
    - DWEER (Dual Work Exchanger Energy Recovery system), on which two pistons each one equipped with 2 check valves, working harmonically in a manner similar to a double acting piston pump
    - SalTec device developed by KSB [441]

Other energy recovery devices are being developed with the aim of reducing the energy consumption of SWRO below 2 kWh/m^3 [441].

Materials of construction for pipes, valves, and energy recovery devices are chosen based on their mechanical strength to withstand the pressure, and their corrosion resistance in chloride containing environments with focus on the resistance to pitting and crevice corrosion. Olsson [442,443] recommends the use of highly alloyed austenitic grades or duplex stainless steel, for the high corrosion resistance and the reduction in gauge, weight, and cost. Below is a summary of applications of different stainless steel grades in the RO plant [427]:

- 316L for permeate and low salinity brackish water
- 904L duplex stainless for permeate and high salinity brackish water
- 254 SMO super austenitic stainless steel, and SAF2507 super duplex stainless steel for all applications
- PVC for low pressure permeate lines

Operation pressure and flow in RO systems are limited by high and low bounds for pressure where the high bound represents the membrane mechanical resistance and the low bound is the pressure to achieve the desired permeate concentration. The pressure in fact does not affect the rejection of the salt, but merely increases the water flux, thus appearing to increase the salt rejection [427]. For the flow, the upper bound represents mechanical loads, and the lower bound is the lowest recommended flow to avoid fouling [444,445].

From an operational review for 50 SWRO and BWRO plants worldwide, the following parameters can be used to benchmark an RO plant from operational prospective [427]:

- Meeting the design specifications, for the product quantity and quality
- Energy use kWh/m^3
- Operation and maintenance costs per m^3
- Plant operational availability (percent of time per year)

- Cartridge filter replacement frequency
- RO membrane cleaning frequency
- RO membrane replacement rate

One of the aspects of the permeate quality that can be handled by adjusting operation parameters is the born concentration. Based on data from toxicological tests on animals, the World Health Organization (WHO) [446] have set a provisional guideline for boron in drinking water at a value of 0.5 mg/L. WHO justifies designating the guideline value as provisional, because of the difficulty to achieve this concentration with the technology available. The concentration of boron in seawater has an average value of 5-6 mg/L [447], desalinated water from thermal methods is essentially free of boron, but boron in water produced from membrane desalination is a big challenge, since boron exists in seawater mainly as uncharged boric acid [448] which has low rejection in RO membranes.

Hilal et al. [449] discussed the importance of boron removal from seawater, as it may have adverse effect on flora and fauna if its concentration is more than required or more than tolerable [447,450]. In seawater, boric acid and borate ion exists in an equilibrium that is a function of pH, temperature, salinity, and pressure (Fig. 12). The importance of this equilibrium is that borate ion is much easier to remove in RO membranes (95% rejection) compared to boric acid (~50% rejection).

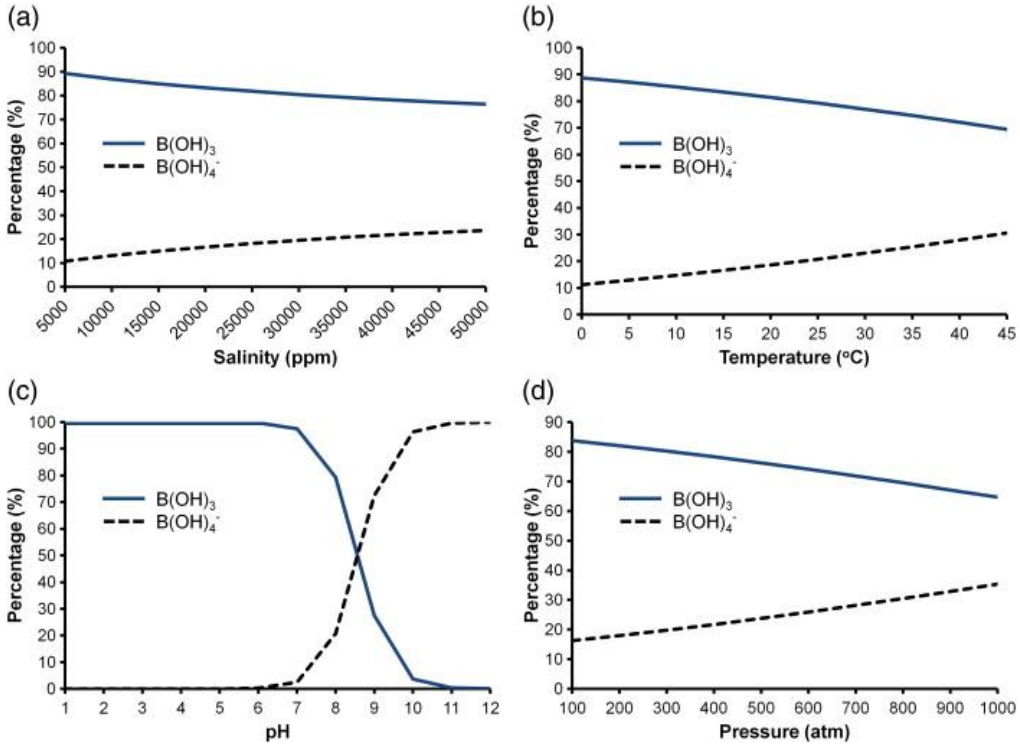

Fig. 12. The distribution of boric acid and borate in seawater by the changes of each parameter. Notes. (a) pH = 8, temperature = 25 °C, pressure = 1 atm (b) pH = 8, salinity = 35,000 ppm, pressure = 1 atm (c) temperature = 25 °C, salinity = 35,000 ppm, pressure = 1 atm (d) pH = 8, temperature = 10 °C, salinity = 34,800 ppm (adopted from [449])

Since the equilibrium is strongly dependent on the pH (as shown in Fig. 12) it is common to operate the RO plant at high pH (8.8 or more) in order to achieve high rejection of boron [23]. Boron rejection is directly proportional to pH, feed pressure [451], and feed boron concentration [452], and is inversely proportional to feed temperature, feed salinity, and recovery [452–454]. Feed flow at constant membrane pressure has no effect on boron rejection [455].

6. Energy and economic considerations

Compared to the other desalination methods, RO today has the lowest energy demand and the lowest unit water cost. This is believed to be a result of research supported by federal governments in the US and elsewhere mainly between 1952 and 1982 and dissemination of the obtained information.

The cost of water produced by RO has dropped from $\$2/m^3$ in 1998 to $\$0.5/m^3$ in 2004 [428]. This drop in the TWP is attributed to the competition, as well as to the improvements in process and membrane technology. Ghaffour et al. [441] further discussed these developments and mentioned that the cost of desalination, in general, has dropped to values that made it a viable option, comparable even to conventional water treatment methods [456]. These developments include: increased salt rejection, reaching 99.8% in commercially available membranes [186], increased efficiency of the energy recovery, thus reducing the specific energy consumption [17], increased flux [297], development of low fouling membranes [183], and development of high boron rejection membranes, eliminating the need for a second pass [457]. Improved membrane performance also leads to decreased need for chemical use, improved membrane life, and increased capacity to work at higher pressure. An insight on how RO technology developed, it can be concluded from the affirmation that the values for the permeate flux in the membranes available today are the highest practical flux. Further increase in the flux will not result in considerable savings in power, when the osmotic pressure of the concentrate increases [428]. Moreover, the decrease in cost has led to increase in plant capacity, which in turn leads to lower capital cost per unit volume of product [456]. Beside the improvements in performance as the technology matures, other factors contributing to the cost drop include the nature of the BOO/BOOT contracts [458,459], which has led to optimization of design and operation, hence reducing the cost.

For the combination of low cost and energy consumption, membrane desalination plants account for 70% of the desalination plants installed in the past 20 years [460]. Nevertheless, RO is still energy intensive [461], highly dependent on the energy prices, and affects the environment by its energy footprint.

Blank et al. [462] discussed the limitations in the economic studies that evaluate the desalination processes. Factors that often get neglected when quoting the total water price are subsidization for the energy or the water price for the consumer, inflation rates, distribution cost, financing cost, and overall cost for desalinated water supply at the consumer's tap. Blank et al. [462] suggested that considering merely the transportation and storage costs (and not the real cost of energy) has

actually resulted in an underestimation of the real cost of desalination. This has, in turn, resulted in a "standstill of the technological progress" as claimed by Blank et al. [462].

Economic analysis from Garg and Joshi [463] agrees with Blank et al. [462] that government subsidy is a factor affecting the techno-economic performance of hybrid systems. Ghaffour et al. [441] also discussed the reasons why reported total cost varies between one plant and another, and administrative costs, including the profit to the provider, are commonly ignored. Suggestions are also made to consider impact on environment and apply life cycle assessment (LCA) instead of the \$/m^3 unit costs [40]. Cherif and Belhadj [464] presented a breakdown for the water cost in SWRO and BWRO plants as shown in Fig. 13.

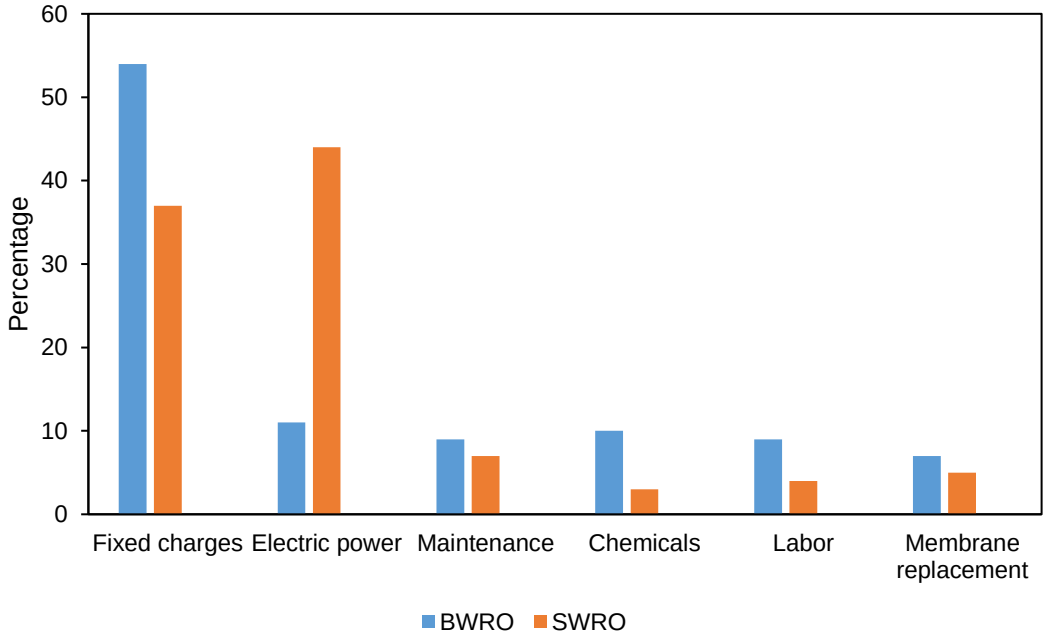

Fig. 13. Water cost breakdown for BWRO and SWRO [464]

Electric power has high contribution to the water cost, especially in SWRO plants. The power needed to drive a certain flow at a certain pressure is $P = Q_f \cdot p_f$, for RO the minimum pressure is the osmotic pressure, which is a function of the solute concentration. For infinitely small number of moles n_w processed at recovery close to zero, the power can be expressed as the product of osmotic pressure, molar volume of water, and the number of moles processed as $\pi_s \cdot \bar{V}_w \cdot n_w$. Incorporating the recovery R to account for the change in concentration, the energy needed for the processes is $E_{thermodynamic,min} = \frac{1}{R}\int_0^R \pi \, dR$ [464].

In SWRO, the highest operating cost goes for energy, and the most energy intensive part of the process is the membrane process itself [17,439], a recent study suggests 2.54 kWh/m^3 amounting for 71% of the total plant energy consumption. The rest of the energy goes as: 10.8% for the pre-treatment, 5.0% for the product water delivery, 5.3% for the intake, and 7.6% for other facilities

[461]. This typical 71% share of the energy referred as the specific energy consumption which ranges between 2.5 to 4 kWh/m^3 in SWRO [439], which can be compared to a thermodynamic limit of a minimum theoretical 0.76 kWh/m^3 of permeate for a 35 g/L feed [465]. However, the practical recovery range around 50% raises limit to 1.1 kWh/m^3 [466]. Karabelas et al. [467] further breaks down the specific energy cost within the membrane process into: 50% to overcome the osmotic pressure, 25% on membrane filtration resistance, 20% on pump and energy recovery device inefficiency, 2.5% for the concentration polarization, 2.5% friction losses in the permeate and the concentrate. Percentage of energy consumption data from [461] and [467] are compiled in Fig. 14.

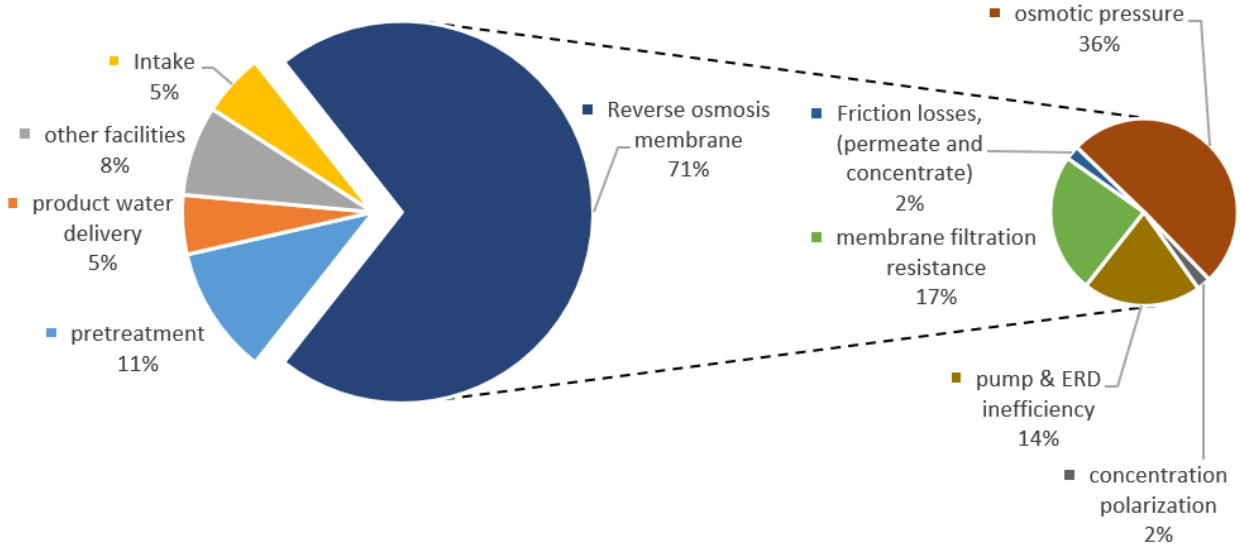

Fig. 14. Percentage of energy consumption in SWRO. Data from [461] and [467]

The following points suggested in literature in order to help reduce the cost of water produced from RO:

- Savings in capital costs are achieved by the shift from the current 8 inch widely adopted pressure vessel industry standard to higher pressure vessel diameters. This leads to fewer element connections, and possible footprint reduction. A report prepared by a consortium of membrane suppliers recommended using 16 inch pressure vessels. It reduces the RO facility construction cost by 15% for SWRO and 30% for BWRO, respectively, which is translated into savings of 5% and 10% in life cycle cost. Use of pressure vessels with diameters bigger than 16 inch have less pronounced effect on cost savings as reported Bartels et al. [468], and will have less flexibility in meeting the market demand.

- High productivity membranes are suggested as a way of improvement in cost savings [461]. However, the improvement can be limited. Operating at low recovery can result in increase in capital and operational cost, while at high recovery the specific energy increases [465,469]. Investigation of the effect of permeability on the specific energy consumption for SWRO and BWRO shows diminishing return beyond the permeability of the membranes available today, as frictional forces increase, the system will hit a "practical energy consumption limit" [470]. Improving the selectivity of the membranes is suggested, the new generation of membranes should overcome the permeability/rejection trade off [15].
- Carbon nanotubes and synthetic nano-channels are good candidates for high selectivity membranes that will acts as a molecular sieve. Although the carbon nanotubes can have high permeability due to low friction, the gains are expected to come from the high selectivity [471]
- Inter stage design (ISD) also referred to as HID (Hybrid membrane inter-stage design) where flux distribution from the membrane elements in a pressure vessel is equalized by using elements of different productivity and rejection [461]. This lowers the pressure requirements by 2 to 6 bars and allows for 26% smaller plants, thus contributing to cuts in both capital and operational costs [438]. In practice, there are variation in performance between one element and another, leading to possible overestimation of the savings from such configurations [427]
- Use of subsurface intakes (SSI) instead of open intake improves the feed water quality, reduces the operation cost, and increases the life expectancy of the membranes. Existing plants incorporating SSI show feed water with low turbidity, low SDI, and near zero algae cells count [472]. This can highly reduce biofouling to which RO membranes are less tolerant compared to thermal desalination [473–475]. Following are three main types of subsurface intakes as discussed elsewhere [424,476]:
    - Vertical, slanted, horizontal and radial collector intake wells, (Sur, Oman SWRO plant with 160,000 m^3/day intake [477])
    - Infiltration galleries: horizontal well with a trench, which is in essence a slow sand filter.
    - Reverbed/seabed filtration system (Fukuoka, Japan SWRO 100,000 m^3/day intake [477])

  For small and medium plants, subsurface intakes (offshore or onshore) overcome the entrainment problems providing savings in operational cost and in capital cost as well, by eliminating the need for rigorous pre-treatment. In large scale plants, the savings are mainly in the operational, as the modular design for subsurface intakes does not benefit much from economy of scale [476] nevertheless, they are better than wells in this aspect [477]. Savings in operation cost should be analyzed then and compared against the needed extra capital [476]. Technical and economic feasibility was investigated for seabed infiltration gallery and beach gallery for a 180 m^3/day plant [477], although the two SSI were technically

feasible the investigators arrived at a conclusion that they are not economically feasible, the savings in pre-treatment operation cost was low compared to the additional capital required. The results are site specific, and the outcome depends on the expected water price and the discount rate [478]

- Seven membrane elements per pressure vessel is widely used in practice. Use of more elements will lower the number of pressure vessels needed in the plant. A plant using six membrane elements in a pressure vessel will require 34% more pressure vessels than if 8 elements are used [149]. By adding an extra membrane element to the 6, 7, and 8 elements arrangement, the capital cost is reduced by 11.3%, 9.4%, and 7.9%, respectively [479]
- Blank et al. [462] presented suggestions to further reduce the cost of fresh water produced from desalination. These include improving the availability of the plant by avoiding shutdowns and designing for easy maintenance, improving the efficiency of the system by improving the pre-treatment and optimizing the energy consumption, and optimizing the combination of energy and water systems

7. Hybrids systems

RO plants can be coupled with power plants, other thermal desalination plants, and with renewable energy sources. Two or more desalination processes can be combined or coupled with a power plant in a hybrid configuration to produce water at a low cost [480].

RO can be coupled with a thermal desalination plant, where the RO can operate at low recovery, producing permeate with relatively high TDS to be blended with a low TDS product from thermal desalination. More integration can be done by feeding the brine from RO to the thermal desalination unit, thereby, the pre-treatment for the thermal plant can be reduced. The hybrid benefits from shared intake and outfall facilities and feed to the RO can be preheated allowing for operation at higher flux and extended membrane life [481]. The aforementioned applies to existing powers plants and thermal desalination plants, i.e., adding an RO plant will decrease the water cost and increase the plant flexibility. However, for a new plant, RO provides water at lower cost. In spite of that, thermal desalination is popular in the Middle East, partly because the plants were established when RO technology was not developed, and partly because of the operational problems linked with the pre-treatment required, high salinity, and hot climate encouraging biological activity [482]. These operational challenges may affect the reliability and availability of RO plants. Another alleged reason is the low cost of energy, Kamal [483] discusses the “myth” that favors thermal desalination, showing that regardless of the energy cost, thermal desalination is more costly than RO, concluding that a new hybrid of thermal and RO desalination is not justified economically. A review for the thermal methods in the GCC suggests that installation of new MSF units is not recommended [484].

7.1. Renewable energy

The environmental impacts from RO, and desalination methods in general, can be shown to have less weight compared to other alternatives like pumping water treated with conventional methods for long distances [456]. The environmental impact from power consumption of the desalination water plants should also be put into prospective. The percentage of the energy that desalination plants consume, as a percentage of the global energy is 0.4% [485], this value agrees with the national levels reported in [486,487]. The social benefit, and the water security the technology provides, should also be taken into account. Nevertheless, incorporation of renewable energy can further reduce the environmental impact of desalination.

Worldwide, 52% of the desalination plants powered using photovoltaic (PV) modules or solar collectors are RO plants [488], 40% of it being PV RO, 8% PV-wind RO, and 4% solar Rankine RO.

7.2. Photovoltaic cells

Herold et al. [489] presented the treatment cost for small scale SWRO PV powered RO (1 m^3/day) at \$16/m^3. A study by Garg and Joshi [463] for a BWRO plant with similar capacity reported the cost at \$5/m^3 and the cost decreases to \$1.37/m^3 when the RO powered by PV is operated in hybrid with NF.

Later studies [490] investigated the economic feasibilities of PV powered SWRO system and reports the TWP as \$0.825/m^3 with payback period of 23.3 years. The savings in the costs are mainly from eliminating the need for batteries by exchanging the power with the grid.

A study on the effect of solar irradiance fluctuation on the productivity of PV powered RO showed that for a wide range of solar constant irradiance values (400–1200 W/m^2), a flux of 5 L/m^2h can be maintained at recovery values above 20% [491]. Improvement on the productivity of the system can be obtained by adding axis tracking to a PV panels. Ahmad et al. [492] reported that the yearly permeate gain made by single and double axis continuous tracking PV panels can be up to 60%.

PV and wind powered RO has been shown to reduce the environmental impact quantified as savings in emissions [480,493]. When used in rural areas where there is no other supplies of water, other factors rather than the TWP are important in choosing the water treatment process and the energy source, such as the ease of operation and maintenance.

7.3. Solar Rankine cycle

Davies [494] designed RO working in a batch mode where the mechanical power in the form of steam is supplied from a solar Rankine cycle to drive the piston pump to pressurize feed water into the RO membrane. Such system can be coupled to existing solar Rankine cycle plants originally designed to produce electricity. However, TWP was not presented and economic evaluation was not provided. It was suggested that the method utilizing solar collector would be less costly than PV cells. Other studies [436,495] also investigated retrofitting a SWRO plant with solar Rankine

cycle and considered the environmental impacts in designing the system. The retrofitting increased the cost from \$1.21/m^3 to \$1.38/m^3 (14% higher) at the expense of reducing CO_2 emissions by 55%. A BWRO in combination with solar cycle operated with CO_2 (where the CO_2 is cooled by recovering the cryogenic energy of LNG was) presented by Xia et al. [496]. A bibliography of the work published in the PV modules and solar thermal collectors with RO is provided elsewhere [497].

7.4. Wind energy

In coastal areas, wind powered RO plants are favorable [149,498] where the wind power can be converted to electrical power to run the pump or directly used to run the pump shaft [499]. To overcome the intermittence in power supply, the following is suggested: adjustment of the RO capacity, combining wind power with another source of power, or to the grid, and the option of storage batteries or a fly wheel energy storage device [498,500]. García-Rodríguez et al. [501] quantified the effect of plant capacity, wind speed, and energy requirement for the plant on the cost of the produced water were studied.

Economic feasibility of wind powered RO plants shows that the costs are almost entirely fixed costs (83%), since energy, which is the main contributor to the variable cost, is not applicable, and the wind turbine maintenance cost for the amounts to only 1% of the water cost. So reduction in cost can be achieved if high water production can be obtained from the available power [502].

7.5. Forward osmosis (FO)

Forward osmosis can be combined with RO, where wastewater can be used to dilute seawater, thereby reducing the specific energy required from 2.5-4 kWh/m^3 to 1.5 kWh/m^3 [503]. In a study by Yangali-Quintanilla et al. [503] seawater was used as a draw solution without pretreatment, the effect of fouling on the FO membrane was reversed by air scouring, and the flux was restored to 98.8% of the initial flux [503]. A similar setup with focus on reducing the pre-treatment sludge in SWRO, directed the sludge from media filter backwash to an FO membrane, where concentrate from the SWRO was used as a draw solution. The results of the study showed decrease in sludge volumes, increase in water recovery, and increase in the solid contents of the sludge [504]. Applications for FO/RO hybrid were also investigated for use in space missions, where FO, together with osmotic distillation (OD) is used as pretreatment for RO. OD was added because high rejection for urea was required [505]. The FO/OD/RO hybrid had the advantage of being lighter in weight, consumed low energy, and exhibited a recovery close to 100%. RO and FO can also be coupled to a membrane bioreactor (MBR) for wastewater treatment. In this combination, FO membrane is immersed in an MBR and the draw solution is treated by RO. The permeate is the clear product and the concentrate is recycled as a draw solution [506].

7.6. Pressure retarded osmosis (PRO)

The theoretically proved concept of pressure retarded osmosis (PRO) still needs improvements to make it a viable solution. The difference in osmotic pressure between seawater and SWRO plant

concentrate can be used to drive flow that can be used to produce power from a hydraulic turbine. The feed solution can also be wastewater, although biofouling in this case can be high due to presence of microorganisms in the wastewater [507].

In two stage SWRO configurations, concentrate streams from the first and the second stage will have different concentrations. Harnessing this driving force using PRO has been investigated, and since the concentrate from the second stage is usually available only at low flowrates, the energy recovery from such integration was found to be limited [508].

7.7. Waves energy

Kinetic and potential energy from ocean waves can be harvested and utilized in desalination plants, which are commonly placed at seashores. Wave energy converters are available in different designs such as [509]:

- Oscillating water columns: The height of a water column, with an opening at the top, is allowed to change by the waves movement. The pressurized air at the top of the column is used to run a turbine
- Overtopping systems: Operates in a similar way to hydro-generation, the potential energy from waves overtopping a barrier at the seashore, is used to fill a reservoir and run a turbine at the bottom of the reservoir

These wave energy converters can be used to generate electricity to be used in desalination, as in the 10 m^3/day plant described by Sharmila et al. [510], or can be used to directly drive the RO pump by the head of the water column obtained from wave energy (WaveCatcher), or using a buoy on the ocean surface directly connected to the RO pump at the sea bed (Delbuoy). Plants with 1.1 m^3/day capacity were tested, and resulted in 20% recovery as presented by Leijon and Boström [509]. The hybrid is still in early development stages, but is expected to give production in the range of 1000 to 3000 m^3/day at a cost of 0.7 to 1.2 \$/m^3 [485,511].

8. Technological challenges

In spite of the fact that RO is a well-established and the most widely used water desalination technology, extensive research efforts and innovations are currently being made in order to address the key challenges faced by the RO desalination process. RO membrane fouling can be considered as the top challenge [512]. Recent studies on novel membrane synthesis and membrane modification (discussed in this review) have made an attempt to enhance the membrane fouling resistance. However, the applicability of such membranes beyond the laboratory still needs to be explored. Nanotechnology has been of great interest to researchers for the synthesis of fouling-resistant TFN RO membranes. However, the high cost, scale-up difficulty, and health and safety concerns pertinent to the use of nanoparticle additives is still a concern that needs to be addressed [186]. In addition, the surface modification techniques need to be further investigated in order to validate their effectiveness in long-term operations. Therefore, future research efforts on the modified RO membranes should be directed towards long-term fouling tests in order to investigate

the stability of the employed modifier/coating material. Furthermore, the trade-off between membrane transport properties and antifouling characteristics needs to be optimized.

Another key challenge related to the utilization of the polyamide RO membranes is the fast degradation and disintegration of the membranes in the presence of chlorine (one of the most common disinfectants in water treatment systems). Chorine is defined as a biological microorganism inhibitor that is usually used in the pretreatment unit in order to prevent membrane degradation. Thus, new studies have focused the use of new novel membrane materials such as sulfonated polysulfone composite membranes that are characterized mainly by their significant resistant towards chlorine. The development of such chlorine-resistant membrane materials may have a significant and direct impact on the overall cost of the RO technology as it would minimize the need of de-chlorination of RO feed and re-chlorination of treated water [34,513]. Studies have indicated that in spite of the promising findings regarding the development of chlorine-tolerant RO membranes, producing a highly reliable and stable membranes is one of the key challenges and significant efforts are still needed to attain progress [184]. As a result, continued efforts are required to further investigate the chlorine resistance of TFC RO membranes.

The discharge of brine is another challenge that needs to be further investigated. RO brine is usually discharged to local water bodies or directly to the sea which has significant negative environmental impacts and establishes a real threat to the ecosystem. Usually the brine reject is discharged to the sea which would result in changing the alkalinity, salinity, and average temperature of seawater. Brine flowrates are usually high and can reach around 40% of the intake flowrate. The reject brine characteristics depend strongly on the feed water quality, the desalination technology implemented, additives used, and recovery percentage. The current brine discharge methods that are currently in use include direct discharge into surface water, deep well injection, and evaporation ponds [514]. These options are still limited and are not yet providing practical solutions to the environmental challenges. Efforts are currently done to find more environmentally friendly and economically feasible options to solve this issue [515]. Zero Liquid Discharge (ZLD) or near Zero Liquid Discharge operations are developed to reduce the brine volume, either by thermal means (like evaporators and crystallizers) or by integration of processes (like forward osmosis [516], membrane distillation [517], or electrodialysis [518]). Possible brine treatment options include reducing/eliminating brine disposal, salt recovery, and brine industrial use [515]. In such cases, salts recovered from the concentrate are a by-product from the desalination process [519]. A new possible approach is through reacting the reject brine with CO_2 by which the modified Solvay process is utilized to convert the brine into reusable solid product namely sodium bicarbonate while the treated water can be utilized for irrigation purposes [514,520].

Another interesting area that needs further investigation and study is the performance of RO treatment as a physical barrier against organic contaminants, contaminants of emerging concern (CECs), and pharmaceuticals compounds contained in the water [521,522]. Few studies have indicated the potential of using RO technology for the removal of organic contaminants especially the hydrophilic organic compounds as the conventional treatment technologies did not show an

effective and acceptable removals. However, the main concern in this case would be the need for a well-design RO pretreatment system. The use of RO membranes for the removal of organic/pharmaceutical compounds could be very challenging particularly for the wastewater streams due to the fact that such streams usually encompass high organic contaminants content as well as the high chances of containing calcium phosphate precipitates which would maximize the membrane fouling problems [34,523].

Although many studies have shown that RO membranes are still permeable to some small micropollutants [524], many other studies have suggested the use of RO as an additional step in wastewater treatment due to its ability to remove organic micropollutants such as bisphenol-A (BPA), salicylic acid, ibuprofen, diclofenac, sulfamethoxazole (SMX), antibiotics, sulfonamides, trimethoprim (TMP), and macrolides [525–529]. Moreover, research needs to be expanded regarding the RO removal efficiency of the disinfection by products as such by-products may pose potential risks to both human health as well as aquatic organisms [530]. Very limited studies have investigated the occurrence, formation, and the behavior of the disinfection by-products in RO desalination plants. In one study [531], the formation of the halogenated byproducts formed in two full-scale RO desalination plants was assessed. Results have revealed that the disinfection by products formed during the prechlorination were removed efficiently [531]. Another study have investigated the fate of the chlorination by-products including trihalomethanes, dihaloacetonitriles, haloacetic acids, and bromophenols under certain conditions [532]. Moreover, another study have studied the formation of 21 disinfection by-products during chlorination in two different desalinated seawater blends (treated drinking water blended with RO permeate and post-treatment (PT) product water). Results have revealed that around sixteen disinfection by-products were detected in both blends during chlorination [533].

Hybrid RO desalination plants require further attention with special focus on the economics of such plants. With its specific energy consumption put at the range of 1.8-2.2 KWh/m^3 [23], RO is less energy intensive when compared to other desalination methods. The technology is believed to have reached a practical limit imposed by the thermodynamic limits and the tradeoff between membrane permeability and selectivity [465]. However, improvements emerge from the possibility of reducing the environmental impacts, and possibly the cost of produced water [490], by using renewable energy sources in hybrid with RO. Most of the studies, however, show higher water prices when renewable energy is used [534].

9. Concluding remarks

Although RO technology was commercialized only 50 years ago, it has become now a well-developed and well-optimized desalination process. Owing to its low specific energy and high reliability, RO has already overtaken the thermal desalination methods. Reductions in cost and energy consumption are attributed to many improvements in the technology including improved membrane properties and performance, optimization of process configuration, and the use of energy recovery devices. The extent of development is demonstrated by the approach to the

thermodynamic limit of the lowest possible energy consumption. However, improvements are still possible in many areas including pre-treatment, integration with renewable energy, brine management, and development of membranes targeting chlorine resistance, fouling, and specific contaminants.

References

[1] M.A. Abdelkareem, M. El Haj Assad, E.T. Sayed, B. Soudan, Recent progress in the use of renewable energy sources to power water desalination plants, Desalination. 435 (2018) 97–113. doi:10.1016/j.desal.2017.11.018.

[2] A. Alkaisi, R. Mossad, A. Sharifian-Barforoush, A Review of the Water Desalination Systems Integrated with Renewable Energy, in: Energy Procedia, 2017: pp. 268–274. doi:10.1016/j.egypro.2017.03.138.

[3] W.L. Ang, A.W. Mohammad, N. Hilal, C.P. Leo, A review on the applicability of integrated/hybrid membrane processes in water treatment and desalination plants, Desalination. 363 (2015) 2–18. doi:10.1016/j.desal.2014.03.008.

[4] United Nations, Water scarcity, (2014). http://www.un.org/waterforlifedecade/scarcity.shtml (accessed January 30, 2019).

[5] S. Jamaly, N.N. Darwish, I. Ahmed, S.W. Hasan, A short review on reverse osmosis pretreatment technologies, Desalination. 354 (2014) 30–38. doi:http://dx.doi.org/10.1016/j.desal.2014.09.017.

[6] S.S. Shenvi, A.M. Isloor, A.F. Ismail, A review on RO membrane technology: Developments and challenges, Desalination. 368 (2015) 10–26. doi:10.1016/j.desal.2014.12.042.

[7] M. Qasim, N.A. Darwish, S. Sarp, N. Hilal, Water desalination by forward (direct) osmosis phenomenon: A comprehensive review, Desalination. 374 (2015) 47–69. doi:10.1016/j.desal.2015.07.016.

[8] M.F.A. Goosen, W.H. Shayya, Water Management, Purification, and Conservation in Arid Climates, 1st ed., Technomic Pub., Lancaster, 1999.

[9] N. Prihasto, Q.F. Liu, S.H. Kim, Pre-treatment strategies for seawater desalination by reverse osmosis system, Desalination. 249 (2009) 308–316. doi:10.1016/j.desal.2008.09.010.

[10] S. Xia, X. Li, Q. Zhang, B. Xu, G. Li, Ultrafiltration of surface water with coagulation pretreatment by streaming current control, Desalination. 204 (2007) 351–358. doi:10.1016/j.desal.2006.03.544.

[11] A. Ali, R.A. Tufa, F. Macedonio, E. Curcio, E. Drioli, Membrane technology in renewable-energy-driven desalination, Renew. Sustain. Energy Rev. 81 (2018) 1–21. doi:10.1016/j.rser.2017.07.047.

[12] G. Micale, A. Cipollina, L. Rizzuti, Seawater Desalination: Conventional and Renewable Energy Processes, in: Seawater Desalin. Conv. Renew. Energy Process., 2009: pp. 1–15. doi:10.1007/978-3-642-01150-4.

[13] P.G. Youssef, R.K. Al-Dadah, S.M. Mahmoud, Comparative analysis of desalination technologies, in: Energy Procedia, 2014: pp. 2604–2607. doi:10.1016/j.egypro.2014.12.258.

[14] P. Cay-Durgun, M.L. Lind, Nanoporous materials in polymeric membranes for desalination, Curr. Opin. Chem. Eng. 20 (2018) 19–27. doi:10.1016/j.coche.2018.01.001.

[15] J.R. Werber, A. Deshmukh, M. Elimelech, The Critical Need for Increased Selectivity,

Not Increased Water Permeability, for Desalination Membranes, Environ. Sci. Technol. Lett. 3 (2016) 112–120. doi:10.1021/acs.estlett.6b00050.

[16] M. Qasim, N.N. Darwish, S. Mhiyo, N.A. Darwish, N. Hilal, The use of ultrasound to mitigate membrane fouling in desalination and water treatment, Desalination. 443 (2018) 143–164. doi:10.1016/j.desal.2018.04.007.

[17] G. Amy, N. Ghaffour, Z. Li, L. Francis, R.V. Linares, T. Missimer, S. Lattemann, Membrane-based seawater desalination: Present and future prospects, Desalination. 401 (2017) 16–21. doi:10.1016/j.desal.2016.10.002.

[18] K. Wang, A. a. Abdalla, M. a. Khaleel, N. Hilal, M.K. Khraisheh, Mechanical properties of water desalination and wastewater treatment membranes, Desalination. 401 (2017) 190–205. doi:10.1016/j.desal.2016.06.032.

[19] A. Altaee, G. Zaragoza, H.R. van Tonningen, Comparison between Forward Osmosis-Reverse Osmosis and Reverse Osmosis processes for seawater desalination, Desalination. 336 (2014) 50–57. doi:10.1016/j.desal.2014.01.002.

[20] P.K. Park, S. Lee, J.S. Cho, J.H. Kim, Full-scale simulation of seawater reverse osmosis desalination processes for boron removal: Effect of membrane fouling, Water Res. 46 (2012) 3796–3804. doi:10.1016/j.watres.2012.04.021.

[21] M. Sarai Atab, A.J. Smallbone, A.P. Roskilly, An operational and economic study of a reverse osmosis desalination system for potable water and land irrigation, Desalination. 397 (2016) 174–184. doi:10.1016/j.desal.2016.06.020.

[22] P.S. Goh, W.J. Lau, M.H.D. Othman, a. F. Ismail, Membrane fouling in desalination and its mitigation strategies, Desalination. 425 (2018) 130–155. doi:10.1016/j.desal.2017.10.018.

[23] S. Burn, S. Gray, Efficient Desalination by Reverse Osmosis : A guide to RO practice, IWA Publishing, London, UNITED KINGDOM, 2015. http://ebookcentral.proquest.com/lib/aus-ebooks/detail.action?docID=4354916.

[24] M.E. Williams, A brief review of reverse osmosis membrane technology, EET Corporation and Williams Engineering Services Company, Harriman, TN, 2003.

[25] T.Y. Cath, A.E. Childress, M. Elimelech, Forward osmosis: Principles, applications, and recent developments, J. Memb. Sci. 281 (2006) 70–87. doi:10.1016/j.memsci.2006.05.048.

[26] J.P. Chen, E.S.K. Chian, P.-X. Sheng, K.G.N. Nanayakkara, L.K. Wang, Y.-P. Ting, Desalination of Seawater by Reverse Osmosis, in: L.K. Wang, J.P. Chen, Y.-T. Hung, N.K. Shammas (Eds.), Membr. Desalin. Technol., Humana Press, Totowa, NJ, 2011: pp. 559–601. doi:10.1007/978-1-59745-278-6_13.

[27] N.B. Singh, S.S. Das, A.K. Singh, Physical Chemistry, Volume 2, New Age International, Daryaganj, India, 2000. http://ebookcentral.proquest.com/lib/aus-ebooks/detail.action?docID=3017399.

[28] A. Yokozeki, Osmotic pressures studied using a simple equation-of-state and its applications, Appl. Energy. 83 (2006) 15–41. doi:10.1016/j.apenergy.2004.10.015.

[29] V.T. Granik, B.R. Smith, S.C. Lee, M. Ferrari, Osmotic pressures for binary solutions of

non-electrolytes, Biomed. Microdevices. 4 (2002) 309–321. doi:10.1023/A:1020910407962.

[30] L. Song, S. Yu, Concentration polarization in cross-flow reverse osmosis, AIChE J. 45 (1999) 921–928. doi:10.1002/aic.690450502.

[31] Z.A. Hu, H.Y. Wu, J.Z. Gao, Calculation of osmotic pressure difference across membranes in hyperfiltration, Desalination. 121 (1999) 131–137. doi:10.1016/S0011-9164(99)00014-4.

[32] J.D. Seader, E.J. Henley, Separation Process Principles, John Wiley & Sons, New York, 1998.

[33] J. Kucera, Reverse Osmosis: Design, Processes, and Applications for Engineers, Wiley, 2010.

[34] L.F. Greenlee, D.F. Lawler, B.D. Freeman, B. Marrot, P. Moulin, Reverse osmosis desalination: Water sources, technology, and today's challenges, Water Res. 43 (2009) 2317–2348. doi:10.1016/j.watres.2009.03.010.

[35] I. Sutzkover, D. Hasson, R. Semiat, Simple technique for measuring the concentration polarization level in a reverse osmosis system, Desalination. 131 (2000) 117–127. doi:10.1016/S0011-9164(00)90012-2.

[36] C. Fritzmann, J. Löwenberg, T. Wintgens, T. Melin, State-of-the-art of reverse osmosis desalination, Desalination. 216 (2007) 1–76. doi:10.1016/j.desal.2006.12.009.

[37] K. Jamal, M.A. Khan, M. Kamil, Mathematical modeling of reverse osmosis systems, Desalination. 160 (2004) 29–42. doi:10.1016/S0011-9164(04)90015-X.

[38] E.M. V Hoek, M. Elimelech, Cake-Enhanced Concentration Polarization: A New Fouling Mechanism for Salt-Rejecting Membranes, Environ. Sci. Technol. 37 (2003) 5581–5588. doi:10.1021/es0262636.

[39] K. NATH, Membrane Separation Processes, PHI Learning Pvt. Ltd., Dehli, 2017.

[40] S. Sablani, M. Goosen, R. Al-Belushi, M. Wilf, Concentration polarization in ultrafiltration and reverse osmosis: A critical review, Desalination. 141 (2001) 269–289. doi:10.1016/S0011-9164(01)85005-0.

[41] R. Salcedo-Díaz, P. García-Algado, M. García-Rodríguez, J. Fernández-Sempere, F. Ruiz-Beviá, Visualization and modeling of the polarization layer in crossflow reverse osmosis in a slit-type channel, J. Memb. Sci. 456 (2014) 21–30. doi:10.1016/j.memsci.2014.01.019.

[42] A.H. Haidari, S.G.J. Heijman, W.G.J. van der Meer, Optimal design of spacers in reverse osmosis, Sep. Purif. Technol. 192 (2018) 441–456. doi:10.1016/j.seppur.2017.10.042.

[43] S. Tielen, Enhancing reverse osmosis with feed spacer technology, Filtr. Sep. 53 (2016) 24–27. doi:10.1016/S0015-1882(16)30039-8.

[44] R.W. Baker, Membrane Technology and Applications, 2nd ed., John Wiley & Sons Ltd., New York, 2004. doi:10.1016/S0376-7388(00)83139-7.

[45] R. Guha, B. Xiong, M. Geitner, T. Moore, T.K. Wood, D. Velegol, M. Kumar, Reactive micromixing eliminates fouling and concentration polarization in reverse osmosis membranes, J. Memb. Sci. 542 (2017) 8–17. doi:10.1016/j.memsci.2017.07.044.

[46] T.J. Kennedy, R.L. Merson, B.J. McCoy, Improving permeation flux by pulsed reverse osmosis, Chem. Eng. Sci. 29 (1974) 1927–1931. doi:10.1016/0009-2509(74)85010-4.

[47] E.M. V Hoek, J. Allred, T. Knoell, B.H. Jeong, Modeling the effects of fouling on full-scale reverse osmosis processes, J. Memb. Sci. 314 (2008) 33–49. doi:10.1016/j.memsci.2008.01.025.

[48] A.L. Zydney, Stagnant film model for concentration polarization in membrane systems, J. Memb. Sci. 130 (1997) 275–281. doi:10.1016/S0376-7388(97)00006-9.

[49] S. Kim, E.M. V Hoek, Modeling concentration polarization in reverse osmosis processes, Desalination. 186 (2005) 111–128. doi:10.1016/j.desal.2005.05.017.

[50] Z.V.P. Murthy, S.K. Gupta, Estimation of mass transfer coefficient using a combined nonlinear membrane transport and film theory model, Desalination. 109 (1997) 39–49. doi:10.1016/s0011-9164(97)00051-9.

[51] G. Schock, A. Miquel, Mass transfer and pressure loss in spiral wound modules, Desalination. 64 (1987) 339–352. doi:10.1016/0011-9164(87)90107-X.

[52] T.Y. Qiu, P. a. Davies, Concentration polarization model of spiral-wound membrane modules with application to batch-mode RO desalination of brackish water, Desalination. 368 (2015) 36–47. doi:10.1016/j.desal.2014.12.048.

[53] S. Bhattacharya, S.T. Hwang, Concentration polarization, separation factor, and Peclet number in membrane processes, J. Memb. Sci. 132 (1997) 73–90. doi:10.1016/S0376-7388(97)00047-1.

[54] E. Lyster, Y. Cohen, Numerical study of concentration polarization in a rectangular reverse osmosis membrane channel: Permeate flux variation and hydrodynamic end effects, J. Memb. Sci. 303 (2007) 140–153. doi:10.1016/j.memsci.2007.07.003.

[55] S. De, P.K. Bhattacharya, Prediction of mass-transfer coefficient with suction in the applications of reverse osmosis and ultrafiltration, J. Memb. Sci. 128 (1997) 119–131. doi:10.1016/S0376-7388(96)00313-4.

[56] R.I.U. Benito J. Mariñas, Modeling Concentration-Polarization in Reverse Osmosis Spiral-Wound Elements, J. Environ. Eng. 122 (1996) 292–298. doi:10.1061/(ASCE)0733-9372(1996)122:4(292).

[57] L. Song, M. Elimelech, Theory of concentration polarization in crossflow filtration, J. Chem. Soc. Faraday Trans. 91 (1995) 3389–3398. doi:10.1039/FT9959103389.

[58] L. Song, C. Liu, A total salt balance model for concentration polarization in crossflow reverse osmosis channels with shear flow, J. Memb. Sci. 401–402 (2012) 313–322. doi:10.1016/j.memsci.2012.02.023.

[59] L. Song, Concentration polarization in a narrow reverse osmosis membrane channel, AIChE J. 56 (2010) 143–149. doi:10.1002/aic.11958.

[60] M. Elimelech, S. Bhattacharjee, A novel approach for modeling concentration polarization in crossflow membrane filtration based on the equivalence of osmotic pressure model and filtration theory, 145 (1998) 223–241.

[61] V. Geraldes, M.D. Afonso, Prediction of the concentration polarization in the nanofiltration/reverse osmosis of dilute multi-ionic solutions, J. Memb. Sci. 300 (2007)

20–27. doi:10.1016/j.memsci.2007.04.025.

[62] K. Madireddi, R.B. Babcock, B. Levine, J.H. Kim, M.K. Stenstrom, An unsteady-state model to predict concentration polarization in commercial spiral wound membranes, J. Memb. Sci. 157 (1999) 13–34. doi:10.1016/S0376-7388(98)00340-8.

[63] D.E. Wiley, D.F. Fletcher, Techniques for computational fluid dynamics modelling of flow in membrane channels, J. Memb. Sci. 211 (2003) 127–137. doi:10.1016/S0376-7388(02)00412-X.

[64] S. Ma, L. Song, S.L. Ong, W.J. Ng, A 2-D streamline upwind Petrov/Galerkin finite element model for concentration polarization in spiral wound reverse osmosis modules, J. Memb. Sci. 244 (2004) 129–139. doi:10.1016/j.memsci.2004.06.048.

[65] U. Merten, H.K. Lonsdale, R.L. Riley, Boundary-layer effects in reverse osmosis, Ind. Eng. Chem. Fundam. 3 (1964) 210–213. doi:10.1021/i160011a006.

[66] W. Zhou, L. Song, T.K. Guan, A numerical study on concentration polarization and system performance of spiral wound RO membrane modules, J. Memb. Sci. 271 (2006) 38–46. doi:10.1016/j.memsci.2005.07.007.

[67] A. Subramani, S. Kim, E.M. V Hoek, Pressure, flow, and concentration profiles in open and spacer-filled membrane channels, J. Memb. Sci. 277 (2006) 7–17. doi:10.1016/j.memsci.2005.10.021.

[68] T. Ishigami, H. Matsuyama, Numerical modeling of concentration polarization in spacer-filled channel with permeation across reverse osmosis membrane, Ind. Eng. Chem. Res. 54 (2015) 1665–1674. doi:10.1021/ie5039665.

[69] M. Li, T. Bui, S. Chao, Three-dimensional CFD analysis of hydrodynamics and concentration polarization in an industrial RO feed channel, Desalination. 397 (2016) 194–204. doi:10.1016/j.desal.2016.07.005.

[70] B. Bernales, P. Haldenwang, P. Guichardon, N. Ibaseta, Prandtl model for concentration polarization and osmotic counter-effects in a 2-D membrane channel, Desalination. 404 (2017) 341–359. doi:10.1016/j.desal.2016.09.026.

[71] A. Chaudhuri, A. Jogdand, Permeate flux decrease due to concentration polarization in a closed roto-dynamic reverse osmosis filtration system, Desalination. 402 (2017) 152–161. doi:10.1016/j.desal.2016.10.005.

[72] S. Jain, S.K. Gupta, Analysis of modified surface force pore flow model with concentration polarization and comparison with Spiegler-Kedem model in reverse osmosis systems, J. Memb. Sci. 232 (2004) 45–61. doi:10.1016/j.memsci.2003.11.021.

[73] J. Wang, D.S. Dlamini, A.K. Mishra, M.T.M. Pendergast, M.C.Y. Wong, B.B. Mamba, V. Freger, A.R.D. Verliefde, E.M. V Hoek, A critical review of transport through osmotic membranes, J. Memb. Sci. 454 (2014) 516–537. doi:10.1016/j.memsci.2013.12.034.

[74] F. Peng, X. Huang, A. Jawor, E.M. V Hoek, Transport, structural, and interfacial properties of poly(vinyl alcohol)-polysulfone composite nanofiltration membranes, J. Memb. Sci. 353 (2010) 169–176. doi:10.1016/j.memsci.2010.02.044.

[75] D. Van Gauwbergen, J. Baeyens, Modelling reverse osmosis by irreversible thermodynamics, Sep. Purif. Technol. 13 (1998) 117–128. doi:10.1016/S1383-

5866(97)00065-8.

[76] H. Mehdizadeh, Modelling of transport phenomena in reverse osmosis membranes, McMaster Unversity, 1990.

[77] L.W. Jye, A.F. Ismail, Nanofiltration Membranes: Synthesis, Characterization, and Applications, 1st ed., CRC Press, Boca Raton, 2016.

[78] L. Onsager, R.R. In, L. Onsager, R.R. In, Reciprocal relations in irreversible processes. I., Phys. Rev. 37 (1931) 405–426. doi:10.1103/PhysRev.37.405.

[79] L. Onsager, Reciprocal relations in irreversible processes. II, Phys. Rev. 38 (1931) 2265–2279. doi:10.1103/PhysRev.38.2265.

[80] G. Jonsson, F. Macedonio, 2.01 – Fundamentals in Reverse Osmosis, in: E. Drioli, L. Giorno, E. Fontananova (Eds.), Compr. Membr. Sci. Eng., Elsevier, 2010: pp. 1–22. doi:10.1016/B978-0-08-093250-7.00026-8.

[81] O. Kedem, A. Katchalsky, Thermodynamic analysis of the permeability of biological membranes to non-electrolytes, BBA - Biochim. Biophys. Acta. 27 (1958) 229–246. doi:10.1016/0006-3002(58)90330-5.

[82] K.S. Spiegler, O. Kedem, Thermodynamics of hyperfiltration (reverse osmosis): criteria for efficient membranes, Desalination. 1 (1966) 311–326. doi:10.1016/S0011-9164(00)80018-1.

[83] M. Jarzyńska, M. Pietruszka, Derivation of Practical Kedem - Katchalsky Equations for Membrane Substance Transport, Old New Concepts Phys. 5 (2008) 459–474. doi:10.2478/v10005-007-0041-8.

[84] M. Soltanieh, W.N. Gill, Review of reverse osmosis membranes and transport models, Chem. Eng. Commun. 12 (1981) 279–363. doi:10.1080/00986448108910843.

[85] V.M. Starov, N. V Churaev, Separation of electrolyte solutions by reverse osmosis, Adv. Colloid Interface Sci. 43 (1993) 145–167. doi:https://doi.org/10.1016/0001-8686(93)80016-5.

[86] M.S. Hall, V.M. Starov, D.R. Lloyd, Reverse osmosis of multicomponent electrolyte solutions. Part I. Theoretical development, J. Memb. Sci. (1997). doi:10.1016/S0376-7388(96)00300-6.

[87] M.S. Hall, D.R. Lloyd, V.M. Starov, Reverse osmosis of multicomponent electrolyte solutions. Part II. Experimental verification, J. Memb. Sci. (1997). doi:10.1016/S0376-7388(96)00301-8.

[88] J.G. Wijmans, R.W. Baker, The solution-diffusion model: a review, J. Memb. Sci. 107 (1995) 1–21. doi:10.1016/0376-7388(95)00102-I.

[89] T. Mohammadi, M. Kazemimoghadam, M. Saadabadi, Modeling of membrane fouling and flux decline in reverse osmosis during separation of oil in water emulsions, Desalination. 157 (2003) 369–375. doi:10.1016/S0011-9164(03)00419-3.

[90] B. Gu, X.Y. Xu, C.S. Adjiman, A predictive model for spiral wound reverse osmosis membrane modules: The effect of winding geometry and accurate geometric details, Comput. Chem. Eng. 96 (2017) 248–265. doi:10.1016/j.compchemeng.2016.07.029.

[91] D. Bhattacharyya, M.E. Williams, Theory, in: W.S.W. Ho, K.K. Sirkar (Eds.), Membr.

Handb., Springer US, Boston, MA, 1992: pp. 269–280. doi:10.1007/978-1-4615-3548-5_22.

[92] E.A. Mason, H.K. Lonsdale, Statistical-mechanical theory of membrane transport, J. Memb. Sci. 51 (1990) 1–81. doi:10.1016/S0376-7388(00)80894-7.

[93] S. Sourirajan, Reverse osmosis, Academic Press, New York, 1970.

[94] W. Ho, K. Sirkar, Membrane Handbook, Van Nostrand Reinhold, New York, 1992. doi:10.1007/978-1-4615-3548-5.

[95] T. Matsuura, S. Sourlrajan, Reverse Osmosis Transport through Capillary Pores under the Influence of Surface Forces, Ind. Eng. Chem. Process Des. Dev. 20 (1981) 273–282. doi:10.1021/i200013a015.

[96] H. Mehdizadeh, J.M. Dickson, Theoretical modification of the surface force-pore flow model for reverse osmosis transport, J. Memb. Sci. 42 (1989) 119–145. doi:10.1016/S0376-7388(00)82369-8.

[97] H. Mehdizadeh, J.M. Dickson, Evaluation of surface force-pore flow and modified surface force-pore flow models for reverse osmosis transport, Chem. Eng. Commun. 103 (1991) 65–82. doi:10.1080/00986449108910863.

[98] J. Corson MacNeil, Membrane separation technologies for treatment of hazardous wastes, Crit. Rev. Environ. Control. 18 (1988) 91–131. doi:10.1080/10643388809388344.

[99] G. BELFORT, 7 - Desalting Experience by Hyperfiltration (Reverse Osmosis) in the United States, in: G.B.T.-S.M.P. BELFORT (Ed.), Academic Press, 1984: pp. 221–280. doi:https://doi.org/10.1016/B978-0-12-085480-6.50013-X.

[100] J. Kucera, Desalination: Water from Water, Wiley-Scrivener, Salem, 2014. doi:10.1002/9781118904855.

[101] R.R. Dupont, T.N. Eisenberg, E.J. Middlebrooks, Reverse osmosis in the treatment of drinking water, Utah, 1982. https://digitalcommons.usu.edu/cgi/viewcontent.cgi?article=1504&context=water_rep.

[102] Accepta, A guide of cost-effective membrane technologies for minimizing wastes and effluents, (1997). http://www.spice3.eu/GR/component/docman/doc_download/336-accepta-membrane-technology (accessed October 1, 2018).

[103] A. Figoli, J. Hoinkis, J. Bundschuh, eds., Membrane Technologies for Water Treatment: Removal of Toxic Trace Elements with Emphasis on Arsenic, Fluoride and Uranium, CRC Press, London, 2016.

[104] P. Pal, J. Sikder, S. Roy, L. Giorno, Process intensification in lactic acid production: A review of membrane based processes, Chem. Eng. Process. Process Intensif. 48 (2009) 1549–1559. doi:10.1016/j.cep.2009.09.003.

[105] J.W. McCutchan, V. Goel, Systems analysis of a multi-stage tubular module reverse osmosis plant for sea water desalination, Desalination. 14 (1974) 57–76. doi:10.1016/S0011-9164(00)80047-8.

[106] D.E. Wiley, C.J.D. Fell, A.G. Fane, Optimisation of membrane module design for brackish water desalination, Desalination. 52 (1985) 249–265. doi:10.1016/0011-9164(85)80036-9.

[107] H. Tsuge, C. Yanagi, K. Mori, Desalination of sea water by reverse osmosis using tubular module, Desalination. 23 (1977) 235–243. doi:https://doi.org/10.1016/S0011-9164(00)82526-6.

[108] A. Kumano, M. Sekino, Y. Matsui, N. Fujiwara, H. Matsuyama, Study of mass transfer characteristics for a hollow fiber reverse osmosis module, J. Memb. Sci. 324 (2008) 136–141. doi:10.1016/j.memsci.2008.07.011.

[109] M.G. Marcovecchio, N.J. Scenna, P.A. Aguirre, Improvements of a hollow fiber reverse osmosis desalination model: Analysis of numerical results, Chem. Eng. Res. Des. 88 (2010) 789–802. doi:10.1016/j.cherd.2009.12.003.

[110] A. Nakayama, Y. Sano, An application of the Sano-Nakayama membrane transport model in hollow fiber reverse osmosis desalination systems, Desalination. 311 (2013) 95–102. doi:10.1016/j.desal.2012.11.012.

[111] S. Senthilmurugan, S.K. Gupta, Separation of inorganic and organic compounds by using a radial flow hollow-fiber reverse osmosis module, Desalination. 196 (2006) 221–236. doi:10.1016/j.desal.2006.02.001.

[112] Toyobo Co. Ltd., HOLLOSEP®, (2006). http://www.toyobo-global.com/seihin/ro/tokucho.htm (accessed October 3, 2018).

[113] C.Y. Tang, Y.N. Kwon, J.O. Leckie, Probing the nano- and micro-scales of reverse osmosis membranes-A comprehensive characterization of physiochemical properties of uncoated and coated membranes by XPS, TEM, ATR-FTIR, and streaming potential measurements, J. Memb. Sci. 287 (2007) 146–156. doi:10.1016/j.memsci.2006.10.038.

[114] K.L. Tung, K.S. Chang, T.T. Wu, N.J. Lin, K.R. Lee, J.Y. Lai, Recent advances in the characterization of membrane morphology, Curr. Opin. Chem. Eng. 4 (2014) 121–127. doi:10.1016/j.coche.2014.03.002.

[115] L. Malaeb, G.M. Ayoub, Reverse osmosis technology for water treatment: State of the art review, Desalination. 267 (2011) 1–8. doi:10.1016/j.desal.2010.09.001.

[116] K.C. Khulbe, C.Y. Feng, T. Matsuura, Membrane characterization, in desalination and water resources (DESWARE) - Membrane process, Encycl. Life Support Syst. (EOLSS), Dev. under Auspices UNESCO. VOL I (2010) 131–172.

[117] K. Košutić, L. Kaštelan-Kunst, B. Kunst, Porosity of some commercial reverse osmosis and nanofiltration polyamide thin-film composite membranes, J. Memb. Sci. 168 (2000) 101–108. doi:10.1016/S0376-7388(99)00309-9.

[118] T. Fujioka, N. Oshima, R. Suzuki, W.E. Price, L.D. Nghiem, Probing the internal structure of reverse osmosis membranes by positron annihilation spectroscopy: Gaining more insight into the transport of water and small solutes, J. Memb. Sci. 486 (2015) 106–118. doi:10.1016/j.memsci.2015.02.007.

[119] K. Chan, T. Liu, T. Matsuura, S. Sourirajan, Effect of shrinkage on pore size and pore size distribution of cellulose acetate reverse osmosis membranes, Ind. Eng. Chem. Prod. Res. Dev. 23 (1984) 124–133. doi:10.1021/i300013a026.

[120] M. Khayet, T. Matsuura, Determination of surface and bulk pore sizes of flat-sheet and hollow-fiber membranes by atomic force microscopy, gas permeation and solute transport methods, Desalination. 158 (2003) 57–64. doi:10.1016/S0011-9164(03)00433-8.

[121] K. Košutić, D. Dolar, B. Kunst, On experimental parameters characterizing the reverse osmosis and nanofiltration membranes' active layer, J. Memb. Sci. 282 (2006) 109–114. doi:10.1016/j.memsci.2006.05.010.

[122] L. Kaštelan-Kunst, V. Dananić, B. Kunst, K. Košutić, Preparation and porosity of cellulose triacetate reverse osmosis membranes, J. Memb. Sci. 109 (1996) 223–230. doi:10.1016/0376-7388(95)00191-3.

[123] Y. Kiso, K. Muroshige, T. Oguchi, M. Hirose, T. Ohara, T. Shintani, Pore radius estimation based on organic solute molecular shape and effects of pressure on pore radius for a reverse osmosis membrane, J. Memb. Sci. 369 (2011) 290–298. doi:10.1016/j.memsci.2010.12.005.

[124] L.C. Powell, N. Hilal, C.J. Wright, Atomic force microscopy study of the biofouling and mechanical properties of virgin and industrially fouled reverse osmosis membranes, Desalination. 404 (2017) 313–321. doi:10.1016/j.desal.2016.11.010.

[125] N. Hilal, A.F. Ismail, T. Matsuura, D. Oatley-Radcliffe, eds., Membrane Characterization, Elsevier, 2017.

[126] J.C. Dore, R.E. Benfield, D. Grandjean, G. Schmid, M. Kröll, D. Le Bolloc'h, Structural studies of mesoporous alumina membranes by small angle X-ray scattering, Stud. Surf. Sci. Catal. 144 (2002) 163–170. doi:10.1016/S0167-2991(02)80130-6.

[127] Y.C. Jean, W.-S. Hung, C.-H. Lo, H. Chen, G. Liu, L. Chakka, M.-L. Cheng, D. Nanda, K.-L. Tung, S.-H. Huang, K.-R. Lee, J.-Y. Lai, Y.-M. Sun, C.-C. Hu, C.-C. Yu, Applications of positron annihilation spectroscopy to polymeric membranes, Desalination. 234 (2008) 89–98. doi:10.1016/j.desal.2007.09.074.

[128] Z. Chen, K. Ito, H. Yanagishita, N. Oshima, R. Suzuki, Y. Kobayashi, Correlation study between free-volume holes and molecular separations of composite membranes for reverse osmosis processes by means of variable-energy positron annihilation techniques, J. Phys. Chem. C. 115 (2011) 18055–18060. doi:10.1021/jp203888m.

[129] T. Shintani, A. Shimazu, S. Yahagi, H. Matsuyama, Characterization of methyl-substituted polyamides used for reverse osmosis membranes by positron annihilation lifetime spectroscopy and MD simulation, J. Appl. Polym. Sci. 113 (2009) 1757–1762. doi:10.1002/app.29885.

[130] J. Lee, C.M. Doherty, A.J. Hill, S.E. Kentish, Water vapor sorption and free volume in the aromatic polyamide layer of reverse osmosis membranes, J. Memb. Sci. 425–426 (2013) 217–226. doi:10.1016/j.memsci.2012.08.054.

[131] A. Shimazu, K. Ikeda, T. Miyazaki, Y. Ito, Application of positron annihilation technique to reverse osmosis membrane materials, in: Radiat. Phys. Chem., 2000: pp. 555–561. doi:10.1016/S0969-806X(00)00217-6.

[132] K.C. Khulbe, T. Matsuura, Recent progresses in preparation and characterization of RO membranes, J. Membr. Sci. Res. 3 (2017).

[133] R.N. Kapadia, V.P. Pandya, Scanning electron microscopy study on reverse osmosis membranes prepared from Indian cellulosic polymers, Desalination. 34 (1980) 199–215. doi:10.1016/S0011-9164(00)88590-2.

[134] G. Mossa, A study of the structure of reverse osmosis membranes by means of the

scanning electron microscope, J. Microsc. 107 (1976) 67–77. doi:10.1111/j.1365-2818.1976.tb02424.x.

[135] D.J. Johnson, D.L. Oatley-Radcliffe, N. Hilal, State of the art review on membrane surface characterisation: Visualisation, verification and quantification of membrane properties, Desalination. 434 (2018) 12–36. doi:10.1016/j.desal.2017.03.023.

[136] C.Y. Tang, Z. Yang, Chapter 8 - Transmission Electron Microscopy (TEM), in: N. Hilal, A.F. Ismail, T. Matsuura, D. Oatley-Radcliffe (Eds.), Membr. Charact., Elsevier, 2017: pp. 145–159. doi:https://doi.org/10.1016/B978-0-444-63776-5.00008-5.

[137] G.R. Guillen, Y. Pan, M. Li, E.M. V Hoek, Preparation and characterization of membranes formed by nonsolvent induced phase separation: A review, Ind. Eng. Chem. Res. 50 (2011) 3798–3817. doi:10.1021/ie101928r.

[138] M. Hirose, H. Ito, Y. Kamiyama, Effect of skin layer surface structures on the flux behaviour of RO membranes, J. Memb. Sci. 121 (1996) 209–215. doi:10.1016/S0376-7388(96)00181-0.

[139] M. Liu, D. Wu, S. Yu, C. Gao, Influence of the polyacyl chloride structure on the reverse osmosis performance, surface properties and chlorine stability of the thin-film composite polyamide membranes, J. Memb. Sci. 326 (2009) 205–214. doi:10.1016/j.memsci.2008.10.004.

[140] K.C. Khulbe, C. Feng, T. Matsuura, G. Lamarche, A.M. Lamarche, Study of the structure and transport of asymmetric polyamide membranes for reverse osmosis using the electron spin resonance (ESR) method, Desalination. 154 (2003) 1–8. doi:10.1016/S0011-9164(03)00202-9.

[141] K.C. Khulbe, T. Matsuura, Characterization of synthetic membranes by Raman spectroscopy, electron spin resonance, and atomic force microscopy; a review., Polymer (Guildf). 41 (1999) 1917–1935. doi:10.1016/S0032-3861(99)00359-6.

[142] B. Mi, O. Coronell, B.J. Mariñas, F. Watanabe, D.G. Cahill, I. Petrov, Physico-chemical characterization of NF/RO membrane active layers by Rutherford backscattering spectrometry, J. Memb. Sci. 282 (2006) 71–81. doi:10.1016/j.memsci.2006.05.015.

[143] H. Kim, Fabrication of reverse osmosis membrane via low temperature plasma polymerization, J. Memb. Sci. 190 (2001) 21–33. doi:10.1016/S0376-7388(01)00380-5.

[144] R. Manjumeena, D. Duraibabu, J. Sudha, P.T. Kalaichelvan, Biogenic nanosilver incorporated reverse osmosis membrane for antibacterial and antifungal activities against selected pathogenic strains: An enhanced eco-friendly water disinfection approach, J. Environ. Sci. Heal. - Part A Toxic/Hazardous Subst. Environ. Eng. 49 (2014) 1125–1133. doi:10.1080/10934529.2014.897149.

[145] S. Jiang, Y. Li, B.P. Ladewig, A review of reverse osmosis membrane fouling and control strategies, Sci. Total Environ. 595 (2017) 567–583. doi:10.1016/j.scitotenv.2017.03.235.

[146] L.N. Sim, T.H. Chong, A.H. Taheri, S.T. V Sim, L. Lai, W.B. Krantz, A.G. Fane, A review of fouling indices and monitoring techniques for reverse osmosis, Desalination. 434 (2018) 169–188. doi:10.1016/j.desal.2017.12.009.

[147] W. Guo, H.H. Ngo, J. Li, A mini-review on membrane fouling, Bioresour. Technol. 122 (2012) 27–34. doi:10.1016/j.biortech.2012.04.089.

[148] G.Z. Ramon, T.V. Nguyen, E.M. V Hoek, Osmosis-assisted cleaning of organic-fouled seawater RO membranes, Chem. Eng. J. 218 (2013) 173–182. doi:10.1016/j.cej.2012.12.006.

[149] B. Peñate, L. Garc\'\ia-Rodr\'\iguez, Current trends and future prospects in the design of seawater reverse osmosis desalination technology, Desalination. 284 (2012) 1–8. doi:10.1016/j.desal.2011.09.010.

[150] F.C. Kent, K. Farahbakhsh, B. Mahendran, M. Jaklewicz, S.N. Liss, H. Zhou, Water reclamation using reverse osmosis: Analysis of fouling propagation given tertiary membrane filtration and MBR pretreatments, J. Memb. Sci. 382 (2011) 328–338. doi:10.1016/j.memsci.2011.08.028.

[151] C.Y. Tang, T.H. Chong, A.G. Fane, Colloidal interactions and fouling of NF and RO membranes: A review, Adv. Colloid Interface Sci. 164 (2011) 126–143. doi:10.1016/j.cis.2010.10.007.

[152] A.J. Karabelas, D.C. Sioutopoulos, New insights into organic gel fouling of reverse osmosis desalination membranes, Desalination. 368 (2015) 114–126. doi:10.1016/j.desal.2015.01.029.

[153] M.F.A. Goosen, S.S. Sablani, H. Al-Hinai, S. Al-Obeidani, R. Al-Belushi, D. Jackson, Fouling of reverse osmosis and ultrafiltration membranes: A critical review, Sep. Sci. Technol. 39 (2004) 2261–2297. doi:10.1081/SS-120039343.

[154] S.G. Yiantsios, D. Sioutopoulos, A.J. Karabelas, Colloidal fouling of RO membranes: An overview of key issues and efforts to develop improved prediction techniques, Desalination. 183 (2005) 257–272. doi:10.1016/j.desal.2005.02.052.

[155] S.F.E. Boerlage, M. Kennedy, M.P. Aniye, J.C. Schippers, Applications of the MFI-UF to measure and predict particulate fouling in RO systems, J. Memb. Sci. 220 (2003) 97–116. doi:10.1016/S0376-7388(03)00222-9.

[156] L.N. Sim, Y. Ye, V. Chen, A.G. Fane, Crossflow Sampler Modified Fouling Index Ultrafiltration (CFS-MFIUF)-An alternative Fouling Index, J. Memb. Sci. 360 (2010) 174–184. doi:10.1016/j.memsci.2010.05.010.

[157] J.S. Choi, T.M. Hwang, S. Lee, S. Hong, A systematic approach to determine the fouling index for a RO/NF membrane process, Desalination. (2009). doi:10.1016/j.desal.2008.01.042.

[158] A. Ruiz-García, N. Melián-Martel, I. Nuez, Short Review on Predicting Fouling in RO Desalination, Membr. . 7 (2017). doi:10.3390/membranes7040062.

[159] Y. Ju, I. Hong, S. Hong, Multiple MFI measurements for the evaluation of organic fouling in SWRO desalination, Desalination. (2015). doi:10.1016/j.desal.2015.02.035.

[160] Y. Yu, S. Lee, K. Hong, S. Hong, Evaluation of membrane fouling potential by multiple membrane array system (MMAS): Measurements and applications, J. Memb. Sci. (2010). doi:10.1016/j.memsci.2010.06.038.

[161] Y. Jin, H. Lee, Y.O. Jin, S. Hong, Application of multiple modified fouling index (MFI) measurements at full-scale SWRO plant, Desalination. (2017). doi:10.1016/j.desal.2016.12.006.

[162] A.H. Taheri, S.T. V Sim, L.N. Sim, T.H. Chong, W.B. Krantz, A.G. Fane, Development of a new technique to predict reverse osmosis fouling, J. Memb. Sci. 448 (2013) 12–22. doi:10.1016/j.memsci.2013.06.040.

[163] A.H. Taheri, L.N. Sim, T.H. Chong, W.B. Krantz, A.G. Fane, Prediction of reverse osmosis fouling using the feed fouling monitor and salt tracer response technique, J. Memb. Sci. 475 (2015) 433–444. doi:10.1016/j.memsci.2014.10.043.

[164] S. Lee, C.H. Lee, Effect of operating conditions on CaSO4 scale formation mechanism in nanofiltration for water softening, Water Res. 34 (2000) 3854–3866. doi:10.1016/S0043-1354(00)00142-1.

[165] A. Antony, J.H. Low, S. Gray, A.E. Childress, P. Le-Clech, G. Leslie, Scale formation and control in high pressure membrane water treatment systems: A review, J. Memb. Sci. 383 (2011) 1–16. doi:10.1016/j.memsci.2011.08.054.

[166] S. Shirazi, C.J. Lin, D. Chen, Inorganic fouling of pressure-driven membrane processes - A critical review, Desalination. 250 (2010) 236–248. doi:10.1016/j.desal.2009.02.056.

[167] G. Amy, Fundamental understanding of organic matter fouling of membranes, Desalination. 231 (2008) 44–51. doi:10.1016/j.desal.2007.11.037.

[168] W. Yuan, A.L. Zydney, Humic acid fouling during microfiltration, J. Memb. Sci. 157 (1999) 1–12. doi:10.1016/S0376-7388(98)00329-9.

[169] Y. Yu, S. Lee, S. Hong, Effect of solution chemistry on organic fouling of reverse osmosis membranes in seawater desalination, J. Memb. Sci. 351 (2010) 205–213. doi:10.1016/j.memsci.2010.01.051.

[170] R. Komlenic, Rethinking the causes of membrane biofouling, Filtr. Sep. 47 (2010) 26–28. doi:10.1016/S0015-1882(10)70211-1.

[171] V. Kochkodan, N. Hilal, A comprehensive review on surface modified polymer membranes for biofouling mitigation, Desalination. 356 (2015) 187–207. doi:10.1016/j.desal.2014.09.015.

[172] Z. Hu, A. Antony, G. Leslie, P. Le-Clech, Real-time monitoring of scale formation in reverse osmosis using electrical impedance spectroscopy, J. Memb. Sci. 453 (2014) 320–327. doi:10.1016/j.memsci.2013.11.014.

[173] T.H. Chong, F.S. Wong, A.G. Fane, Fouling in reverse osmosis: Detection by non-invasive techniques, Desalination. 204 (2007) 148–154. doi:10.1016/j.desal.2006.02.031.

[174] E. Kujundzic, A. Cristina Fonseca, E.A. Evans, M. Peterson, A.R. Greenberg, M. Hernandez, Ultrasonic monitoring of early-stage biofilm growth on polymeric surfaces, J. Microbiol. Methods. 68 (2007) 458–467. doi:10.1016/j.mimet.2006.10.005.

[175] M. Uchymiak, A. Rahardianto, E. Lyster, J. Glater, Y. Cohen, A novel RO ex situ scale observation detector (EXSOD) for mineral scale characterization and early detection, J. Memb. Sci. 291 (2007) 86–95. doi:10.1016/j.memsci.2006.12.038.

[176] J.M. Kavanagh, S. Hussain, T.C. Chilcott, H.G.L. Coster, Fouling of reverse osmosis membranes using electrical impedance spectroscopy: Measurements and simulations, Desalination. 236 (2009) 187–193. doi:10.1016/j.desal.2007.10.066.

[177] L.N. Sim, Z.J. Wang, J. Gu, H.G.L. Coster, A.G. Fane, Detection of reverse osmosis

membrane fouling with silica, bovine serum albumin and their mixture using in-situ electrical impedance spectroscopy, J. Memb. Sci. 443 (2013) 45–53. doi:10.1016/j.memsci.2013.04.047.

[178] A. Antony, T. Chilcott, H. Coster, G. Leslie, In situ structural and functional characterization of reverse osmosis membranes using electrical impedance spectroscopy, J. Memb. Sci. 425–426 (2013) 89–97. doi:10.1016/j.memsci.2012.09.028.

[179] M. Wilf, K. Klinko, Performance of commercial seawater membranes, Desalination. 96 (1994) 465–478. doi:https://doi.org/10.1016/0011-9164(94)85196-4.

[180] A. Abbas, N. Al-Bastaki, Performance decline in brackish water Film Tec spiral wound RO membranes, Desalination. (2001). doi:10.1016/S0011-9164(01)00191-6.

[181] M. Zhu, M.M. El-Halwagi, M. Al-Ahmad, Optimal design and scheduling of flexible reverse osmosis networks, J. Memb. Sci. (1997). doi:10.1016/S0376-7388(96)00310-9.

[182] A. Ruiz-García, I. Nuez, Long-term performance decline in a brackish water reverse osmosis desalination plant. Predictive model for the water permeability coefficient, Desalination. (2016). doi:10.1016/j.desal.2016.06.027.

[183] G.D. Kang, Y.M. Cao, Development of antifouling reverse osmosis membranes for water treatment: A review, Water Res. 46 (2012) 584–600. doi:10.1016/j.watres.2011.11.041.

[184] N. Misdan, W.J. Lau, a. F. Ismail, Seawater Reverse Osmosis (SWRO) desalination by thin-film composite membrane-Current development, challenges and future prospects, Desalination. 287 (2012) 228–237. doi:10.1016/j.desal.2011.11.001.

[185] D. Li, H. Wang, Recent developments in reverse osmosis desalination membranes, J. Mater. Chem. 20 (2010) 4551–4566. doi:10.1039/b924553g.

[186] K.P. Lee, T.C. Arnot, D. Mattia, A review of reverse osmosis membrane materials for desalination-Development to date and future potential, J. Memb. Sci. 370 (2011) 1–22. doi:10.1016/j.memsci.2010.12.036.

[187] M. Asadollahi, D. Bastani, S.A. Musavi, Enhancement of surface properties and performance of reverse osmosis membranes after surface modification: A review, Desalination. 420 (2017) 330–383. doi:10.1016/j.desal.2017.05.027.

[188] E. Curcio, E. Drioli, Membranes for Desalination BT - Seawater Desalination: Conventional and Renewable Energy Processes, in: G. Micale, L. Rizzuti, A. Cipollina (Eds.), Springer Berlin Heidelberg, Berlin, Heidelberg, 2009: pp. 41–75. doi:10.1007/978-3-642-01150-4_3.

[189] R.C.B. A.K. Ghosh S. Prabhakar and P.K.Tewari, Composite Polyamide Reverse Osmosis (RO) Membranes – Recent Developments and Future Directions, BARC Newsl. 321 (2011) 43–51.

[190] I. Pinnau, B.D. Freeman, Formation and Modification of Polymeric Membranes: Overview, in: Membr. Form. Modif., American Chemical Society, 1999: p. 1. doi:doi:10.1021/bk-2000-0744.ch001.

[191] F. Ismail, K.C. Khulbe, T. Matsuura, Reverse Osmosis, Elsevier, Amsterdam, 2019.

[192] A.P. Duarte, J.C. Bordado, 12 - Smart composite reverse-osmosis membranes for energy generation and water desalination processes, in: M.F.B.T.-S.C.C. Montemor, Membranes

(Eds.), Woodhead Publ. Ser. Compos. Sci. Eng., Woodhead Publishing, 2016: pp. 329–350. doi:https://doi.org/10.1016/B978-1-78242-283-9.00012-9.

[193] Y.-N. Wang, R. Wang, Chapter 1 - Reverse Osmosis Membrane Separation Technology, in: A.F. Ismail, M.A. Rahman, M.H.D. Othman, T.B.T.-M.S.P. Matsuura, Applications (Eds.), Handbooks Sep. Sci., Elsevier, 2019: pp. 1–45. doi:https://doi.org/10.1016/B978-0-12-812815-2.00001-6.

[194] M. Mulder, Preparation of Synthetic Membranes BT - Basic Principles of Membrane Technology, in: M. Mulder (Ed.), Springer Netherlands, Dordrecht, 1996: pp. 71–156. doi:10.1007/978-94-009-1766-8_3.

[195] A.K. Pabby, S.S.H. Rizvi, A.M.S. Requena, eds., Handbook of Membrane Separations, 2nd Editio, CRC Press, Boca Raton, 2015.

[196] K.C. Khulbe, C.Y. Feng, T. Matsuura, eds., Synthetic Membranes for Membrane Processes BT - Synthetic Polymeric Membranes: Characterization by Atomic Force Microscopy, in: Springer Berlin Heidelberg, Berlin, Heidelberg, 2008: pp. 5–18. doi:10.1007/978-3-540-73994-4_2.

[197] B.S. Lalia, V. Kochkodan, R. Hashaikeh, N. Hilal, A review on membrane fabrication: Structure, properties and performance relationship, Desalination. 326 (2013) 77–95. doi:10.1016/j.desal.2013.06.016.

[198] Applied Membranes Inc., CTA commercial/industrial RO membranes, (2018). https://www.appliedmembranes.com/cta-ro-membranes.html (accessed October 12, 2018).

[199] Suez Water Technologies, CD series high rejection brackish water RO elements (cellulose acetate), (2018). https://www.suezwatertechnologies.com/kcpguest/documents/Fact (accessed October 15, 2018).

[200] Suez Water Technologies, CE series brackish water RO elements (cellulose acetate), (2018). https://www.suezwatertechnologies.com/kcpguest/documents/Fact (accessed October 15, 2018).

[201] S. LOEB, S. SOURIRAJAN, Sea Water Demineralization by Means of an Osmotic Membrane, in: Saline Water Conversion—II, AMERICAN CHEMICAL SOCIETY, 1963: pp. 117--132 SE-- 9. doi:doi:10.1021/ba-1963-0038.ch009.

[202] S. LOEB, The Loeb-Sourirajan Membrane: How It Came About, in: Synth. Membr., AMERICAN CHEMICAL SOCIETY, 1981: p. 1. doi:doi:10.1021/bk-1981-0153.ch001.

[203] S. Loeb, S. Sourirajan, High flow porous membranes for separating water from saline solutions, (1964).

[204] S. Kimura, S. Sourirajan, Analysis of data in reverse osmosis with porous cellulose acetate membranes used, AIChE J. 13 (1967) 497–503. doi:10.1002/aic.690130319.

[205] M. Ulbricht, Advanced functional polymer membranes, Polymer (Guildf). 47 (2006) 2217–2262. doi:10.1016/j.polymer.2006.01.084.

[206] J. Glater, The early history of reverse osmosis membrane development, Desalination. 117 (1998) 297–309. doi:10.1016/S0011-9164(98)00122-2.

[207] H. El-Saied, A.H. Basta, B.N. Barsoum, M.M. Elberry, Cellulose membranes for reverse osmosis Part I. RO cellulose acetate membranes including a composite with

polypropylene, Desalination. 159 (2003) 171–181. doi:10.1016/S0011-9164(03)90069-5.

[208] R. Singh, Chapter 1 - Introduction to Membrane Technology, in: R.B.T.-M.T. Singh, E. for Water Purification (Second Edition) (Eds.), Butterworth-Heinemann, Oxford, 2015: pp. 1–80. doi:https://doi.org/10.1016/B978-0-444-63362-0.00001-X.

[209] G.D. Mehta, S. Loeb, Performance of permasep B-9 and B-10 membranes in various osmotic regions and at high osmotic pressures, J. Memb. Sci. 4 (1978) 335–349. doi:10.1016/S0376-7388(00)83312-8.

[210] S. Senthilmurugan, S.K. Gupta, Modeling of a radial flow hollow fiber module and estimation of model parameters for aqueous multi-component mixture using numerical techniques, J. Memb. Sci. 279 (2006) 466–478. doi:10.1016/j.memsci.2005.12.041.

[211] L.C. Sawyer, R.S. Jones, Observations on the structure of first generation polybenzimidazole reverse osmosis membranes, J. Memb. Sci. 20 (1984) 147–166. doi:10.1016/S0376-7388(00)81329-0.

[212] W. Brinegar, Reverse osmosis process employing polybenzimidazole membranes, (1970).

[213] N.S. Trouw, Method for the preparation of polybenzimidazole membranes, (1987).

[214] M. Senoo, S. Hara, S. Ozawa, Permselective polymeric membrane prepared from polybenzimidazoles, (1971).

[215] R.L. Goldsmith, B.A. Wechsler, S. Hara, K. Mori, Y. Taketani, Development of PBIL low pressure brackish-water reverse osmosis membranes, Desalination. 22 (1977) 311–333. doi:10.1016/S0011-9164(00)88387-3.

[216] H. Murakami, N. Igarashi, PBIL tubular reverse osmosis. Application as low-energy concentrators, Ind. Eng. Chem. Prod. Res. Dev. 20 (1981) 501–508. doi:10.1021/i300003a015.

[217] L. Credali, A. Chiolle, P. Parrini, New polymer materials for reverse osmosis membranes., Desalination. 14 (1974) 137–150. doi:10.1016/S0011-9164(00)82047-0.

[218] L. Credali, G. Baruzzi, V. Guidotti, Reverse osmosis anisotropic membranes based on polypiperazine amides, (1978).

[219] P. Parrini, Polypiperazinamides: new polymers useful for membrane processes, Desalination. 48 (1983) 67–78. doi:10.1016/0011-9164(83)80006-X.

[220] L. Credali, P. Parrini, Properties of piperazine homopolyamide films, Polymer (Guildf). 12 (1971) 717–729. doi:10.1016/0032-3861(71)90087-5.

[221] C.W. Alegranti, Asymmetric polyimide membranes, (1974).

[222] R.L. Fox, Process for preparing an asymmetric permselective membrane, (1980).

[223] H. Sekiguchi, F. Sato, K. Sadamitsu, K. Yoshida, Solute-separating membrane, (1978). US.

[224] A. El-Gendi, H. Abdallah, A. Amin, S.K. Amin, Investigation of polyvinylchloride and cellulose acetate blend membranes for desalination, J. Mol. Struct. 1146 (2017) 14–22. doi:10.1016/j.molstruc.2017.05.122.

[225] E. Saljoughi, T. Mohammadi, Cellulose acetate (CA)/polyvinylpyrrolidone (PVP) blend asymmetric membranes: Preparation, morphology and performance, Desalination. 249

(2009) 850–854. doi:10.1016/j.desal.2008.12.066.

[226] C.H. Worthley, K.T. Constantopoulos, M. Ginic-Markovic, R.J. Pillar, J.G. Matisons, S. Clarke, Surface modification of commercial cellulose acetate membranes using surface-initiated polymerization of 2-hydroxyethyl methacrylate to improve membrane surface biofouling resistance, J. Memb. Sci. 385–386 (2011) 30–39. doi:10.1016/j.memsci.2011.09.017.

[227] E. Ferjani, S. Roudesli, A. Deratani, Desalination of brackish water from Tunisian Sahel using composite polymethylhydrosiloxane-cellulose acetate membranes, Desalination. 162 (2004) 103–109. doi:10.1016/S0011-9164(04)00032-3.

[228] E. Ferjani, M. Mejdoub, M.S. Roudesli, M.M. Chehimi, D. Picard, M. Delamar, XPS characterization of poly(methylhydrosiloxane)-modified cellulose diacetate membranes, J. Memb. Sci. 165 (2000) 125–133. doi:10.1016/S0376-7388(99)00227-6.

[229] I. Guezguez, B. Mrabet, E. Ferjani, XPS and contact angle characterization of surface modified cellulose acetate membranes by mixtures of PMHS/PDMS, Desalination. 313 (2013) 208–211. doi:10.1016/j.desal.2012.11.018.

[230] A. Morsy, S. Ebrahim, E.R. Kenawy, T. Abdel-Fattah, S. Kandil, Grafted cellulose acetate reverse osmosis membrane using 2-acrylamido-2-methylpropanesulfonic acid for water desalination, Water Sci. Technol. Water Supply. 16 (2016) 1046–1056. doi:10.2166/ws.2016.025.

[231] P. Fei, L. Liao, J. Meng, B. Cheng, X. Hu, J. Song, Non-leaching antibacterial cellulose triacetate reverse osmosis membrane via covalent immobilization of quaternary ammonium cations, Carbohydr. Polym. 181 (2018) 1102–1111. doi:10.1016/j.carbpol.2017.11.036.

[232] J.E. Cadotte, K.E. Cobian, R.H. Forester, R.J. Petersen, Continued evaluation of in situ-formed condensation polymers for reverse osmosis membranes, NTIS Report No. PB-253193, 1976.

[233] J.E. Cadotte, M.J. Steuck, R.J. Petersen, Research on in-situ-formed condensation polymers for reverse osmosis membranes, NTIS Report No. PB- 288387, n.d.

[234] R.J. Petersen, Composite reverse osmosis and nanofiltration membranes, J. Memb. Sci. 83 (1993) 81–150. doi:10.1016/0376-7388(93)80014-O.

[235] D. Li, Y. Yan, H. Wang, Recent advances in polymer and polymer composite membranes for reverse and forward osmosis processes, Prog. Polym. Sci. 61 (2016) 104–155. doi:10.1016/j.progpolymsci.2016.03.003.

[236] Axeon, HF1 – Series Membrane Elements, (2017). http://www.axeonwater.com/skin/common_files/admin/overview/MKTF_133_E_HF1_MEMBRANE_ELEMENT_SPEC_SHEET.pdf (accessed November 1, 2018).

[237] Dow, DOW FILMTEC™ BW30-365 Element, (2015). http://www.dupont.com/content/dam/Dupont2.0/Products/water/literature/609-00153.pdf (accessed November 1, 2018).

[238] Dow, DOW FILMTEC™ SW30HR–380 Element, (2018). http://www.dupont.com/content/dam/Dupont2.0/Products/water/literature/609-00390.pdf (accessed November 1, 2018).

[239] Toray Industries Inc., Standard BWRO TM700, (2014). https://www.toraywater.com/products/ro/pdf/TM700.pdf (accessed November 1, 2018).

[240] Toray Industries Inc., Standard SWRO TM800C, (2014). https://www.toraywater.com/products/ro/pdf/TM800C.pdf (accessed November 1, 2018).

[241] Suez Water Technologies, OSMO HR(PA) Series, (2015). https://www.suezwatertechnologies.com/kcpguest/documents/Fact (accessed November 1, 2018).

[242] Hydranautics, CPA2, (2018). http://membranes.com/wp-content/uploads/2017/03/CPA2.pdf (accessed November 1, 2018).

[243] Hydranautics, SWC4-LD, (2018). http://membranes.com/wp-content/uploads/2017/03/SWC4-LD.pdf (accessed November 1, 2018).

[244] Koch Membrane Systems, FLUID SYSTEMS® TFC® HR 8" ELEMENTS, (2018). https://www.kochmembrane.com/KochMembraneSolutions/media/Product-Datasheets/Spiral (accessed November 1, 2018).

[245] Koch Membrane Systems, FLUID SYSTEMS® TFC® SW 8" ELEMENTS, (2018). https://www.kochmembrane.com/KochMembraneSolutions/media/Product-Datasheets/Spiral (accessed November 1, 2018).

[246] J.E. Cadotte, Reverse osmosis membrane, (1977).

[247] R.L. Riley, R.L. Fox, C.R. Lyons, C.E. Milstead, M.W. Seroy, M. Tagami, Spiral-wound poly (ether/amide) thin-film composite membrane systems, Desalination. 19 (1976) 113–126. doi:10.1016/S0011-9164(00)88022-4.

[248] P.L. Riley, C.E. Milstead, A.L. Lloyd, M.W. Seroy, M. Tagami, Spiral-wound thin-film composite membrane systems for brackish and seawater desalination by reverse osmosis, Desalination. 23 (1977) 331–355. doi:https://doi.org/10.1016/S0011-9164(00)82535-7.

[249] J.E. Cadotte, Interfacially synthesized reverse osmosis membrane, (1981).

[250] R.E. Larson, J.E. Cadotte, R.J. Petersen, The FT-30 seawater reverse osmosis membrane--element test results, Desalination. 38 (1981) 473–483. doi:10.1016/S0011-9164(00)86092-0.

[251] W.J. Lau, A.F. Ismail, N. Misdan, M.A. Kassim, A recent progress in thin film composite membrane: A review, Desalination. 287 (2012) 190–199. doi:10.1016/j.desal.2011.04.004.

[252] T. Uemura, Y. Himeshima, M. Kurihara, Interfacially synthesized reverse osmosis membrane, (1988).

[253] T.A. Otitoju, R.A. Saari, A.L. Ahmad, Progress in the modification of reverse osmosis (RO) membranes for enhanced performance, J. Ind. Eng. Chem. 67 (2018) 52–71. doi:https://doi.org/10.1016/j.jiec.2018.07.010.

[254] L. Li, S. Zhang, X. Zhang, G. Zheng, Polyamide thin film composite membranes prepared from 3,4′,5-biphenyl triacyl chloride, 3,3′,5,5′-biphenyl tetraacyl chloride and m-phenylenediamine, J. Memb. Sci. 289 (2007) 258–267. doi:https://doi.org/10.1016/j.memsci.2006.12.007.

[255] L. Li, S. Zhang, X. Zhang, G. Zheng, Polyamide thin film composite membranes prepared from isomeric biphenyl tetraacyl chloride and m-phenylenediamine, J. Memb. Sci. 315

(2008) 20–27. doi:10.1016/j.memsci.2008.02.022.

[256] G. Chen, S. Li, X. Zhang, S. Zhang, Novel thin-film composite membranes with improved water flux from sulfonated cardo poly(arylene ether sulfone) bearing pendant amino groups, J. Memb. Sci. 310 (2008) 102–109. doi:10.1016/j.memsci.2007.10.039.

[257] H. Wang, L. Li, X. Zhang, S. Zhang, Polyamide thin-film composite membranes prepared from a novel triamine 3,5-diamino-N-(4-aminophenyl)-benzamide monomer and m-phenylenediamine, J. Memb. Sci. 353 (2010) 78–84. doi:https://doi.org/10.1016/j.memsci.2010.02.033.

[258] G.N.B. Baroña, J. Lim, B. Jung, High performance thin film composite polyamide reverse osmosis membrane prepared via m-phenylenediamine and 2,2'-benzidinedisulfonic acid, Desalination. 291 (2012) 69–77. doi:10.1016/j.desal.2012.02.001.

[259] T. Wang, L. Dai, Q. Zhang, A. Li, S. Zhang, Effects of acyl chloride monomer functionality on the properties of polyamide reverse osmosis (RO) membrane, J. Memb. Sci. 440 (2013) 48–57. doi:10.1016/j.memsci.2013.03.066.

[260] M. Said, S. Ebrahim, A. Gad, S. Kandil, Toward energy efficient reverse osmosis polyamide thin-film composite membrane based on diaminotoluene, Desalin. Water Treat. 71 (2017) 261–270. doi:10.1111/j.1540-6237.2012.00854.x.

[261] J. Hu, Y. Pu, M. Ueda, X. Zhang, L. Wang, Charge-aggregate induced (CAI) reverse osmosis membrane for seawater desalination and boron removal, J. Memb. Sci. 520 (2016) 1–7. doi:10.1016/j.memsci.2016.07.053.

[262] J. Zheng, Y. Yao, M. Li, L. Wang, X. Zhang, A non-MPD-type reverse osmosis membrane with enhanced permselectivity for brackish water desalination, J. Memb. Sci. 565 (2018) 104–111. doi:10.1016/j.memsci.2018.08.015.

[263] S.J. Park, S.J. Kwon, H.E. Kwon, M.G. Shin, S.H. Park, H. Park, Y.I. Park, S.E. Nam, J.H. Lee, Aromatic solvent-assisted interfacial polymerization to prepare high performance thin film composite reverse osmosis membranes based on hydrophilic supports, Polymer (Guildf). 144 (2018) 159–167. doi:10.1016/j.polymer.2018.04.060.

[264] S. Yu, M. Liu, Z. Lü, Y. Zhou, C. Gao, Aromatic-cycloaliphatic polyamide thin-film composite membrane with improved chlorine resistance prepared from m-phenylenediamine-4-methyl and cyclohexane-1,3,5-tricarbonyl chloride, J. Memb. Sci. 344 (2009) 155–164. doi:10.1016/j.memsci.2009.07.046.

[265] S.G. Kim, S.Y. Park, J.H. Chun, B.H. Chun, S.H. Kim, Novel thin-film composite membrane for seawater desalination with sulfonated poly(arylene ether sulfone) containing amino Groups, Desalin. Water Treat. 43 (2012) 230–237. doi:10.1080/19443994.2012.672177.

[266] T. Shintani, H. Matsuyama, N. Kurata, Effect of heat treatment on performance of chlorine-resistant polyamide reverse osmosis membranes, Desalination. 247 (2009) 370–377. doi:10.1016/j.desal.2008.09.003.

[267] S.P. Hong, I.C. Kim, T. Tak, Y.N. Kwon, Interfacially synthesized chlorine-resistant polyimide thin film composite (TFC) reverse osmosis (RO) membranes, Desalination. 309 (2013) 18–26. doi:10.1016/j.desal.2012.09.025.

[268] S.K. Jewrajka, A.V.R. Reddy, H.H. Rana, S. Mandal, S. Khullar, S. Haldar, N. Joshi, P.K.

Ghosh, Use of 2,4,6-pyridinetricarboxylic acid chloride as a novel co-monomer for the preparation of thin film composite polyamide membrane with improved bacterial resistance, J. Memb. Sci. 439 (2013) 87–95. doi:10.1016/j.memsci.2013.03.047.

[269] J. Qin, S. Lin, S. Song, L. Zhang, H. Chen, 4-Dimethylaminopyridine promoted interfacial polymerization between hyperbranched polyesteramide and trimesoyl chloride for preparing ultralow-pressure reverse osmosis composite membrane, ACS Appl. Mater. Interfaces. 5 (2013) 6649–6656. doi:10.1021/am401345y.

[270] A.K. Ghosh, R.C. Bindal, Impacts of Heat Treatment Medium on Performance of Aliphatic-aromatic and Aromatic-aromatic based Thin-film composite (TFC) polyamide Reverse Osmosis (RO) Membrane, J. Polym. Mater. 34 (2017) 759–772.

[271] A.F. Ismail, M. Padaki, N. Hilal, T. Matsuura, W.J. Lau, Thin film composite membrane - Recent development and future potential, Desalination. 356 (2015) 140–148. doi:10.1016/j.desal.2014.10.042.

[272] J. Li, M. Wei, Y. Wang, Substrate matters: The influences of substrate layers on the performances of thin-film composite reverse osmosis membranes, Chinese J. Chem. Eng. 25 (2017) 1676–1684. doi:10.1016/j.cjche.2017.05.006.

[273] J. Wei, X. Jian, C. Wu, S. Zhang, C. Yan, Influence of polymer structure on thermal stability of composite membranes, J. Memb. Sci. 256 (2005) 116–121. doi:10.1016/j.memsci.2005.02.012.

[274] E.S. Kim, Y.J. Kim, Q. Yu, B. Deng, Preparation and characterization of polyamide thin-film composite (TFC) membranes on plasma-modified polyvinylidene fluoride (PVDF), J. Memb. Sci. 344 (2009) 71–81. doi:10.1016/j.memsci.2009.07.036.

[275] H. Il Kim, S.S. Kim, Plasma treatment of polypropylene and polysulfone supports for thin film composite reverse osmosis membrane, J. Memb. Sci. 286 (2006) 193–201. doi:10.1016/j.memsci.2006.09.037.

[276] S.H. Maruf, A.R. Greenberg, J. Pellegrino, Y. Ding, Fabrication and characterization of a surface-patterned thin film composite membrane, J. Memb. Sci. 452 (2014) 11–19. doi:10.1016/j.memsci.2013.10.017.

[277] H.M. Park, K.Y. Jee, Y.T. Lee, Preparation and characterization of a thin-film composite reverse osmosis membrane using a polysulfone membrane including metal-organic frameworks, J. Memb. Sci. 541 (2017) 510–518. doi:10.1016/j.memsci.2017.07.034.

[278] C. Ba, J. Economy, Preparation of PMDA/ODA polyimide membrane for use as substrate in a thermally stable composite reverse osmosis membrane, J. Memb. Sci. 363 (2010) 140–148. doi:10.1016/j.memsci.2010.07.019.

[279] M. Son, H. gyu Choi, L. Liu, E. Celik, H. Park, H. Choi, Efficacy of carbon nanotube positioning in the polyethersulfone support layer on the performance of thin-film composite membrane for desalination, Chem. Eng. J. 266 (2015) 376–384. doi:10.1016/j.cej.2014.12.108.

[280] M. Son, H. Park, L. Liu, H. Choi, J.H. Kim, H. Choi, Thin-film nanocomposite membrane with CNT positioning in support layer for energy harvesting from saline water, Chem. Eng. J. 284 (2016) 68–77. doi:10.1016/j.cej.2015.08.134.

[281] B. Sabzi Dizajikan, M. Asadollahi, S.A. Musavi, D. Bastani, Preparation of poly(vinyl

chloride) (PVC) ultrafiltration membranes from PVC/additive/solvent and application of UF membranes as substrate for fabrication of reverse osmosis membranes, J. Appl. Polym. Sci. 135 (2018). doi:10.1002/app.46267.

[282] G.Z. Ramon, M.C.Y. Wong, E.M. V Hoek, Transport through composite membrane, Part 1: Is there an optimal support membrane?, J. Memb. Sci. 415–416 (2012) 298–305. doi:10.1016/j.memsci.2012.05.013.

[283] P.S. Singh, S. V Joshi, J.J. Trivedi, C. V Devmurari, A.P. Rao, P.K. Ghosh, Probing the structural variations of thin film composite RO membranes obtained by coating polyamide over polysulfone membranes of different pore dimensions, J. Memb. Sci. 278 (2006) 19–25. doi:10.1016/j.memsci.2005.10.039.

[284] W. Yan, Z. Wang, J. Wu, S. Zhao, J. Wang, S. Wang, Enhancing the flux of brackish water TFC RO membrane by improving support surface porosity via a secondary pore-forming method, J. Memb. Sci. 498 (2016) 227–241. doi:10.1016/j.memsci.2015.10.029.

[285] J. Wang, R. Xu, F. Yang, J. Kang, Y. Cao, M. Xiang, Probing influences of support layer on the morphology of polyamide selective layer of thin film composite membrane, J. Memb. Sci. 556 (2018) 374–383. doi:10.1016/j.memsci.2018.04.011.

[286] B. Khorshidi, T. Thundat, D. Pernitsky, M. Sadrzadeh, A parametric study on the synergistic impacts of chemical additives on permeation properties of thin film composite polyamide membrane, J. Memb. Sci. 535 (2017) 248–257. doi:10.1016/j.memsci.2017.04.052.

[287] Z. Liu, G. Zhu, Y. Wei, D. Zhang, L. Jiang, H. Wang, C. Gao, Enhanced flux performance of polyamide composite membranes prepared via interfacial polymerization assisted with ethyl formate, Water Sci. Technol. 76 (2017) 1884–1894. doi:10.2166/wst.2017.349.

[288] C. Kong, T. Shintani, T. Kamada, V. Freger, T. Tsuru, Co-solvent-mediated synthesis of thin polyamide membranes, J. Memb. Sci. 384 (2011) 10–16. doi:10.1016/j.memsci.2011.08.055.

[289] S.H. Kim, S.Y. Kwak, T. Suzuki, Positron annihilation spectroscopic evidence to demonstrate the flux-enhancement mechanism in morphology-controlled thin-film-composite (TFC) membrane, Environ. Sci. Technol. 39 (2005) 1764–1770. doi:10.1021/es049453k.

[290] S. Qiu, L. Wu, L. Zhang, H. Chen, C. Gao, Preparation of reverse osmosis composite membrane with high flux by interfacial polymerization of MPD and TMC, J. Appl. Polym. Sci. 112 (2009) 2066–2072. doi:10.1002/app.29639.

[291] B. Khorshidi, B. Soltannia, T. Thundat, M. Sadrzadeh, Synthesis of thin film composite polyamide membranes: Effect of monohydric and polyhydric alcohol additives in aqueous solution, J. Memb. Sci. 523 (2017) 336–345. doi:10.1016/j.memsci.2016.09.062.

[292] B.J. Abu Tarboush, D. Rana, T. Matsuura, H.A. Arafat, R.M. Narbaitz, Preparation of thin-film-composite polyamide membranes for desalination using novel hydrophilic surface modifying macromolecules, J. Memb. Sci. 325 (2008) 166–175. doi:10.1016/j.memsci.2008.07.037.

[293] D. Rana, Y. Kim, T. Matsuura, H.A. Arafat, Development of antifouling thin-film-composite membranes for seawater desalination, J. Memb. Sci. 367 (2011) 110–118.

doi:10.1016/j.memsci.2010.10.050.

[294] M. Duan, Z. Wang, J. Xu, J. Wang, S. Wang, Influence of hexamethyl phosphoramide on polyamide composite reverse osmosis membrane performance, Sep. Purif. Technol. 75 (2010) 145–155. doi:10.1016/j.seppur.2010.08.004.

[295] R.M. Gol, S.K. Jewrajka, Facile in situ PEGylation of polyamide thin film composite membranes for improving fouling resistance, J. Memb. Sci. 455 (2014) 271–282. doi:10.1016/j.memsci.2013.12.058.

[296] A. Bera, R.M. Gol, S. Chatterjee, S.K. Jewrajka, PEGylation and incorporation of triazine ring into thin film composite reverse osmosis membranes for enhancement of anti-organic and anti-biofouling properties, Desalination. 360 (2015) 108–117. doi:10.1016/j.desal.2015.01.018.

[297] L. Zhao, P.C.Y. Chang, W.S.W. Ho, High-flux reverse osmosis membranes incorporated with hydrophilic additives for brackish water desalination, Desalination. 308 (2013) 225–232. doi:10.1016/j.desal.2012.07.020.

[298] Y. Zhang, X. Miao, G. Pan, H. Shi, H. Yan, J. Xu, M. Guo, S. Li, Y. Zhang, Y. Liu, Highly improved permeation property of thin-film-composite polyamide membrane for water desalination, J. Polym. Res. 24 (2016). doi:10.1007/s10965-016-1167-2.

[299] F. Wu, X. Liu, C. Au, Effects of DMSO and glycerol additives on the property of polyamide reverse osmosis membrane, Water Sci. Technol. 74 (2016) 1619–1625. doi:10.2166/wst.2016.367.

[300] B.H. Jeong, E.M. V Hoek, Y. Yan, A. Subramani, X. Huang, G. Hurwitz, A.K. Ghosh, A. Jawor, Interfacial polymerization of thin film nanocomposites: A new concept for reverse osmosis membranes, J. Memb. Sci. 294 (2007) 1–7. doi:10.1016/j.memsci.2007.02.025.

[301] M. Fathizadeh, A. Aroujalian, A. Raisi, Effect of added NaX nano-zeolite into polyamide as a top thin layer of membrane on water flux and salt rejection in a reverse osmosis process, J. Memb. Sci. 375 (2011) 88–95. doi:10.1016/j.memsci.2011.03.017.

[302] H. Dong, L. Zhao, L. Zhang, H. Chen, C. Gao, W.S. Winston Ho, High-flux reverse osmosis membranes incorporated with NaY zeolite nanoparticles for brackish water desalination, J. Memb. Sci. 476 (2015) 373–383. doi:10.1016/j.memsci.2014.11.054.

[303] M. Safarpour, V. Vatanpour, A. Khataee, H. Zarrabi, P. Gholami, M.E. Yekavalangi, High flux and fouling resistant reverse osmosis membrane modified with plasma treated natural zeolite, Desalination. 411 (2017) 89–100. doi:10.1016/j.desal.2017.02.012.

[304] P. Cay-Durgun, C. McCloskey, J. Konecny, A. Khosravi, M.L. Lind, Evaluation of thin film nanocomposite reverse osmosis membranes for long-term brackish water desalination performance, Desalination. 404 (2017) 304–312. doi:10.1016/j.desal.2016.10.014.

[305] M. Bao, G. Zhu, L. Wang, M. Wang, C. Gao, Preparation of monodispersed spherical mesoporous nanosilica-polyamide thin film composite reverse osmosis membranes via interfacial polymerization, Desalination. 309 (2013) 261–266. doi:10.1016/j.desal.2012.10.028.

[306] A. Peyki, A. Rahimpour, M. Jahanshahi, Preparation and characterization of thin film composite reverse osmosis membranes incorporated with hydrophilic SiO2nanoparticles, Desalination. 368 (2015) 152–158. doi:10.1016/j.desal.2014.05.025.

[307] J. Yin, E.S. Kim, J. Yang, B. Deng, Fabrication of a novel thin-film nanocomposite (TFN) membrane containing MCM-41 silica nanoparticles (NPs) for water purification, J. Memb. Sci. 423–424 (2012) 238–246. doi:10.1016/j.memsci.2012.08.020.

[308] M. Zargar, Y. Hartanto, B. Jin, S. Dai, Hollow mesoporous silica nanoparticles: A peculiar structure for thin film nanocomposite membranes, J. Memb. Sci. 519 (2016) 1–10. doi:10.1016/j.memsci.2016.07.052.

[309] M. Zargar, Y. Hartanto, B. Jin, S. Dai, Polyethylenimine modified silica nanoparticles enhance interfacial interactions and desalination performance of thin film nanocomposite membranes, J. Memb. Sci. 541 (2017) 19–28. doi:10.1016/j.memsci.2017.06.085.

[310] H.R. Chae, J. Lee, C.H. Lee, I.C. Kim, P.K. Park, Graphene oxide-embedded thin-film composite reverse osmosis membrane with high flux, anti-biofouling, and chlorine resistance, J. Memb. Sci. 483 (2015) 128–135. doi:10.1016/j.memsci.2015.02.045.

[311] M.E.A. Ali, L. Wang, X. Wang, X. Feng, Thin film composite membranes embedded with graphene oxide for water desalination, Desalination. 386 (2016) 67–76. doi:10.1016/j.desal.2016.02.034.

[312] M. Safarpour, A. Khataee, V. Vatanpour, Thin film nanocomposite reverse osmosis membrane modified by reduced graphene oxide/TiO<inf>2</inf> with improved desalination performance, J. Memb. Sci. 489 (2015) 43–54. doi:10.1016/j.memsci.2015.04.010.

[313] J. Yin, G. Zhu, B. Deng, Graphene oxide (GO) enhanced polyamide (PA) thin-film nanocomposite (TFN) membrane for water purification, Desalination. 379 (2016) 93–101. doi:https://doi.org/10.1016/j.desal.2015.11.001.

[314] Y. Baek, H.J. Kim, S.H. Kim, J.C. Lee, J. Yoon, Evaluation of carbon nanotube-polyamide thin-film nanocomposite reverse osmosis membrane: Surface properties, performance characteristics and fouling behavior, J. Ind. Eng. Chem. 56 (2017) 327–334. doi:10.1016/j.jiec.2017.07.028.

[315] I. Wan Azelee, P.S. Goh, W.J. Lau, A.F. Ismail, M. Rezaei-DashtArzhandi, K.C. Wong, M.N. Subramaniam, Enhanced desalination of polyamide thin film nanocomposite incorporated with acid treated multiwalled carbon nanotube-titania nanotube hybrid, Desalination. 409 (2017) 163–170. doi:10.1016/j.desal.2017.01.029.

[316] H. Zhao, S. Qiu, L. Wu, L. Zhang, H. Chen, C. Gao, Improving the performance of polyamide reverse osmosis membrane by incorporation of modified multi-walled carbon nanotubes, J. Memb. Sci. 450 (2014) 249–256. doi:10.1016/j.memsci.2013.09.014.

[317] W.F. Chan, E. Marand, S.M. Martin, Novel zwitterion functionalized carbon nanotube nanocomposite membranes for improved RO performance and surface anti-biofouling resistance, J. Memb. Sci. 509 (2016) 125–137. doi:10.1016/j.memsci.2016.02.014.

[318] V. Vatanpour, M. Safarpour, A. Khataee, H. Zarrabi, M.E. Yekavalangi, M. Kavian, A thin film nanocomposite reverse osmosis membrane containing amine-functionalized carbon nanotubes, Sep. Purif. Technol. 184 (2017) 135–143. doi:10.1016/j.seppur.2017.04.038.

[319] J. Farahbaksh, M. Delnavaz, V. Vatanpour, Investigation of raw and oxidized multiwalled carbon nanotubes in fabrication of reverse osmosis polyamide membranes for

improvement in desalination and antifouling properties, Desalination. 410 (2017) 1–9. doi:10.1016/j.desal.2017.01.031.

[320] A.U.H. Khan, Z. Khan, I.H. Aljundi, Improved hydrophilicity and anti-fouling properties of polyamide TFN membrane comprising carbide derived carbon, Desalination. 420 (2017) 125–135. doi:10.1016/j.desal.2017.07.002.

[321] Y. Li, S. Li, K. Zhang, Influence of hydrophilic carbon dots on polyamide thin film nanocomposite reverse osmosis membranes, J. Memb. Sci. 537 (2017) 42–53. doi:10.1016/j.memsci.2017.05.026.

[322] M. Fathizadeh, H.N. Tien, K. Khivantsev, Z. Song, F. Zhou, M. Yu, Polyamide/nitrogen-doped graphene oxide quantum dots (N-GOQD) thin film nanocomposite reverse osmosis membranes for high flux desalination, Desalination. (2017). doi:https://doi.org/10.1016/j.desal.2017.07.014.

[323] A.S. Al-Hobaib, J. El Ghoul, I. Ghiloufi, L. El Mir, Synthesis and characterization of polyamide thin-film nanocomposite membrane reached by aluminum doped ZnO nanoparticles, Mater. Sci. Semicond. Process. 42 (2016) 111–114. doi:10.1016/j.mssp.2015.07.058.

[324] D. Emadzadeh, W.J. Lau, M. Rahbari-Sisakht, A. Daneshfar, M. Ghanbari, A. Mayahi, T. Matsuura, A.F. Ismail, A novel thin film nanocomposite reverse osmosis membrane with superior anti-organic fouling affinity for water desalination, Desalination. 368 (2015) 106–113. doi:10.1016/j.desal.2014.11.019.

[325] L. Liu, G. Zhu, Z. Liu, C. Gao, Effect of MCM-48 nanoparticles on the performance of thin film nanocomposite membranes for reverse osmosis application, Desalination. 394 (2016) 72–82. doi:10.1016/j.desal.2016.04.028.

[326] R. Ma, Y.L. Ji, Y.S. Guo, Y.F. Mi, Q.F. An, C.J. Gao, Fabrication of antifouling reverse osmosis membranes by incorporating zwitterionic colloids nanoparticles for brackish water desalination, Desalination. 416 (2017) 35–44. doi:10.1016/j.desal.2017.04.016.

[327] M. Ben-Sasson, X. Lu, E. Bar-Zeev, K.R. Zodrow, S. Nejati, G. Qi, E.P. Giannelis, M. Elimelech, In situ formation of silver nanoparticles on thin-film composite reverse osmosis membranes for biofouling mitigation, Water Res. 62 (2014) 260–270. doi:10.1016/j.watres.2014.05.049.

[328] J. Duan, E. Litwiller, I. Pinnau, Preparation and water desalination properties of POSS-polyamide nanocomposite reverse osmosis membranes, J. Memb. Sci. 473 (2015) 157–164. doi:10.1016/j.memsci.2014.09.022.

[329] J. Duan, Y. Pan, F. Pacheco, E. Litwiller, Z. Lai, I. Pinnau, High-performance polyamide thin-film-nanocomposite reverse osmosis membranes containing hydrophobic zeolitic imidazolate framework-8, J. Memb. Sci. 476 (2015) 303–310. doi:10.1016/j.memsci.2014.11.038.

[330] H. Dong, L. Wu, L. Zhang, H. Chen, C. Gao, Clay nanosheets as charged filler materials for high-performance and fouling-resistant thin film nanocomposite membranes, J. Memb. Sci. 494 (2015) 92–103. doi:10.1016/j.memsci.2015.07.049.

[331] Y. Xu, X. Gao, X. Wang, Q. Wang, Z. Ji, X. Wang, T. Wu, C. Gao, Highly and stably water permeable thin film nanocomposite membranes doped with MIL-101 (Cr)

nanoparticles for reverse osmosis application, Materials (Basel). 9 (2016). doi:10.3390/ma9110870.

[332] A. Al Mayyahi, TiO2 Polyamide Thin Film Nanocomposite Reverses Osmosis Membrane for Water Desalination, Membranes (Basel). 8 (2018) 66. doi:10.3390/membranes8030066.

[333] H. Choi, J. Park, T. Tak, Y.N. Kwon, Surface modification of seawater reverse osmosis (SWRO) membrane using methyl methacrylate-hydroxy poly(oxyethylene) methacrylate (MMA-HPOEM) comb-polymer and its performance, Desalination. 291 (2012) 1–7. doi:10.1016/j.desal.2012.01.018.

[334] C. Zhou, D. Ye, H. Jia, S. Yu, M. Liu, C. Gao, Surface mineralization of commercial thin-film composite polyamide membrane by depositing barium sulfate for improved reverse osmosis performance and antifouling property, Desalination. 351 (2014) 228–235. doi:10.1016/j.desal.2014.07.040.

[335] H. Karkhanechi, R. Takagi, H. Matsuyama, Biofouling resistance of reverse osmosis membrane modified with polydopamine, Desalination. 336 (2014) 87–96. doi:10.1016/j.desal.2013.12.033.

[336] Y. Zhang, Y. Wan, G. Pan, H. Shi, H. Yan, J. Xu, M. Guo, Z. Wang, Y. Liu, Surface modification of polyamide reverse osmosis membrane with sulfonated polyvinyl alcohol for antifouling, Appl. Surf. Sci. 419 (2017) 177–187. doi:10.1016/j.apsusc.2017.05.047.

[337] S. Yu, Z. Lü, Z. Chen, X. Liu, M. Liu, C. Gao, Surface modification of thin-film composite polyamide reverse osmosis membranes by coating N-isopropylacrylamide-co-acrylic acid copolymers for improved membrane properties, J. Memb. Sci. 371 (2011) 293–306. doi:10.1016/j.memsci.2011.01.059.

[338] S. Yu, X. Liu, J. Liu, D. Wu, M. Liu, C. Gao, Surface modification of thin-film composite polyamide reverse osmosis membranes with thermo-responsive polymer (TRP) for improved fouling resistance and cleaning efficiency, Sep. Purif. Technol. 76 (2011) 283–291. doi:10.1016/j.seppur.2010.10.017.

[339] S. Azari, L. Zou, Using zwitterionic amino acid l-DOPA to modify the surface of thin film composite polyamide reverse osmosis membranes to increase their fouling resistance, J. Memb. Sci. 401–402 (2012) 68–75. doi:10.1016/j.memsci.2012.01.041.

[340] Y. Wang, Z. Wang, X. Han, J. Wang, S. Wang, Improved flux and anti-biofouling performances of reverse osmosis membrane via surface layer-by-layer assembly, J. Memb. Sci. 539 (2017) 403–411. doi:10.1016/j.memsci.2017.06.029.

[341] D. Saeki, T. Tanimoto, H. Matsuyama, Prevention of bacterial adhesion on polyamide reverse osmosis membranes via electrostatic interactions using a cationic phosphorylcholine polymer coating, Colloids Surfaces A Physicochem. Eng. Asp. 443 (2014) 171–176. doi:10.1016/j.colsurfa.2013.11.007.

[342] T. Ishigami, K. Amano, A. Fujii, Y. Ohmukai, E. Kamio, T. Maruyama, H. Matsuyama, Fouling reduction of reverse osmosis membrane by surface modification via layer-by-layer assembly, Sep. Purif. Technol. 99 (2012) 1–7. doi:10.1016/j.seppur.2012.08.002.

[343] S. Yu, G. Yao, B. Dong, H. Zhu, X. Peng, J. Liu, M. Liu, C. Gao, Improving fouling resistance of thin-film composite polyamide reverse osmosis membrane by coating natural

hydrophilic polymer sericin, Sep. Purif. Technol. 118 (2013) 285–293. doi:10.1016/j.seppur.2013.07.018.

[344] A. Zhang, Y. Zhang, G. Pan, J. Xu, H. Yan, Y. Liu, In situ formation of copper nanoparticles in carboxylated chitosan layer: Preparation and characterization of surface modified TFC membrane with protein fouling resistance and long-lasting antibacterial properties, Sep. Purif. Technol. 176 (2017) 164–172. doi:10.1016/j.seppur.2016.12.006.

[345] C. Wang, G.K. Such, A. Widjaya, H. Lomas, G. Stevens, F. Caruso, S.E. Kentish, Click poly(ethylene glycol) multilayers on RO membranes: Fouling reduction and membrane characterization, J. Memb. Sci. 409–410 (2012) 9–15. doi:10.1016/j.memsci.2012.02.049.

[346] J. Nikkola, X. Liu, Y. Li, M. Raulio, H.L. Alakomi, J. Wei, C.Y. Tang, Surface modification of thin film composite RO membrane for enhanced anti-biofouling performance, J. Memb. Sci. 444 (2013) 192–200. doi:10.1016/j.memsci.2013.05.032.

[347] J. Nikkola, J. Sievänen, M. Raulio, J. Wei, J. Vuorinen, C.Y. Tang, Surface modification of thin film composite polyamide membrane using atomic layer deposition method, J. Memb. Sci. 450 (2014) 174–180. doi:10.1016/j.memsci.2013.09.005.

[348] J.S. Louie, I. Pinnau, I. Ciobanu, K.P. Ishida, A. Ng, M. Reinhard, Effects of polyether-polyamide block copolymer coating on performance and fouling of reverse osmosis membranes, J. Memb. Sci. 280 (2006) 762–770. doi:10.1016/j.memsci.2006.02.041.

[349] A.C. Sagle, E.M. Van Wagner, H. Ju, B.D. McCloskey, B.D. Freeman, M.M. Sharma, PEG-coated reverse osmosis membranes: Desalination properties and fouling resistance, J. Memb. Sci. 340 (2009) 92–108. doi:10.1016/j.memsci.2009.05.013.

[350] A. Sarkar, P.I. Carver, T. Zhang, A. Merrington, K.J. Bruza, J.L. Rousseau, S.E. Keinath, P.R. Dvornic, Dendrimer-based coatings for surface modification of polyamide reverse osmosis membranes, J. Memb. Sci. 349 (2010) 421–428. doi:10.1016/j.memsci.2009.12.005.

[351] Y. Zhou, S. Yu, C. Gao, X. Feng, Surface modification of thin film composite polyamide membranes by electrostatic self deposition of polycations for improved fouling resistance, Sep. Purif. Technol. 66 (2009) 287–294. doi:10.1016/j.seppur.2008.12.021.

[352] M. Liu, Z. Chen, S. Yu, D. Wu, C. Gao, Thin-film composite polyamide reverse osmosis membranes with improved acid stability and chlorine resistance by coating N-isopropylacrylamide-co-acrylamide copolymers, Desalination. 270 (2011) 248–257. doi:10.1016/j.desal.2010.11.052.

[353] F. Shao, L. Dong, H. Dong, Q. Zhang, M. Zhao, L. Yu, B. Pang, Y. Chen, Graphene oxide modified polyamide reverse osmosis membranes with enhanced chlorine resistance, J. Memb. Sci. 525 (2017) 9–17. doi:10.1016/j.memsci.2016.12.001.

[354] J. Sun, L.P. Zhu, Z.H. Wang, F. Hu, P. Bin Zhang, B.K. Zhu, Improved chlorine resistance of polyamide thin-film composite membranes with a terpolymer coating, Sep. Purif. Technol. 157 (2016) 112–119. doi:10.1016/j.seppur.2015.11.034.

[355] L. Ni, J. Meng, X. Li, Y. Zhang, Surface coating on the polyamide TFC RO membrane for chlorine resistance and antifouling performance improvement, J. Memb. Sci. 451 (2014) 205–215. doi:10.1016/j.memsci.2013.09.040.

[356] Y.N. Kwon, S. Hong, H. Choi, T. Tak, Surface modification of a polyamide reverse

osmosis membrane for chlorine resistance improvement, J. Memb. Sci. 415–416 (2012) 192–198. doi:10.1016/j.memsci.2012.04.056.

[357] J. Xu, X. Feng, C. Gao, Surface modification of thin-film-composite polyamide membranes for improved reverse osmosis performance, J. Memb. Sci. 370 (2011) 116–123. doi:10.1016/j.memsci.2011.01.001.

[358] A. Kulkarni, D. Mukherjee, W.N. Gill, Flux enhancement by hydrophilization of thin film composite reverse osmosis membranes, J. Memb. Sci. 114 (1996) 39–50. doi:10.1016/0376-7388(95)00271-5.

[359] R. Reis, L.F. Dumée, A. Merenda, J.D. Orbell, J.A. Schütz, M.C. Duke, Plasma-induced physicochemical effects on a poly(amide) thin-film composite membrane, Desalination. 403 (2017) 3–11. doi:10.1016/j.desal.2016.06.009.

[360] R. Reis, M. Duke, A. Merenda, B. Winther-Jensen, L. Puskar, M.J. Tobin, J.D. Orbell, L.F. Dumée, Customizing the surface charge of thin-film composite membranes by surface plasma thin film polymerization, J. Memb. Sci. 537 (2017) 1–10. doi:10.1016/j.memsci.2017.05.013.

[361] G. Kang, H. Yu, Z. Liu, Y. Cao, Surface modification of a commercial thin film composite polyamide reverse osmosis membrane by carbodiimide-induced grafting with poly(ethylene glycol) derivatives, Desalination. 275 (2011) 252–259. doi:10.1016/j.desal.2011.03.007.

[362] S. Azari, L. Zou, Fouling resistant zwitterionic surface modification of reverse osmosis membranes using amino acid l-cysteine, Desalination. 324 (2013) 79–86. doi:10.1016/j.desal.2013.06.005.

[363] J. Xu, Z. Wang, J. Wang, S. Wang, Positively charged aromatic polyamide reverse osmosis membrane with high anti-fouling property prepared by polyethylenimine grafting, Desalination. 365 (2015) 398–406. doi:10.1016/j.desal.2015.03.026.

[364] D. Saeki, S. Nagao, I. Sawada, Y. Ohmukai, T. Maruyama, H. Matsuyama, Development of antibacterial polyamide reverse osmosis membrane modified with a covalently immobilized enzyme, J. Memb. Sci. 428 (2013) 403–409. doi:10.1016/j.memsci.2012.10.038.

[365] D. Nikolaeva, C. Langner, A. Ghanem, M.A. Rehim, B. Voit, J. Meier-Haack, Hydrogel surface modification of reverse osmosis membranes, J. Memb. Sci. 476 (2015) 264–276. doi:10.1016/j.memsci.2014.11.051.

[366] Y. Hu, K. Lu, F. Yan, Y. Shi, P. Yu, S. Yu, S. Li, C. Gao, Enhancing the performance of aromatic polyamide reverse osmosis membrane by surface modification via covalent attachment of polyvinyl alcohol (PVA), J. Memb. Sci. 501 (2016) 209–219. doi:10.1016/j.memsci.2015.12.003.

[367] Z. Zhang, Z. Wang, J. Wang, S. Wang, Enhancing chlorine resistances and anti-biofouling properties of commercial aromatic polyamide reverse osmosis membranes by grafting 3-allyl-5,5-dimethylhydantoin and N,N'-Methylenebis(acrylamide), Desalination. 309 (2013) 187–196. doi:10.1016/j.desal.2012.10.019.

[368] D. Saeki, T. Tanimoto, H. Matsuyama, Anti-biofouling of polyamide reverse osmosis membranes using phosphorylcholine polymer grafted by surface-initiated atom transfer

radical polymerization, Desalination. 350 (2014) 21–27. doi:10.1016/j.desal.2014.07.004.

[369] H. Isawi, M.H. El-Sayed, X. Feng, H. Shawky, M.S. Abdel Mottaleb, Surface nanostructuring of thin film composite membranes via grafting polymerization and incorporation of ZnO nanoparticles, Appl. Surf. Sci. 385 (2016) 268–281. doi:10.1016/j.apsusc.2016.05.141.

[370] V. Vatanpour, N. Zoqi, Surface modification of commercial seawater reverse osmosis membranes by grafting of hydrophilic monomer blended with carboxylated multiwalled carbon nanotubes, Appl. Surf. Sci. 396 (2017) 1478–1489. doi:https://doi.org/10.1016/j.apsusc.2016.11.195.

[371] Q. Cheng, Y. Zheng, S. Yu, H. Zhu, X. Peng, J. Liu, J. Liu, M. Liu, C. Gao, Surface modification of a commercial thin-film composite polyamide reverse osmosis membrane through graft polymerization of N-isopropylacrylamide followed by acrylic acid, J. Memb. Sci. 447 (2013) 236–245. doi:10.1016/j.memsci.2013.07.025.

[372] J. Wang, Z. Wang, J. Wang, S. Wang, Improving the water flux and bio-fouling resistance of reverse osmosis (RO) membrane through surface modification by zwitterionic polymer, J. Memb. Sci. 493 (2015) 188–199. doi:10.1016/j.memsci.2015.06.036.

[373] H.Z. Shafi, Z. Khan, R. Yang, K.K. Gleason, Surface modification of reverse osmosis membranes with zwitterionic coating for improved resistance to fouling, Desalination. 362 (2015) 93–103. doi:10.1016/j.desal.2015.02.009.

[374] G. Ozaydin-Ince, A. Matin, Z. Khan, S.M.J. Zaidi, K.K. Gleason, Surface modification of reverse osmosis desalination membranes by thin-film coatings deposited by initiated chemical vapor deposition, Thin Solid Films. 539 (2013) 181–187. doi:10.1016/j.tsf.2013.04.133.

[375] R. Yang, J. Xu, G. Ozaydin-Ince, S.Y. Wong, K.K. Gleason, Surface-tethered zwitterionic ultrathin antifouling coatings on reverse osmosis membranes by initiated chemical vapor deposition, Chem. Mater. 23 (2011) 1263–1272. doi:10.1021/cm1031392.

[376] J. Xu, Z. Wang, L. Yu, J. Wang, S. Wang, A novel reverse osmosis membrane with regenerable anti-biofouling and chlorine resistant properties, J. Memb. Sci. 435 (2013) 80–91. doi:10.1016/j.memsci.2013.02.010.

[377] S. Lin, H. Huang, Y. Zeng, L. Zhang, L. Hou, Facile surface modification by aldehydes to enhance chlorine resistance of polyamide thin film composite membranes, J. Memb. Sci. 518 (2016) 40–49. doi:10.1016/j.memsci.2016.06.032.

[378] W.S. Ang, N.Y. Yip, A. Tiraferri, M. Elimelech, Chemical cleaning of RO membranes fouled by wastewater effluent: Achieving higher efficiency with dual-step cleaning, J. Memb. Sci. 382 (2011) 100–106. doi:10.1016/j.memsci.2011.07.047.

[379] Y.G. Lee, A. Gambier, E. Badreddin, S. Lee, D.R. Yang, J.H. Kim, Application of hybrid systems techniques for cleaning and replacement of a RO membrane, Desalination. 247 (2009) 25–32. doi:10.1016/j.desal.2008.12.009.

[380] X. Huang, G.R. Guillen, E.M. V Hoek, A new high-pressure optical membrane module for direct observation of seawater RO membrane fouling and cleaning, J. Memb. Sci. 364 (2010) 149–156. doi:10.1016/j.memsci.2010.08.009.

[381] E. Filloux, J. Wang, M. Pidou, W. Gernjak, Z. Yuan, Biofouling and scaling control of

reverse osmosis membrane using one-step cleaning-potential of acidified nitrite solution as an agent, J. Memb. Sci. 495 (2015) 276–283. doi:10.1016/j.memsci.2015.08.034.

[382] X. Li, D. Yan, G. An, D. Jing, J. Li, Fouling and Cleaning of Reverse Osmosis Membranes duing Municipal Tap Water Treatment on a Pilot-Scale Plant, J. Water Sustain. 1 (2011) 139–151.

[383] M.R. Sohrabi, S.S. Madaeni, M. Khosravi, A.M. Ghaedi, Chemical cleaning of reverse osmosis and nanofiltration membranes fouled by licorice aqueous solutions, Desalination. 267 (2011) 93–100. doi:10.1016/j.desal.2010.09.011.

[384] S.S. Madaeni, S. Samieirad, Chemical cleaning of reverse osmosis membrane fouled by wastewater, Desalination. 257 (2010) 80–86. doi:10.1016/j.desal.2010.03.002.

[385] W.S. Ang, A. Tiraferri, K.L. Chen, M. Elimelech, Fouling and cleaning of RO membranes fouled by mixtures of organic foulants simulating wastewater effluent, J. Memb. Sci. 376 (2011) 196–206. doi:10.1016/j.memsci.2011.04.020.

[386] M. Kazemimoghadam, T. Mohammadi, Chemical cleaning of ultrafiltration membranes in the milk industry, Desalination. 204 (2007) 213–218. doi:10.1016/j.desal.2006.04.030.

[387] J.S. Vrouwenvelder, J.C. Kruithof, M.C.M. Van Loosdrecht, Integrated approach for biofouling control, Water Sci. Technol. 62 (2010) 2477–2490. doi:10.2166/wst.2010.747.

[388] M. You, P. Wang, M. Xu, T. Yuan, J. Meng, Fouling resistance and cleaning efficiency of stimuli-responsive reverse osmosis (RO) membranes, Polymer (Guildf). 103 (2016) 457–467. doi:10.1016/j.polymer.2016.03.065.

[389] J.M. Ochando-Pulido, M.D. Victor-Ortega, A. Martínez-Ferez, On the cleaning procedure of a hydrophilic reverse osmosis membrane fouled by secondary-treated olive mill wastewater, Chem. Eng. J. 260 (2015) 142–151. doi:10.1016/j.cej.2014.08.094.

[390] T. Yu, L. Meng, Q.B. Zhao, Y. Shi, H.Y. Hu, Y. Lu, Effects of chemical cleaning on RO membrane inorganic, organic and microbial foulant removal in a full-scale plant for municipal wastewater reclamation, Water Res. 113 (2017) 1–10. doi:10.1016/j.watres.2017.01.068.

[391] S.F. Anis, R. Hashaikeh, N. Hilal, Reverse osmosis pretreatment technologies and future trends: A comprehensive review, Desalination. 452 (2019) 159–195. doi:10.1016/j.desal.2018.11.006.

[392] S.S. Madaeni, N. Ghaemi, Characterization of self-cleaning RO membranes coated with TiO2 particles under UV irradiation, J. Memb. Sci. 303 (2007) 221–233. doi:10.1016/j.memsci.2007.07.017.

[393] N.K. Khanzada, S.J. Khan, P.A. Davies, Performance evaluation of reverse osmosis (RO) pre-treatment technologies for in-land brackish water treatment, Desalination. 406 (2017) 44–50. doi:10.1016/j.desal.2016.06.030.

[394] M. Badruzzaman, N. Voutchkov, L. Weinrich, J.G. Jacangelo, Selection of pretreatment technologies for seawater reverse osmosis plants: A review, Desalination. 449 (2019) 78–91. doi:10.1016/j.desal.2018.10.006.

[395] R. Fabris, C.W.K. Chow, M. Drikas, B. Eikebrokk, Comparison of NOM character in selected Australian and Norwegian drinking waters, Water Res. 42 (2008) 4188–4196.

doi:10.1016/j.watres.2008.06.023.

[396] F.-H. Wang, H.-T. Hao, R. Sun, S. Li, R. Han, C. Papelis, Y. Zhang, Bench-scale and pilot-scale evaluation of coagulation pre-treatment for wastewater reused by reverse osmosis in a petrochemical circulating cooling water system, Desalination. 335 (2014) 64–69. doi:https://doi.org/10.1016/j.desal.2013.12.013.

[397] J. Duan, F. Wilson, N. Graham, J.H. Tay, Adsorption of humic acid by powdered activated carbon in saline water conditions, Desalination. 151 (2003) 53–66. doi:10.1016/S0011-9164(02)00972-4.

[398] S.Y. Lee, G.A. Gagnon, Comparing the growth and structure of flocs from electrocoagulation and chemical coagulation, J. Water Process Eng. 10 (2016) 20–29. doi:10.1016/j.jwpe.2016.01.012.

[399] R.H. Peiris, M. Jaklewicz, H. Budman, R.L. Legge, C. Moresoli, Assessing the role of feed water constituents in irreversible membrane fouling of pilot-scale ultrafiltration drinking water treatment systems, Water Res. 47 (2013) 3364–3374. doi:10.1016/j.watres.2013.03.015.

[400] K. Sadeddin, A. Naser, A. Firas, Removal of turbidity and suspended solids by electro-coagulation to improve feed water quality of reverse osmosis plant, Desalination. 268 (2011) 204–207. doi:10.1016/j.desal.2010.10.027.

[401] D.S. Patil, S.M. Chavan, J.U.K. Oubagaranadin, A review of technologies for manganese removal from wastewaters, J. Environ. Chem. Eng. 4 (2016) 468–487. doi:10.1016/j.jece.2015.11.028.

[402] K. Song, M. Mohseni, F. Taghipour, Application of ultraviolet light-emitting diodes (UV-LEDs) for water disinfection: A review, Water Res. 94 (2016) 341–349. doi:10.1016/j.watres.2016.03.003.

[403] H. Wang, S. Yuan, J. Zhan, Y. Wang, G. Yu, S. Deng, J. Huang, B. Wang, Mechanisms of enhanced total organic carbon elimination from oxalic acid solutions by electro-peroxone process, Water Res. 80 (2015) 20–29. doi:10.1016/j.watres.2015.05.024.

[404] E. Friedler, I. Katz, C.G. Dosoretz, Chlorination and coagulation as pretreatments for greywater desalination, Desalination. 222 (2008) 38–49. doi:10.1016/j.desal.2007.01.130.

[405] M.A. Sanza, V. Bonnélyea, G. Cremerb, Fujairah reverse osmosis plant: 2 years of operation, Desalination. 203 (2007) 91–99. doi:10.1016/j.desal.2006.03.526.

[406] J. Park, Y. Kim, P.K. Kim, H. V Daniels, Effects of two different ozone doses on seawater recirculating systems for black sea bream Acanthopagrus schlegeli (Bleeker): Removal of solids and bacteria by foam fractionation, Aquac. Eng. 44 (2011) 19–24. doi:10.1016/j.aquaeng.2010.11.001.

[407] E. Joyce, S.S. Phull, J.P. Lorimer, T.J. Mason, The development and evaluation of ultrasound for the treatment of bacterial suspensions. A study of frequency, power and sonication time on cultured [i]Bacillus[/i] species, Ultrason. Sonochem. 10 (2003) 315–318. doi:10.1016/S1350-4177(03)00101-9.

[408] S. Broekman, O. Pohlmann, E.S. Beardwood, E.C. de Meulenaer, Ultrasonic treatment for microbiological control of water systems, Ultrason. Sonochem. 17 (2010) 1041–1048. doi:10.1016/j.ultsonch.2009.11.011.

[409] B.K. Pramanik, Y. Gao, L. Fan, F.A. Roddick, Z. Liu, Antiscaling effect of polyaspartic acid and its derivative for RO membranes used for saline wastewater and brackish water desalination, Desalination. 404 (2017) 224–229. doi:https://doi.org/10.1016/j.desal.2016.11.019.

[410] M. Al-Shammiri, M. Safar, M. Al-Dawas, Evaluation of two different antiscalants in real operation at the Doha research plant, Desalination. 128 (2000) 1–16. doi:10.1016/S0011-9164(00)00019-9.

[411] E.A. Rashed, M.M. Elshafei, M.A. Hiekl, M.E. Matta, K.M. Naguib, On-line dosing of Ammonium Biflouride for reduction of silica scaling on RO membranes, HBRC J. 12 (2016) 205–211. doi:10.1016/j.hbrcj.2014.10.001.

[412] M. Nair, D. Kumar, Water desalination and challenges: The Middle East perspective: A review, Desalin. Water Treat. 51 (2013) 2030–2040. doi:10.1080/19443994.2013.734483.

[413] V. Bonnélye, L. Guey, J. Del Castillo, UF/MF as RO pre-treatment: the real benefit, Desalination. 222 (2008) 59–65. doi:10.1016/j.desal.2007.01.129.

[414] K. Chinu, A.H. Johir, S. Vigneswaran, H.K. Shon, J. Kandasamy, Assessment of pretreatment to microfiltration for desalination in terms of fouling index and molecular weight distribution, Desalination. 250 (2010) 644–647. doi:10.1016/j.desal.2009.09.041.

[415] J. Lee, B.S. Oh, S. Kim, S.J. Kim, S.K. Hong, I.S. Kim, Fate of Bacillus sp. and Pseudomonas sp. isolated from seawater during chlorination and microfiltration as pretreatments of a desalination plant, J. Memb. Sci. 349 (2010) 208–216. doi:10.1016/j.memsci.2009.11.045.

[416] A.F. Corral, U. Yenal, R. Strickle, D. Yan, E. Holler, C. Hill, W.P. Ela, R.G. Arnold, Comparison of slow sand filtration and microfiltration as pretreatments for inland desalination via reverse osmosis, Desalination. 334 (2014) 1–9. doi:10.1016/j.desal.2013.11.034.

[417] N. Voutchkov, Considerations for selection of seawater filtration pretreatment system, Desalination. 261 (2010) 354–364. doi:10.1016/j.desal.2010.07.002.

[418] E. Akhondi, B. Wu, S. Sun, B. Marxer, W. Lim, J. Gu, L. Liu, M. Burkhardt, D. McDougald, W. Pronk, A.G. Fane, Gravity-driven membrane filtration as pretreatment for seawater reverse osmosis: Linking biofouling layer morphology with flux stabilization, Water Res. 70 (2015) 158–173. doi:10.1016/j.watres.2014.12.001.

[419] M. Monnot, S. Laborie, C. Cabassud, Granular activated carbon filtration plus ultrafiltration as a pretreatment to seawater desalination lines: Impact on water quality and UF fouling, Desalination. 383 (2016) 1–11. doi:10.1016/j.desal.2015.12.010.

[420] A.R. Guastalli, F.X. Simon, Y. Penru, A. de Kerchove, J. Llorens, S. Baig, Comparison of DMF and UF pre-treatments for particulate material and dissolved organic matter removal in SWRO desalination, Desalination. 322 (2013) 144–150. doi:10.1016/j.desal.2013.05.005.

[421] Y. Song, B. Su, X. Gao, C. Gao, The performance of polyamide nanofiltration membrane for long-term operation in an integrated membrane seawater pretreatment system, Desalination. 296 (2012) 30–36. doi:10.1016/j.desal.2012.03.024.

[422] X. Li, Y. Cao, H. Yu, G. Kang, X. Jie, Z. Liu, Q. Yuan, A novel composite nanofiltration

membrane prepared with PHGH and TMC by interfacial polymerization, J. Memb. Sci. 466 (2014) 82–91. doi:10.1016/j.memsci.2014.04.034.

[423] S. El-Manharawy, A. Hafez, Water type and guidelines for RO system design, Desalination. 139 (2001) 97–113. doi:10.1016/S0011-9164(01)00298-3.

[424] AWWA Staff, Reverse Osmosis and Nanofiltration, American Water Works Assoc., Denver, UNITED STATES, 2006. http://ebookcentral.proquest.com/lib/aus-ebooks/detail.action?docID=3116769.

[425] P. Dorji, J. Choi, D.I. Kim, S. Phuntsho, S. Hong, H.K. Shon, Membrane capacitive deionisation as an alternative to the 2nd pass for seawater reverse osmosis desalination plant for bromide removal, Desalination. 433 (2018) 113–119. doi:10.1016/j.desal.2018.01.020.

[426] S. Rybar, R. Boda, C. Bartels, Split partial second pass design for SWRO plants, Desalin. Water Treat. 13 (2010) 186–194. doi:10.5004/dwt.2010.989.

[427] N. Voutchkov, Desalination Engineering: Operation and Maintenance, McGraw-Hill, New York, 2014.

[428] M. Wilf, C. Bartels, Optimization of seawater RO systems design, Desalination. 173 (2005) 1–12. doi:10.1016/j.desal.2004.06.206.

[429] F. Vince, F. Marechal, E. Aoustin, P. Bréant, Multi-objective optimization of RO desalination plants, Desalination. 222 (2008) 96–118. doi:10.1016/j.desal.2007.02.064.

[430] Y. Du, L. Xie, J. Liu, Y. Wang, Y. Xu, S. Wang, Multi-objective optimization of reverse osmosis networks by lexicographic optimization and augmented epsilon constraint method, Desalination. 333 (2014) 66–81. doi:10.1016/j.desal.2013.10.028.

[431] Y. Saif, A. Almansoori, Synthesis of reverse osmosis desalination network under boron specifications, Desalination. 371 (2015) 26–36. doi:10.1016/j.desal.2015.05.012.

[432] Y. Saif, A. Almansoori, A. Elkamel, Optimal design of split partial second pass reverse osmosis network for desalination applications, AIChE J. 60 (2014) 520–532. doi:10.1002/aic.14271.

[433] B. Djebedjian, H. Gad, I. Khaled, M.A. Rayan, S.D. Authority, Optimization of Reverse Osmosis Desalination System Using Genetic Algorithms Technique, Twelfth Int. Water Technol. Conf. IWTC12. (2008) 1047–1067. doi:10.4025/dialogos.v18i3.996.

[434] C. Guria, P.K. Bhattacharya, S.K. Gupta, Multi-objective optimization of reverse osmosis desalination units using different adaptations of the non-dominated sorting genetic algorithm (NSGA), Comput. Chem. Eng. 29 (2005) 1977–1995. doi:10.1016/j.compchemeng.2005.05.002.

[435] Y.Y. Lu, Y.D. Hu, X.L. Zhang, L.Y. Wu, Q.Z. Liu, Optimum design of reverse osmosis system under different feed concentration and product specification, J. Memb. Sci. 287 (2007) 219–229. doi:10.1016/j.memsci.2006.10.037.

[436] E. Antipova, D. Boer, L.F. Cabeza, G. Guillén-Gosálbez, L. Jiménez, Multi-objective design of reverse osmosis plants integrated with solar Rankine cycles and thermal energy storage, Appl. Energy. 102 (2013) 1137–1147. doi:10.1016/j.apenergy.2012.06.038.

[437] H. Kotb, E.H. Amer, K.A. Ibrahim, On the optimization of RO (Reverse Osmosis) system

arrangements and their operating conditions, Energy. 103 (2016) 127–150. doi:10.1016/j.energy.2016.02.162.

[438] B. Peñate, L. Garc\'\ia-Rodr\'\iguez, Reverse osmosis hybrid membrane inter-stage design: A comparative performance assessment, Desalination. 281 (2011) 354–363. doi:10.1016/j.desal.2011.08.010.

[439] D. Zarzo, D. Prats, Desalination and energy consumption. What can we expect in the near future?, Desalination. 427 (2018) 1–9. doi:10.1016/j.desal.2017.10.046.

[440] N. Voutchkov, Desalination Engineering: Planning and Design, McGraw Hill, New York, 2012.

[441] N. Ghaffour, T.M. Missimer, G.L. Amy, Technical review and evaluation of the economics of water desalination: Current and future challenges for better water supply sustainability, Desalination. 309 (2013) 197–207. doi:10.1016/j.desal.2012.10.015.

[442] J. Olsson, Stainless steels for desalination plants, Desalination. 183 (2005) 217–225. doi:10.1016/j.desal.2005.02.050.

[443] J. Olsson, M. Snis, Duplex - A new generation of stainless steels for desalination plants, Desalination. 205 (2007) 104–113. doi:10.1016/j.desal.2006.02.051.

[444] F. Moreno, A. Pinilla, Preliminary experimental study of a small reverse osmosis wind-powered desalination plant, Desalination. 171 (2005) 257–265. doi:10.1016/j.desal.2004.06.191.

[445] R. Pohl, M. Kaltschmitt, R. Holländer, Investigation of different operational strategies for the variable operation of a simple reverse osmosis unit, Desalination. 249 (2009) 1280–1287. doi:10.1016/j.desal.2009.06.029.

[446] WHO, Boron in Drinking-water, Geneva, 2003. https://www.who.int/water_sanitation_health/dwq/boron.pdf.

[447] N. Kabay, E. Güler, M. Bryjak, Boron in seawater and methods for its separation - A review, Desalination. 261 (2010) 212–217. doi:10.1016/j.desal.2010.05.033.

[448] A. Farhat, F. Ahmad, H. Arafat, Analytical techniques for boron quantification supporting desalination processes: A review, Desalination. (2013). doi:10.1016/j.desal.2011.12.020.

[449] N. Hilal, G.J. Kim, C. Somerfield, Boron removal from saline water: A comprehensive review, Desalination. 273 (2011) 23–35. doi:10.1016/j.desal.2010.05.012.

[450] P. Glueckstern, M. Priel, Optimization of boron removal in old and new SWRO systems, Desalination. 156 (2003) 219–228. doi:10.1016/S0011-9164(03)00344-8.

[451] D. Prats, M.F. Chillon-Arias, M. Rodriguez-Pastor, Analysis of the influence of pH and pressure on the elimination of boron in reverse osmosis, Desalination. 128 (2000) 269–273. doi:10.1016/S0011-9164(00)00041-2.

[452] Y. Magara, A. Tabata, M. Kohki, M. Kawasaki, M. Hirose, Development of boron reduction system for sea water desalination, Desalination. 118 (1998) 25–34. doi:10.1016/S0011-9164(98)00076-9.

[453] H. Hyung, J.H. Kim, A mechanistic study on boron rejection by sea water reverse osmosis membranes, J. Memb. Sci. 286 (2006) 269–278. doi:10.1016/j.memsci.2006.09.043.

[454] P.V.X. Hung, S.H. Cho, S.H. Moon, Prediction of boron transport through seawater reverse osmosis membranes using solution-diffusion model, Desalination. 247 (2009) 33–44. doi:10.1016/j.desal.2008.12.010.

[455] H. Koseoglu, N. Kabay, M. Yüksel, S. Sarp, Ö. Arar, M. Kitis, Boron removal from seawater using high rejection SWRO membranes - impact of pH, feed concentration, pressure, and cross-flow velocity, Desalination. 227 (2008) 253–263. doi:10.1016/j.desal.2007.06.029.

[456] M.H.I. Dore, Forecasting the economic costs of desalination technology, Desalination. 172 (2005) 207–214. doi:10.1016/j.desal.2004.07.036.

[457] S.T. M. Ando, H. Iwahori, R. Nakahara, Design operation and environmental aspects of 40,000 m3/day seawater RO plant in Okinawa, Japan. Development of high boron rejection membrane technology, in: Proc. 4th Annu. IDS Conf., Haifa, Israel, 2001.

[458] M. Wolfs, S. Woodroffe, Structuring and financing international BOO/BOT desalination projects, Desalination. 142 (2002) 101–106. doi:https://doi.org/10.1016/S0011-9164(01)00429-5.

[459] F. Lokiec, G. Kronenberg, Emerging role of BOOT desalination projects, Desalination. 136 (2001) 109–114. doi:10.1016/S0011-9164(01)00172-2.

[460] A. Shrivastava, D. Stevens, Chapter 2 - Energy Efficiency of Reverse Osmosis, in: V.G.B.T.-S.D.H. Gude (Ed.), Butterworth-Heinemann, 2018: pp. 25–54. doi:https://doi.org/10.1016/B978-0-12-809240-8.00002-2.

[461] N. Voutchkov, Energy use for membrane seawater desalination – current status and trends, Desalination. 431 (2018) 2–14. doi:10.1016/j.desal.2017.10.033.

[462] J.E. Blank, G.F. Tusel, S. Nisanc, The real cost of desalted water and how to reduce it further, Desalination. 205 (2007) 298–311. doi:10.1016/j.desal.2006.05.015.

[463] M.C. Garg, H. Joshi, Optimization and economic analysis of small scale nanofiltration and reverse osmosis brackish water system powered by photovoltaics, Desalination. 353 (2014) 57–74. doi:10.1016/j.desal.2014.09.005.

[464] H. Cherif, J. Belhadj, Chapter 15 - Environmental Life Cycle Analysis of Water Desalination Processes, in: V.G.B.T.-S.D.H. Gude (Ed.), Butterworth-Heinemann, 2018: pp. 527–559. doi:https://doi.org/10.1016/B978-0-12-809240-8.00015-0.

[465] J.M. Gordon, T.C. Hui, Thermodynamic perspective for the specific energy consumption of seawater desalination, Desalination. 386 (2016) 13–18. doi:10.1016/j.desal.2016.02.030.

[466] M. Elimelech, W.A. Phillip, The future of seawater desalination: Energy, technology, and the environment, Science (80-.). 333 (2011) 712–717. doi:10.1126/science.1200488.

[467] A.J. Karabelas, C.P. Koutsou, M. Kostoglou, D.C. Sioutopoulos, Analysis of specific energy consumption in reverse osmosis desalination processes, Desalination. 431 (2018) 15–21. doi:10.1016/j.desal.2017.04.006.

[468] C. Bartels, R. Bergman, M. Hallan, L. Henthorne, P. Knappe, J. Lozier, P. Metcalfe, M. Peery, I. Shelby, Industry Consortium Analysis of Large Reverse Osmosis / Nanofiltration Element Diameters, Work. (2005) 197.

[469] A. Zhu, P.D. Christofides, Y. Cohen, On RO membrane and energy costs and associated incentives for future enhancements of membrane permeability, J. Memb. Sci. 344 (2009) 1–5. doi:10.1016/j.memsci.2009.08.006.

[470] A. Shrivastava, S. Rosenberg, M. Peery, Energy efficiency breakdown of reverse osmosis and its implications on future innovation roadmap for desalination, Desalination. 368 (2015) 181–192. doi:10.1016/j.desal.2015.01.005.

[471] J.R. Werber, C.O. Osuji, M. Elimelech, Materials for next-generation desalination and water purification membranes, Nat. Rev. Mater. 1 (2016). doi:10.1038/natrevmats.2016.18.

[472] R.M. Rachman, S. Li, T.M. Missimer, SWRO feed water quality improvement using subsurface intakes in Oman, Spain, Turks and Caicos Islands, and Saudi Arabia, Desalination. 351 (2014) 88–100. doi:10.1016/j.desal.2014.07.032.

[473] S. Boerlage, N. Nada, Algal toxin removal in seawater desalination processes, Desalin. Water Treat. 55 (2015) 2575–2593. doi:10.1080/19443994.2014.947785.

[474] L.O. Villacorte, S.A.A. Tabatabai, D.M. Anderson, G.L. Amy, J.C. Schippers, M.D. Kennedy, Seawater reverse osmosis desalination and (harmful) algal blooms, Desalination. 360 (2015) 61–80. doi:10.1016/j.desal.2015.01.007.

[475] P. Hess, O. Villacorte Loreen, B. Dixon Mike, F. Boerlage Siobhan, M. Anderson Donald, D. Kennedy Maria, C. Schippers Jan, Harmful Algal Blooms (HABs) and Desalination : A Guide to Impacts , Monitoring , and Management, 2017. doi:10.1017/S1049096508080268.

[476] T.M. Missimer, N. Ghaffour, A.H.A. Dehwah, R. Rachman, R.G. Maliva, G. Amy, Subsurface intakes for seawater reverse osmosis facilities: Capacity limitation, water quality improvement, and economics, Desalination. 322 (2013) 37–51. doi:10.1016/j.desal.2013.04.021.

[477] California Coastal Commission and Poseidon Tesources (SUrfside) LLC, Final Report: Technical Feasibility ofSubsurface Intake Designs for the Proposed Poseidon Water Desalination Facility at Huntington Beach, California, 2014.

[478] California Coastal Commission and Poseidon Resources (Surfside) LLC, Phase II Report: Feasibility of Subsurface Intakes Designs for the Proposed Poseidon Water Desalination Facility at Huntington Beach, California, 2015.

[479] M. Brusilovsky, M. Faigon, The impact of varying the number of elements per PV in SWRO plants - Actual and future configurations, Desalination. 184 (2005) 233–240. doi:10.1016/j.desal.2005.03.057.

[480] H. D.G, H. G.E, M. K, Desalination Using Renewable Energy in Australia, Environ. Sci. Div. 513 (1996) 511. doi:10.1016/0960-1481(96)88909-9.

[481] O.A. Hamed, Overview of hybrid desalination systems - Current status and future prospects, Desalination. 186 (2005) 207–214. doi:10.1016/j.desal.2005.03.095.

[482] M. Saeed, G. F. Al-Otaibi, E. S. Al-Thobaiti, FILTRATION AND FOULING PROBLEMS IN A SWRO PLANT ON THE GULF COAST1, 2018.

[483] I. Kamal, Myth and reality of the hybrid desalination process, Desalination. 230 (2008)

269–280. doi:10.1016/j.desal.2007.11.030.

[484] M.A. Darwish, Thermal desalination in GCC and possible development, Desalin. Water Treat. 52 (2014) 27–47. doi:10.1080/19443994.2013.808401.

[485] M.W. Shahzad, M. Burhan, L. Ang, K.C. Ng, Energy-water-environment nexus underpinning future desalination sustainability, Desalination. 413 (2017) 52–64. doi:10.1016/j.desal.2017.03.009.

[486] P. Rao, W.R. Morrow, A. Aghajanzadeh, P. Sheaffer, C. Dollinger, S. Brueske, J. Cresko, Energy considerations associated with increased adoption of seawater desalination in the United States, Desalination. 445 (2018) 213–224. doi:10.1016/j.desal.2018.08.014.

[487] H. Shemer, R. Semiat, Sustainable RO desalination – Energy demand and environmental impact, Desalination. 424 (2017) 10–16. doi:10.1016/j.desal.2017.09.021.

[488] M.T. Ali, H.E.S. Fath, P.R. Armstrong, A comprehensive techno-economical review of indirect solar desalination, Renew. Sustain. Energy Rev. 15 (2011) 4187–4199. doi:10.1016/j.rser.2011.05.012.

[489] D. Herold, V. Horstmann, A. Neskakis, J. Plettner-Marliani, G. Piernavieja, R. Calero, Small scale photovoltaic desalination for rural water supply - demonstration plant in Gran Canaria, Renew. Energy. 14 (1998) 293–298. doi:10.1016/S0960-1481(98)00080-9.

[490] A. Alsheghri, S.A. Sharief, S. Rabbani, N.Z. Aitzhan, Design and Cost Analysis of a Solar Photovoltaic Powered Reverse Osmosis Plant for Masdar Institute, in: Energy Procedia, 2015: pp. 319–324. doi:10.1016/j.egypro.2015.07.365.

[491] B.S. Richards, D.P.S. Capão, W.G. Früh, A.I. Schäfer, Renewable energy powered membrane technology: Impact of solar irradiance fluctuations on performance of a brackish water reverse osmosis system, Sep. Purif. Technol. 156 (2015) 379–390. doi:10.1016/j.seppur.2015.10.025.

[492] N. Ahmad, A.K. Sheikh, P. Gandhidasan, M. Elshafie, Modeling, simulation and performance evaluation of a community scale PVRO water desalination system operated by fixed and tracking PV panels: A case study for Dhahran city, Saudi Arabia, Renew. Energy. 75 (2015) 433–447. doi:10.1016/j.renene.2014.10.023.

[493] A. Joyce, D. Loureiro, C. Rodrigues, S. Castro, Small reverse osmosis units using PV systems for water purification in rural places, Desalination. 137 (2001) 39–44. doi:10.1016/S0011-9164(01)00202-8.

[494] P.A. Davies, A solar-powered reverse osmosis system for high recovery of freshwater from saline groundwater, Desalination. 271 (2011) 72–79. doi:10.1016/j.desal.2010.12.010.

[495] R. Salcedo, E. Antipova, D. Boer, L. Jiménez, G. Guillén-Gosálbez, Multi-objective optimization of solar Rankine cycles coupled with reverse osmosis desalination considering economic and life cycle environmental concerns, Desalination. 286 (2012) 358–371. doi:10.1016/j.desal.2011.11.050.

[496] G. Xia, Q. Sun, X. Cao, J. Wang, Y. Yu, L. Wang, Thermodynamic analysis and optimization of a solar-powered transcritical CO2 (carbon dioxide) power cycle for reverse osmosis desalination based on the recovery of cryogenic energy of LNG (liquefied natural gas), Energy. 66 (2014) 643–653.

doi:https://doi.org/10.1016/j.energy.2013.12.029.

[497] A. Kasaeian, F. Rajaee, W.-M. Yan, Osmotic desalination by solar energy: A critical review, Renew. Energy. 134 (2019) 1473–1490. doi:https://doi.org/10.1016/j.renene.2018.09.038.

[498] J.A. Carta, J. González, V. Subiela, The SDAWES project: An ambitious R and D prototype for wind-powered desalination, Desalination. 161 (2004) 33–48. doi:10.1016/S0011-9164(04)90038-0.

[499] L. Garcíıa-Rodríıguez, Renewable energy applications in desalination: state of the art, Sol. Energy. 75 (2003) 381–393. doi:https://doi.org/10.1016/j.solener.2003.08.005.

[500] S. Loutatidou, N. Liosis, R. Pohl, T.B.M.J. Ouarda, H.A. Arafat, Wind-powered desalination for strategic water storage: Techno-economic assessment of concept, Desalination. 408 (2017) 36–51. doi:10.1016/j.desal.2017.01.002.

[501] L. Garc\'\ia-Rodr\'\iguez, V. Romero-Ternero, C. Gómez-Camacho, Economic analysis of wind-powered desalination, Desalination. 137 (2001) 259–265. doi:10.1016/S0011-9164(01)00235-1.

[502] M. Forstmeier, F. Mannerheim, F. D'Amato, M. Shah, Y. Liu, M. Baldea, A. Stella, Feasibility study on wind-powered desalination, Desalination. (2007). doi:10.1016/j.desal.2006.05.009.

[503] V. Yangali-Quintanilla, Z. Li, R. Valladares, Q. Li, G. Amy, Indirect desalination of Red Sea water with forward osmosis and low pressure reverse osmosis for water reuse, Desalination. (2011). doi:10.1016/j.desal.2011.06.066.

[504] S. Liyanaarachchi, V. Jegatheesan, S. Muthukumaran, S. Gray, L. Shu, Mass balance for a novel RO/FO hybrid system in seawater desalination, J. Memb. Sci. 501 (2016) 199–208. doi:https://doi.org/10.1016/j.memsci.2015.11.047.

[505] T.Y. Cath, S. Gormly, E.G. Beaudry, M.T. Flynn, V.D. Adams, A.E. Childress, Membrane contactor processes for wastewater reclamation in space: Part I. Direct osmotic concentration as pretreatment for reverse osmosis, J. Memb. Sci. 257 (2005) 85–98. doi:10.1016/j.memsci.2004.08.039.

[506] A. Achilli, T.Y. Cath, E.A. Marchand, A.E. Childress, The forward osmosis membrane bioreactor: A low fouling alternative to MBR processes, Desalination. (2009). doi:10.1016/j.desal.2008.02.022.

[507] E. Bar-Zeev, F. Perreault, A.P. Straub, M. Elimelech, Impaired Performance of Pressure-Retarded Osmosis due to Irreversible Biofouling, Environ. Sci. Technol. 49 (2015) 13050–13058. doi:10.1021/acs.est.5b03523.

[508] K. Touati, F. Tadeo, H. Elfil, Osmotic energy recovery from Reverse Osmosis using two-stage Pressure Retarded Osmosis, Energy. 132 (2017) 213–224. doi:https://doi.org/10.1016/j.energy.2017.05.050.

[509] J. Leijon, C. Boström, Freshwater production from the motion of ocean waves – A review, Desalination. (2018). doi:10.1016/j.desal.2017.10.049.

[510] N. Sharmila, P. Jalihal, A.K. Swamy, M. Ravindran, Wave powered desalination system, Energy. (2004). doi:10.1016/j.energy.2004.03.099.

[511] N. Khan, A. Kalair, N. Abas, A. Haider, Review of ocean tidal, wave and thermal energy technologies, Renew. Sustain. Energy Rev. (2017). doi:10.1016/j.rser.2017.01.079.

[512] B.E. Logan, The Global Challenge of Sustainable Seawater Desalination, Environ. Sci. Technol. Lett. 4 (2017) 197. doi:10.1021/acs.estlett.7b00167.

[513] H.B. Park, B.D. Freeman, Z.B. Zhang, M. Sankir, J.E. McGrath, Highly chlorine-tolerant polymers for desalination, Angew. Chemie - Int. Ed. (2008). doi:10.1002/anie.200800454.

[514] M. Abualtayef, H. Al-Najjar, Y. Mogheir, A.K. Seif, Numerical modeling of brine disposal from Gaza central seawater desalination plant, Arab. J. Geosci. (2016). doi:10.1007/s12517-016-2591-7.

[515] J. Morillo, J. Usero, D. Rosado, H. El Bakouri, A. Riaza, F.J. Bernaola, Comparative study of brine management technologies for desalination plants, Desalination. 336 (2014) 32–49. doi:10.1016/j.desal.2013.12.038.

[516] W. Tang, H.Y. Ng, Concentration of brine by forward osmosis: Performance and influence of membrane structure, Desalination. (2008). doi:10.1016/j.desal.2007.04.085.

[517] H. Geng, J. Wang, C. Zhang, P. Li, H. Chang, High water recovery of RO brine using multi-stage air gap membrane distillation, Desalination. (2015). doi:10.1016/j.desal.2014.10.038.

[518] E. Korngold, L. Aronov, N. Daltrophe, Electrodialysis of brine solutions discharged from an RO plant, Desalination. (2009). doi:10.1016/j.desal.2008.04.008.

[519] A. Ravizky, N. Nadav, Salt production by the evaporation of SWRO brine in Eilat: a success story, Desalination. (2007). doi:10.1016/j.desal.2006.03.559.

[520] M.H.E.-N.E.-M. Schorr, Reject Brine Management, in: IntechOpen, Rijeka, 2011: p. Ch. 11. doi:10.5772/13706.

[521] A. Simon, L.D. Nghiem, P. Le-Clech, S.J. Khan, J.E. Drewes, Effects of membrane degradation on the removal of pharmaceutically active compounds (PhACs) by NF/RO filtration processes, J. Memb. Sci. 340 (2009) 16–25. doi:10.1016/j.memsci.2009.05.005.

[522] E. Sahar, I. David, Y. Gelman, H. Chikurel, A. Aharoni, R. Messalem, A. Brenner, The use of RO to remove emerging micropollutants following CAS/UF or MBR treatment of municipal wastewater, Desalination. 273 (2011) 142–147. doi:10.1016/j.desal.2010.11.004.

[523] S.D. Richardson, M.J. Plewa, E.D. Wagner, R. Schoeny, D.M. DeMarini, Occurrence, genotoxicity, and carcinogenicity of regulated and emerging disinfection by-products in drinking water: A review and roadmap for research, Mutat. Res. - Rev. Mutat. Res. (2007). doi:10.1016/j.mrrev.2007.09.001.

[524] Y. Luo, W. Guo, H.H. Ngo, L.D. Nghiem, F.I. Hai, J. Zhang, S. Liang, X.C. Wang, A review on the occurrence of micropollutants in the aquatic environment and their fate and removal during wastewater treatment, Sci. Total Environ. 473–474 (2014) 619–641. doi:10.1016/j.scitotenv.2013.12.065.

[525] Y. Yang, Y.S. Ok, K.H. Kim, E.E. Kwon, Y.F. Tsang, Occurrences and removal of pharmaceuticals and personal care products (PPCPs) in drinking water and water/sewage treatment plants: A review, Sci. Total Environ. 596–597 (2017) 303–320.

doi:10.1016/j.scitotenv.2017.04.102.

[526] A.M. Comerton, R.C. Andrews, D.M. Bagley, P. Yang, Membrane adsorption of endocrine disrupting compounds and pharmaceutically active compounds, J. Memb. Sci. 303 (2007) 267–277. doi:10.1016/j.memsci.2007.07.025.

[527] S.J. Khan, T. Wintgens, P. Sherman, J. Zaricky, A.I. Schäfer, Removal of hormones and pharmaceuticals in the advanced water recycling demonstration plant in Queensland, Australia, Water Sci. Technol. 50 (2004) 15–22.

[528] J. Radjenović, M. Petrović, F. Ventura, D. Barceló, Rejection of pharmaceuticals in nanofiltration and reverse osmosis membrane drinking water treatment, Water Res. 42 (2008) 3601–3610. doi:10.1016/j.watres.2008.05.020.

[529] N. Le-Minh, S.J. Khan, J.E. Drewes, R.M. Stuetz, Fate of antibiotics during municipal water recycling treatment processes, Water Res. 44 (2010) 4295–4323. doi:10.1016/j.watres.2010.06.020.

[530] E. Agus, N. Voutchkov, D.L. Sedlak, Disinfection by-products and their potential impact on the quality of water produced by desalination systems: A literature review, Desalination. 237 (2009) 214–237. doi:10.1016/j.desal.2007.11.059.

[531] J. Le Roux, N. Nada, M.T. Khan, J.P. Croué, Tracing disinfection byproducts in full-scale desalination plants, Desalination. 359 (2015) 141–148. doi:10.1016/j.desal.2014.12.035.

[532] E. Agus, D.L. Sedlak, Formation and fate of chlorination by-products in reverse osmosis desalination systems, Water Res. 44 (2010) 1616–1626. doi:10.1016/j.watres.2009.11.015.

[533] M. Cai, W. Liu, W. Sun, Formation and speciation of disinfection byproducts in desalinated seawater blended with treated drinking water during chlorination, Desalination. 437 (2018) 7–14. doi:10.1016/j.desal.2018.02.009.

[534] I.C. Karagiannis, P.G. Soldatos, Water desalination cost literature: review and assessment, Desalination. (2008). doi:10.1016/j.desal.2007.02.071.